Optimal Performance of a Wind Farm with and without Battery Energy Storage

Mostafa Naemi

Submitted in total fulfilment of the requirements of the degree of

Doctor of Philosophy

Department of Mechanical Engineering
THE UNIVERSITY OF MELBOURNE

December 2019

Abstract

The increasing penetration of wind in power systems can result in various challenges for system security and reliability, as well as wind farm investability. These challenges require further research to develop an understanding of the operation of a wind farm with and without the use of complementary technologies, such as energy storage, particularly, when the wind turbines have Frequency Control Ancillary Services (FCAS) capability.

This thesis therefore first presents a hierarchical, data-driven, reduced order model of a wind farm, which accounts for the correlation between wind turbines' power output. It finds that the cross-correlation between each turbines' power generation is dependant on the frequency of the wind disturbance and the distance between wind turbines, so that the cross-correlation can be related to the convective length scale in the incoming wind. An investigation of the number of wind turbines required to simulate the wind farm's power generation then indicates that there is an inherent trade-off between model accuracy and complexity.

An optimisation model is then developed to investigate the optimal performance of the wind farm participating in the energy and FCAS markets with and without a battery storage system. This requires modelling of the battery costs along with the revenues in the energy and FCAS markets, as well as a simplified version of the Causer Pays Method used in the Australian National Electricity Market (NEM).

The optimal performance of the Mt Mercer wind farm, located in Victoria, Australia, is then examined. It is found that the wind farm participation in the FCAS markets can improve its financial performance. This analysis shows that the wind farm mainly tends to participate in the FCAS lower regulation market due to the higher prices of this service and no requirement for curtailment before starting a dispatch interval (precurtailment). An investigation of the impact of wind generation forecast accuracy on the system performance also finds that with a better forecasting system, the total performance of the wind farm improves.

Finally, the optimal integration of a lithium-ion battery into a wind farm is examined. Assessments find that the battery is not investable without substantial subsidies when the battery participates only in the energy market. However, it is also found that participation in the FCAS markets can significantly improve the battery's investability, but its financial viability is highly sensitive to FCAS prices. In addition, it is found that the introduction of wind farm frequency control capability reduces the optimal value and capacity of battery storage. Investigation of different wind generation forecasting systems identifies that the improvement of forecast accuracy also reduces the optimal battery value and capacity, as there are fewer opportunities for the battery to reduce the wind farm regulation payments.

Declaration

This is to certify that

1. the thesis comprises only my original work towards the PhD,
2. due acknowledgement has been made in the text to all other material used,
3. the thesis is less than 100000 words in length, exclusive of tables, maps, bibliographies and appendices.

Mostafa Naemi, December 2019

Acknowledgement

Firstly I would like to express my sincere appreciation to my supervisors Prof. Michael Brear and Dr. Matthew Jeppesen for their continuous support throughout my PhD. Without their constructive advice, patience and encouragement, this thesis would not have been completed. I would also like to thank the members of my advisory committee, Dr. Robert Gordon and Dr. Mohsen Talei for their guidance.

I am grateful of the financial support from the University of Melbourne through the scholarships and also the studentship funding granted by Prof. Brear to complete this thesis.

My sincere thanks also goes to all my friends and colleagues in the Thermodynamics Group, especially Dr. Dominic Davis, Will Clarke and Reza Yosri for providing a productive and enjoyable working environment.

Finally, I must express my profound gratitude to my family especially my parents, whose support, love and caring are always with me throughout my life. Also, I wish to thank Romina for her emotional support through the latest stages of my PhD work.

To my parents

Contents

List of Figures

List of Tables

Nomenclature

The following nomenclature includes the list of symbols used in the optimisation model presented in this chapter.

Parameters

$\alpha_{RReg}, \alpha_{LReg}$	Fraction of total enabled FCAS raise and lower regulation used by the power system (%).
Δt	Time resolution of the opitmisation model (hr).
δ	Number of time intervals in a day.
η_d, η_c	Battery discharging and charging efficiency (%).
$\mathcal{S}$	Share of the wind farm-battery system in FCAS markets (%).
π	Wholesale price of electricity ($/MWh).
$\pi_{\mathcal{X}}$	Price of FCAS $\mathcal{X}$ service ($/MWh).
$\rho_{RCont}, \rho_{LCont}$	Probability of a contingency event requiring raise or lower services (%).
σ_{g_c}	Maximum unfulfilled curtailment for a controlled group g_c due to the aggregated control of turbines (MW).
θ_{curt}	Maximum allowable wind power curtailment for a turbine as pecentage of the power generation (%).
ε	Error in modelled wind farm power output at each time interval (MW).
C_{rate}^{max}	Maximum recommended C_{rate} for the battery.
$C_{B,E}, C_{B,P}$	Enegy and power related costs of the battery ($/MWh , $/MW).
$D_{\mathcal{X}}$	Demand of FCAS $\mathcal{X}$ service (MW).

DT_{hist}	Historical data of the dispatch target.
f_B, v_B	Battery fixed ($/MW) and variable ($/MWh) O&M costs.
FI	Frequency indictor (MW).
K_{CPP}	Coeficient of the linear model of Causer Pays Method.
L	Battery lifetime (yr).
$l^{max}_{g_c,act}$	Maximum curtailment limit for a controlled group g_c using the measured power (MW).
$l^{max}_{g_c,mdl}$	Maximum curtailment limit for a controlled group g_c using the modelled power (MW).
N_{cyc}	Typical number of daily cylce for a utility scale battery.
P_{TL}	Capacity of transmission line (MW).
$P_{wt,mdl}, P_{g,mdl}$	Modelled power output of wind turbine wt and group g respectively (MW).
r	Discount rate (%).
SOC_{up}, SOC_{low}	Upper and lower limit of battery state of charge (%).
w_{g_c}	Number of turbines in a controlled group g_c.

Sets

$\mathcal{X}$	Set of all FCAS services: LReg, RReg, L5, L60, L6, R5, R60 and R6.
$\mathcal{X}_{LCont}$	Set of all FCAS contingency lower services; L5, L60 and L6.
$\mathcal{X}_{RCont}$	Set of all FCAS contingency raise services; R5, R60 and R6.
g	Set of turbine groups in the wind farm model.
g_c	Set of turbine control groups.
t	Set of time intervals.
wt	Set of turbines of the wind farm.
y	Set of years of the battery life.

Variables

ϵ	Maximum unfulfilled curtailment in the actual scenario due to the error in the wind farm model (MW).
$\mathcal{V}$	The objective value ($).
τ	Unfulfilled requested curtailment in the actual scenario due to the error in the wind farm model (MW).
CPP	Present value of total causer pays payments ($).
Dev	Deviation of the system from the dispatch target (MW).
$DT_{correct}$	Corrected dispatch target of the wind farm considering the pre-curtailment (MW).
E_B	Battery energy level (MWh).
FOM_B, VOM_B	Present value of battery fixed and variable O&M costs ($).
$P_{B,\mathcal{X}}$	Battery FCAS $\mathcal{X}$ serivce enablement (MW).
$P_{B,c}, P_{B,d}$	Battery charging and discharging power in the energy market (MW).
$P_{B,max}$	Battery power rating (MW).
$P^{max}_{g_c,curt}$	Maximum possible curtailment of controlled group g_c using wind farm modelled power (MW).
$P^{req}_{g_c,curt}$	Requested curtailment of controlled group g_c using wind farm modelled power (MW).
$P_{net,mdl}, P_{net,act}$	Net power flow to/from the grid calculated based on the modelled and measured power output of the wind farm respectively (MW).
$P_{wf,\mathcal{X}}, P_{g_c,\mathcal{X}}$	Wind farm and controlled group g_c FCAS $\mathcal{X}$ service enablement repsectively (MW).
$P_{wf,pcurt}, P_{g_c,pcurt}$	Precurtailment of wind farm and turbines in controlled group g_c respectively (MW).
Q_B	Battery capacity (MWh).
R_{Cont}	Present value of earned revenues in FCAS contingency markets ($).
R_{Energy}	Present value of earned revenue in energy market($).

R_{FCAS}	Present value of total earned revenues in FCAS markets ($).
R_{Reg}	Present value of earned revenues in FCAS regulation markets ($).
TC_B	Present value of total cost of battery energy storage ($).

Acronyms

ACPP Avoided Causer Pays Payments.

AEMC Australian Energy Market Commission.

AEMO Australian Energy Market Operator.

AGC Automatic Generation Control.

AWEFS Australian Wind Energy Forecasting System.

CAES Compressed Air Energy Storage.

CPF Causer Pays Factor.

CPM Causer Pays Method.

CPP Causer Pays Payment.

DFIG Doubly Fed Induction Generator.

FCAS Frequency Control Ancillary Services.

FFR Fast Frequency Response.

FI Frequency Indicator.

FOM Fixed Operation and Maintenance Cost.

ISO Independant System Operator.

LCont Lower Contingency.

LP Linear Program.

LReg Lower Regulation.

NEM National Electricity Market.

NEMDE National Electricity Market Dispatch Engine.

NSCAS Networks Support and Control Ancillary Services.

PHES Pumped Hydro Energy Storage.

RCont Raise Contingency.

ROCOF Rate of Change of Frequency.

RReg Raise Regulation.

RTE Round Trip Efficiency.

SOC State of Charge.

SRAS System Restart Ancillary Services.

VOM Variable Operation and Maintenance Cost.

Chapter 1

Introduction

1.1 Challenges of integrating wind energy into power systems

The increasing deployment of wind energy in a power system has resulted in various challenges, and this requires further research to realise the potential of this source of energy [1–4]. In a recent review, Veers et al. [3] identified three grand challenges for the production of energy from wind:

- to develop a deeper understanding of wind power plant flow physics;
- to continue aerodynamic and structural innovation of wind turbine technologies;
- to optimise the integration of wind power plants into the grid.

Wind physics has traditionally been simplified by using various assumptions, such as surface layer similarity, which do not necessarily hold for micro-scale atmospheric flows with length scales less than 1 km. The dynamics of wind motion inside a wind farm with complex terrain and the creation of wakes that potentially impact the power generation of downstream wind turbines are not fully understood [3]. Therefore, further investigation of the impact of wind flow variations inside a wind farm on the performance of the whole wind farm is required.

Challenges associated with the integration of wind power plants into the grid are also critical because high penetrations of converter connected wind power generators can adversely impact grid stability, reliability and planning. These adverse impacts occur over a range of time scales, from less than a second to multiple years and therefore require action to be taken over the corresponding time scales [3]. Conventionally, wind power plants have not provided ancillary services, which are required for power system security. However, with increasing wind penetration, existing ancillary service markets may need to be revised to incentivise the provision of ancillary services by wind farms and other assets, which can ultimately increase the system flexibility. Furthermore, alternative solutions for improving grid integration of intermittent wind energy have also been proposed, such as improving the wind generation forecast accuracy and deploying utility-scale energy storage technologies in power systems. As shown in Figure 1.1, the global installed wind power generation capacity and its share in total electricity generation have increased considerably over the past 10 years [5], which illustrates the importance of studying these challenges and associated solutions.

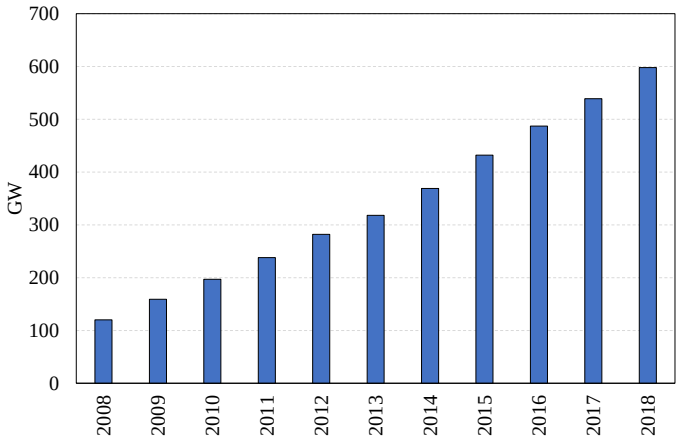

(a)

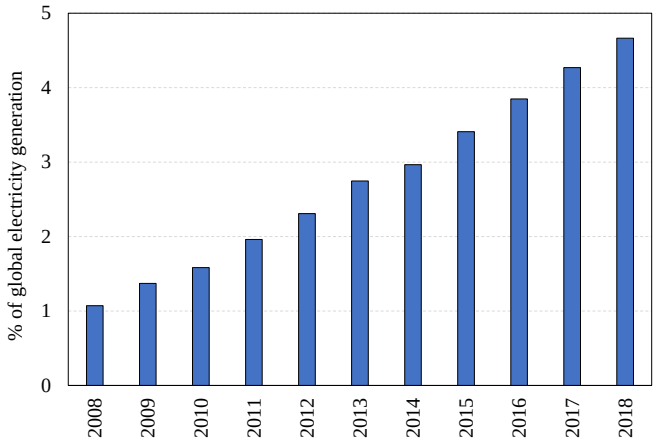

(b)

Figure 1.1: a) Global installed wind power generation capacity [5] and b) share of wind in the global electricity energy generation from 2008 to 2018 [6].

1.2 The Australian National Electricity Market

The transition towards greater penetration of renewable power generation in the power system is also occurring in Australia. This trend is highlighted in Figure 1.2a, which shows the wind installed capacity in different Australian National Electricity Market (NEM) regions [7]. Figure 1.2b demonstrates the historical trend of wind generation's share in total regional generation. It can be seen that in 2018, wind generation accounted for approximately 45% of South Australia's energy generation, which has already imposed challenges on power system operation and frequency control [8, 9]. To date, these challenges have been resolved to a large extent by revising the system requirements and

allowing new participants, such as wind farms and battery storage to provide frequency control ancillary services [10, 11]. However, wind energy penetration in the NEM is forecast to continue growing, such that by 2030 the installed capacity of wind generation is anticipated to reach approximately 10 GW [12].

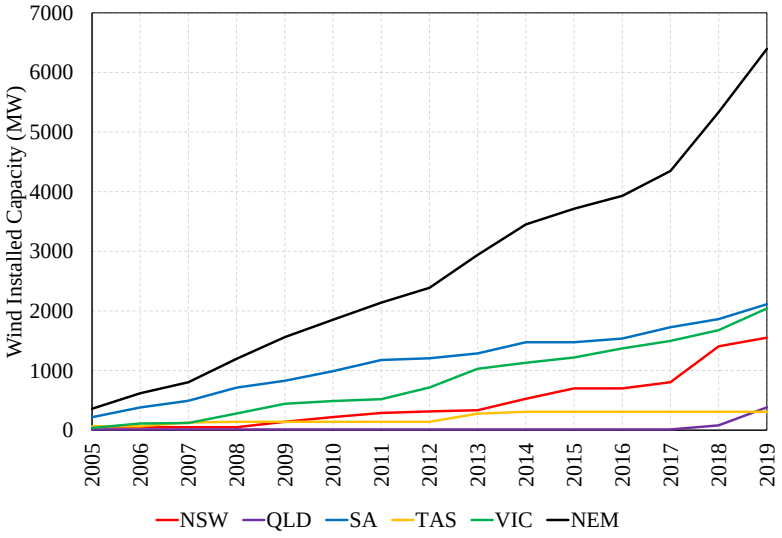

(a)

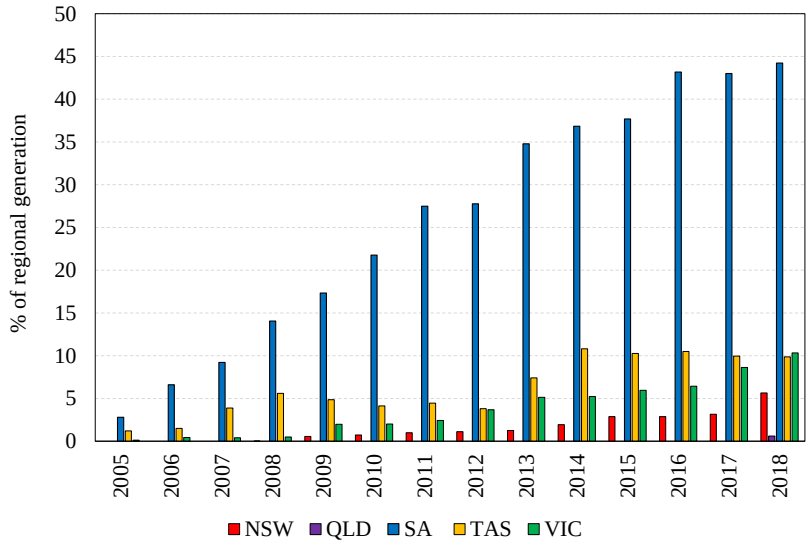

(b)

Figure 1.2: Historical trends of a) installed wind capacity in different regions of the NEM (data obtained from [7]), and b) wind generation as a percentage of total regional generation [13].

The NEM with a total generation capacity of almost 54 GW, is one of the longest interconnected power systems in the world, having a total length of approximately 5000 km compared with the Russian and Chilean systems with approximately 10000 km and 3100 length km, respectively [14, 15]. The NEM is a wholesale spot market, with a wholesale energy market and Frequency Control Ancillary Services (FCAS) markets. FCAS services are used to maintain the power system frequency within the normal operating band (49.85-50.15 Hz). In addition to FCAS services, non-market ancillary services also support the security of the system and are provided using contracts between the Australian Energy Market Operator (AEMO) and the service providers [16]. These include Networks Support and Control Ancillary Services (NSCAS) and System Restart Ancillary Services (SRAS). NSCAS are used for voltage control, power flow control and maintaining the stability of the system following major events in the power system. Finally, SRAS are reserved for use in restarting the system when a complete or partial blackout occurs [17].

FCAS services are classified into *regulation* and *contingency* services. FCAS regulation services are used continuously to correct minor imbalances between generation and demand. Regulation raise services increase generation or decrease load when the frequency is below the nominal value, while lower services decrease generation or increase load to reduce the frequency when it is above the nominal value. In the event of a critical and unexpected disturbance in the power system, such as the loss of a generator causing a significant power imbalance and deviation of the frequency outside of the normal operating band, contingency services are also used [17]. These contingency services include fast (6-second), slow (60-second) and delayed (5-minute) services, which complement one another, as shown in Figure 1.3a. Unlike regulation services which are controlled through the Automatic Generation Control (AGC) signal, the provision of contingency services is a direct response to local measurements of system frequency [12]. Figure 1.3b demonstrates the response time frame of different contingency services to a given frequency deviation.

FCAS regulation services have been traditionally provided by generators raising or lowering their generation. However, the provision of regulation services usually incurs a cost to the provider, such as financial loss in the energy market or inefficiencies due to deviation from optimal operating points. The FCAS regulation costs are recovered from the participants according to a complex approach called the *Causer Pays* method. This method attempts to allocate costs to participants who increase the need for regulation services [17, 18]. On the other hand, since the raise contingency services are required to manage the loss of the largest generator in the system, payments for these services are recovered from the generators. Furthermore, the lower contingency services are used to

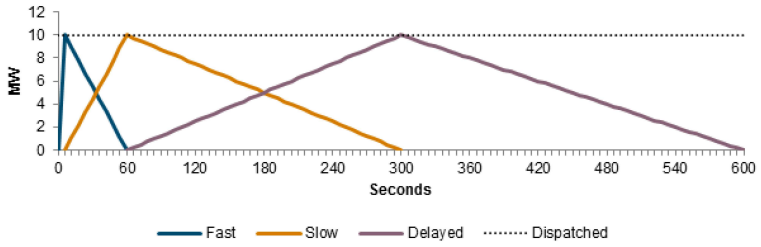

(a)

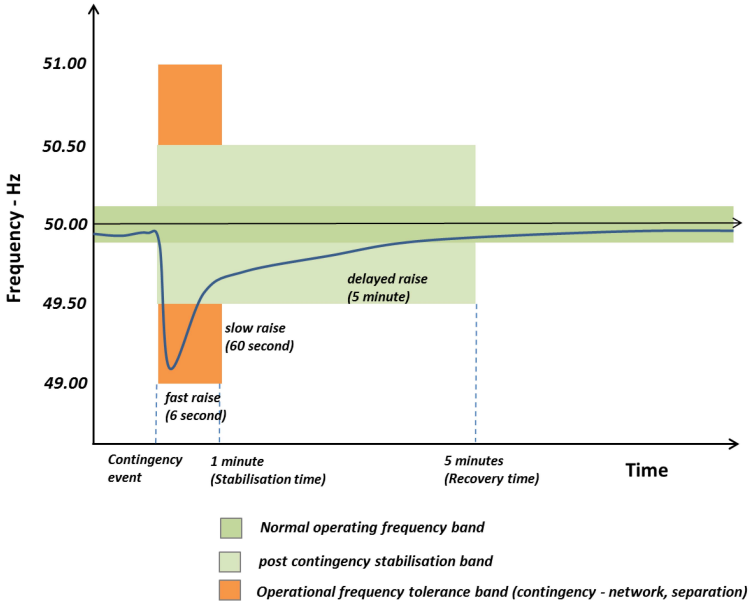

(b)

Figure 1.3: a) The dispatched power profile for 10 MW enabled FCAS fast, slow and delayed contingency services and b) a frequency deviation and consequential response of the FCAS contingency services in the NEM [12].

manage the loss of the largest load in the gird therefore payments of these services are recovered from the customers. These costs are allocated to participants according to their relative generation or consumption in the power system [17].

In recent years, the FCAS markets of Australia's NEM have experienced a significant increase in the price of the various services (Figure 1.4). This can be partially attributed to the increasing penetration of wind generation into the grid, which increases the need for FCAS services to manage their variability [12]. The analysis of the historical data shows that there is no significant increase in the requirement of FCAS services in the NEM. However, a 35 MW local FCAS regulation requirement for South Australia when there is a possibility of islanding mainly contributed to this price increase. This is due to the lack of competition in FCAS markets, as there is a limited number of FCAS services providers in that state. Also, the increasing penetration of renewables in the power system has replaced conventional synchronous generators, which have typically been the major provider of FCAS services. Hence, the increased intermittent power

generation along with a reduction in the number of FCAS providers have contributed to the significant price increase, especially in South Australia [9].

High prices of the FCAS services result in correspondingly high payments of the market participants who increase the need for these services but do not provide them, particularly for renewable generators such as wind power plants. Wind farms are particularly vulnerable to these increased FCAS prices because the Causer Pays method penalises them for deviating from their dispatch targets, which can occur frequently due to imperfect forecasting or control of the wind farm's power generation.

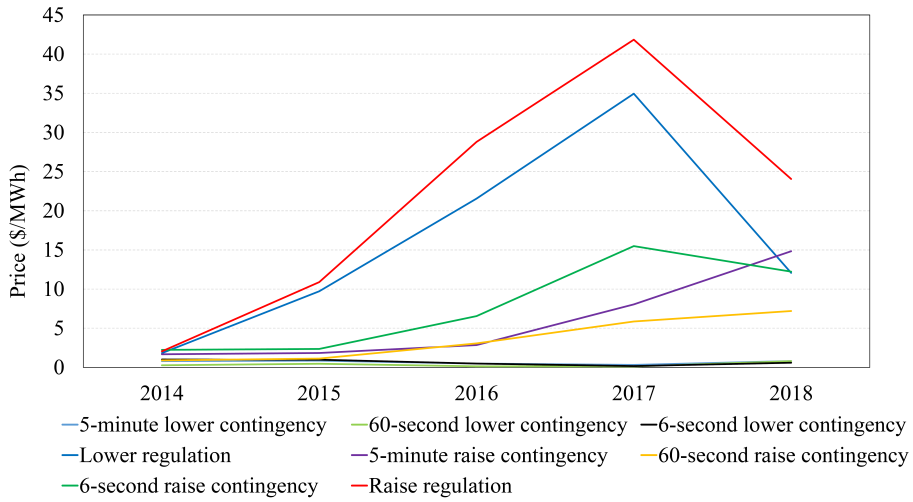

Figure 1.4: Average price of FCAS services in the NEM.

Although FCAS prices have increased significantly from 2015, the total size of these markets (approximately $200 million) is small relative to the wholesale energy market, which had a total size of approximately $17 billion in 2017 [14]. Nevertheless, participation in the FCAS markets is potentially attractive for a generator, a battery, controllable loads and other dispatchable plants. The main feature is that these markets are enablement-based, meaning that the FCAS providers earn revenues based on their ability to provide the FCAS services, not based on what they are asked to provide. It should be noted that the amount of energy dispatched due to the provision of FCAS services provides revenues in the energy market as well. Analysis of NEM data for 2017 showed that 30% and 20% of the total FCAS regulation raise and lower enabled capacity were actually used by the power system. Also, contingency events occur very rarely (approximately 1% of time) [19], showing that providers of FCAS contingency services can also earn revenue for simply being enabled to provide these services, without having to take action for the large majority of the time.

1.3 Thesis overview and contributions

This thesis aims:

- to develop a reduced order model of a wind farm;
- to examine the optimal performance of a wind farm with capability of the frequency control services provision;
- to investigate the optimal integration of battery storage into a wind farm with and without frequency control.

In Chapter 2, different challenges and solutions for increasing wind penetration in power systems are reviewed. Various research gaps are identified in this literature review, which leads to three stated research aims. Chapter 3 then proposes a method to develop a reduced order model of a wind farm, which takes into account the cross-correlation between the power output of wind turbines. This model is suitable for studying fluctuations in power generation due to natural wind variations. Chapter 4 presents the formulation of an optimisation problem to assess the optimal technical and financial performance of a wind farm operating in the wholesale energy and FCAS markets, and with the possibility of an integrated battery storage system. Chapter 5 uses this optimisation model to investigate the optimal performance of a wind farm with frequency control capability. It also studies the impact of wind generation forecast accuracy on the performance of a wind farm-only. Chapter 6 examines the optimal performance of a battery storage system integrated into a wind farm, considering the influence of different input parameters, such as battery capital cost, on the optimal performance of the plant. Again, the impact of wind generation forecast accuracy on the battery investment and the performance of the entire system is investigated. Chapter 7 then provides a summary of the key outcomes of this work and discusses the potential topics for future research.

In terms of the three grand challenges identified by Veers et al. [3] and discussed in Section 1.1, this thesis addresses the first grand challenge by developing a model that incorporates the dynamics of wind power generation and relating the correlation between wind turbines' power output to the convective length scale of the incoming wind. This thesis also contributes to the third challenge by investigating the optimal performance of a wind farm integrated into a power system, both as a stand alone system and in combination with battery storage.

Chapter 2

Literature review

2.1 Introduction

The greater penetration of wind turbine generation into a power system has the important benefit of reducing the system's carbon intensity but also presents significant challenges relating to their effective integration. This chapter reviews the current understanding of these challenges. The fundamental technical aspects of wind turbine operation are explained, followed by a review of different methods for the dynamic modelling of wind farms and their potential capability to offer system frequency control services. In addition, the potential use of energy storage to complement wind farms is reviewed, with regard to the available energy storage technologies and the services they can provide.

2.2 Grid integration challenges of wind energy

The large-scale integration of wind turbine generation into the grid leads to various technical issues that affect grid reliability and security, several of which originate from the intermittent nature of the wind resource. This natural variability in wind energy generation can be classified according to the time scale of the variation into annual, seasonal and diurnal variations, as well as turbulent disturbances. The short time scale variability of wind generation can have a significant impact on the power quality and operation of the power system [4, 20]. Furthermore, most current wind turbines are connected to the grid through power electronics. This presents challenges such as a reduction of the inertia of the power system and the creation of harmonics from power electronics switching, which impacts power system security [1].

2.2.1 Power quality

Electricity grids must have quality standards that ensure the safe and efficient supply of energy to customers. These standards are applied to various power quality properties, such as frequency and voltage. Both wind variability and the use of power electronics has the potential to adversely affect the power quality of the grid, to such an extent that the standards are no longer fulfilled, and which can lead to grid failure and malfunction of electric devices [21, 22].

In particular, if the system frequency is above the nominal operating value, generation is greater than the demand, while system frequency below the nominal value is a symptom of demand being greater than generation [23]. The natural variability in

large-scale wind power generation presents difficulties for the frequency control of the power system. Therefore, the system operator is required to increase the amount of reserve generation in the system to meet demand in the event of an unexpected variation in wind energy generation [24].

Doherty et al. [25] showed that the reserve requirement increases by 20% for increasing wind penetration to 30% in a power system with a total generation capacity of 4500 MW. However, it has also been shown that the aggregation of geographically dispersed wind farms can reduce the short term wind generation variability by 30-50% compared with a single large wind farm of the same capacity [1, 20, 23, 26]. This aggregation results in lower reserve requirements.

To resolve system frequency fluctuations arising from variations of the wind, the dynamic allocation of reserve requirements has also been proposed. In this method, the reserve requirement is updated every 24 hours according to the level of the wind generation [27], which may allow for diurnal variations to be addressed, but provide limited scope for mitigating the impacts of short time scale variations.

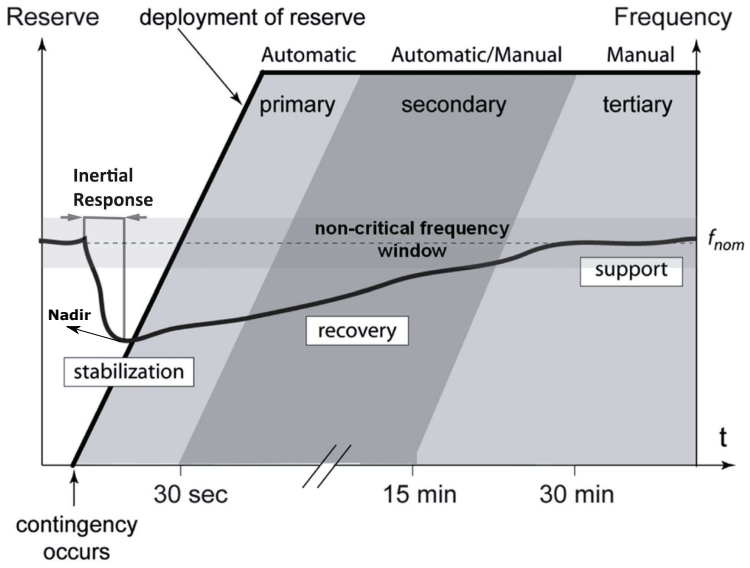

Figure 2.1: Typical response time of different frequency control services to a system contingency [28].

Figure 2.1 presents the typical response time of different frequency control services, showing the various time scales of the response to a *contingency* that pushes frequency outside the non-critical band. The inertial response is the fast and inherent response of the system's synchronous generators to the rate of change of the frequency, in which their kinetic energy is released or absorbed to oppose the frequency change [29]. Unlike conventional synchronous generating units such as coal power plants, wind turbines have asynchronous generators connected to the grid through the power electronics that

makes them insensitive to the changes in frequency [1, 30]. Therefore, the replacement of conventional generators with wind turbines reduces the system's total inertia, and thus affects the Rate of Change of Frequency (ROCOF). The initial ROCOF immediately after a contingency and before the response of any frequency control service providers is related to the inertia as: [29],

$$ROCOF = \frac{df}{dt} = \frac{\Delta P}{2H_{sys}} f_0, \tag{2.1}$$

where ΔP, f_0 and H_{sys} are the power imbalance (contingency size), the rated frequency and the inertia constant of the system, respectively. It can be seen from Equation 2.1 that the lower the value of the system inertia, the greater the ROCOF, which is undesirable for power system security.

Not only the ROCOF but also the minimum frequency (nadir), resulting from a system frequency contingency, will change as a result of the increasing penetration of wind generation. This is because the higher ROCOF will result in the system frequency reducing to lower levels, and there is therefore less time for providers of frequency control services to respond. Figure 2.2 shows the impact of both the penetration of converter connected generators such as wind turbines and the inertia of the synchronous generators operating in the grid on the ROCOF and the frequency nadir. It can be seen that greater penetration of wind generation and less inertia in the power system results in higher ROCOF and lower nadir.

Various approaches have been discussed to address the low inertia of a power system with high penetration of wind. The first approach proposes the provision of different forms of inertia (synchronous and synthetic), whilst the second approach focuses on changing the current power system requirements to cope with large ROCOF [31]. As an example of the first approach, Ref [32] presented a unit commitment model with constraints on the maximum allowable ROCOF to ensure system security.

The intermittent wind power generation of a wind farm, as well as start-up and shut-down of the individual turbines consuming reactive power in their asynchronous generator, can also cause voltage fluctuations in the system [33]. On the other hand, wind farms themselves are susceptible to voltage dips within the electrical grid [34]. In the event of such a fault in the power system, a voltage dip will eventuate at the point of connection between a variable speed wind turbine and the grid. As the voltage decreases, current increases in the stator and rotor windings, which can result in over-current of converters. Therefore, to avoid these adverse impacts, wind farm operators must disconnect the wind farm from the grid during the fault to protect the turbines [35]. This leads to a reduction in power injection to the grid, which exacerbates the challenge

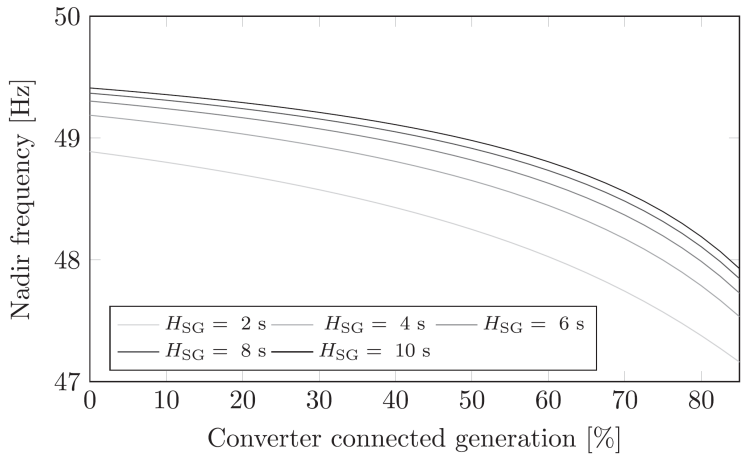

(a)

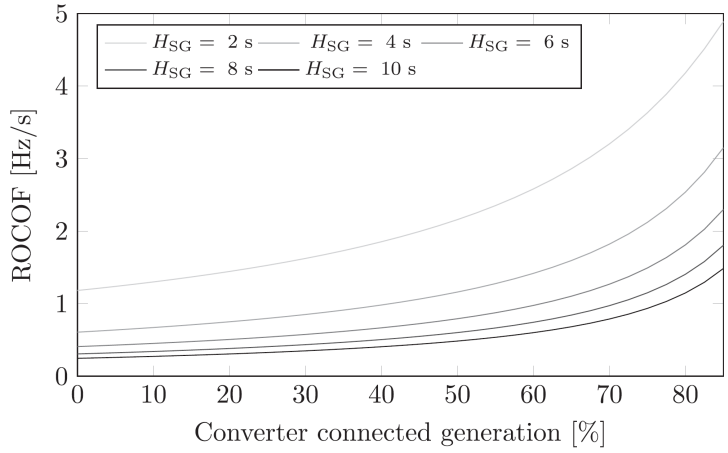

(b)

Figure 2.2: Impact of increasing penetration of converter connected generation such as wind turbines on a) the frequency nadir, and b) the ROCOF resulting from a 10% power imbalance (ΔP), for different values of the inertia constant of synchronous generators (H_{SG}) in a system [31].

of ensuring power system security. Studies such as Ref [35] have proposed modifications in the control system of wind turbines to improve this 'fault ride through'capability.

2.2.2 Power system operational cost

The technical issues associated with large-scale wind integration into a power system also have economic consequences. Wind farms are not dispatchable. Therefore, the system operator must allocate additional reserves to accommodate the uncertainty in the forecast wind generation, as well as to accommodate ramping up or down of the wind power generation [36]. Uncertainty in the expected wind generation and so uncertainty in the commitment of other generators can lead to higher operating costs because system operators have to deal with this uncertainty by regulating the dispatchable generators

[4, 20, 37, 38]. In addition, as the penetration of wind in the power system increases, wind generation curtailment, which is a deliberate reduction of turbine's power generation using its control system, will be inevitable to stabilise the system and minimise the variability. This curtailment has a negative impact on the financial performance of wind power plants and the power system [1, 30, 39]. There is, therefore, an opportunity to improve system efficiency and reduce operational costs with improved forecasting of wind generation. The extent to which these efficiencies and cost reductions are possible needs to be evaluated.

2.2.3 Power system planning

The increasing penetration of wind generation in a power system requires revising the power system infrastructure to incorporate both its natural variability and geographic characteristics. The location of a wind farm is dependent on the local wind speed, so that in regions with desirable wind speed there will be a large amount of wind generation, while local consumption will be usually low due to low population density. This requires a transmission line with enough capacity to export the wind power generation, which can impose a considerable cost on the system [1]. Also, a sudden reduction in power generation of a wind plant, due to a storm, for example, can cause overloading problems in interconnectors and transmission lines and increase the *loss of load probability* [21, 27].

For instance, in September 2016, tornadoes with wind speed more than 190 km/h damaged transmission lines in South Australia (SA), which resulted in a series of faults in the network. This activated the protection system of wind farms, which resulted in a 460 MW reduction in power generation. This significant wind power reduction overloaded the interconnection between Victoria and SA, which finally resulted in blackout for SA [8]. Therefore, it is crucial to investigate the expansion of the power system and potential technologies such as energy storage for improving system security and diminishing the adverse impact of wind variability.

2.3 Wind power plants

Technical innovation in the development of wind turbine technology has resulted in the rapid growth of the capacity of individual turbines, from approximately 100 kW in the 1980s, to capacities of order of 10 MW in the present day [40, 41]. Figure 2.3 depicts the evolution of wind turbine capacity, together with the change in operating rotational speed.

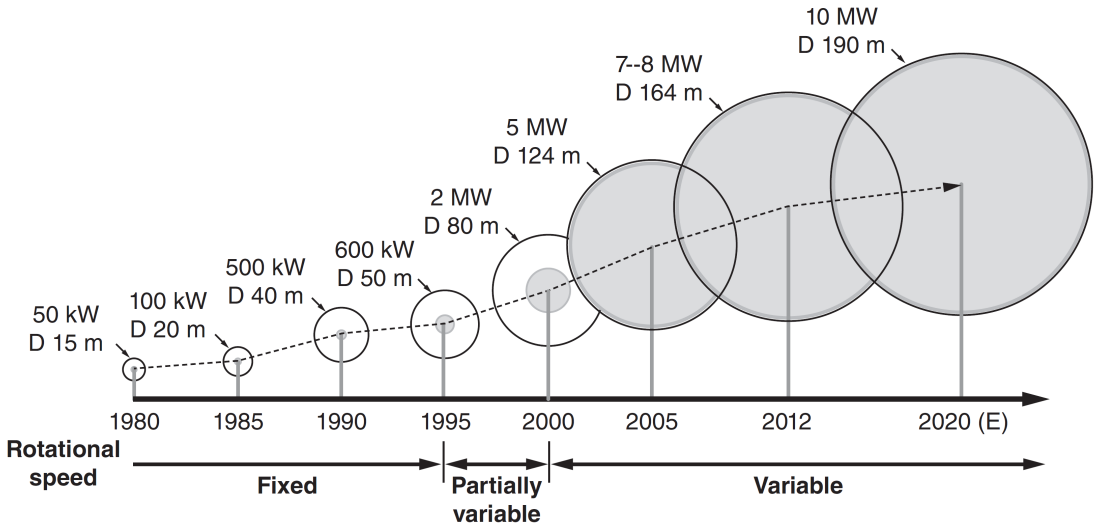

Figure 2.3: Evolution of wind turbine capacity and operating rotational speed [41].

2.3.1 Types of wind turbine

The most common class of wind turbine is the horizontal axis turbine, which can be classified into four main types:

- Type 1: Fixed speed wind turbine,
- Type 2: Variable slip wind turbine,
- Type 3: Doubly Fed Induction Generator wind turbine (DFIG),
- Type 4: Full converter wind turbines.

The schematics of these different types of wind turbine are shown in Figure 2.4.

The earliest type of wind turbine was of fixed speed, which has simpler design and operation, as well as lower cost than other types. The operational speed of this kind of wind turbine can tolerate very slight fluctuations (about 1 % of nominal speed) [43]. The main disadvantage of this type of turbine is non-optimal performance due to the fixed speed of the rotor [43–46].

To resolve the drawbacks of fixed speed turbines, the variable slip wind turbine was introduced, in which a wound rotor induction generator is typically used. The variable resistance in the rotor circuit of this type of generator is controlled by an electronic control system and allows up to 10 % slip in operation. Both fixed speed and variable slip type turbines must operate at super-synchronous speed to generate power; otherwise, they consume electricity like all induction machines [43, 44].

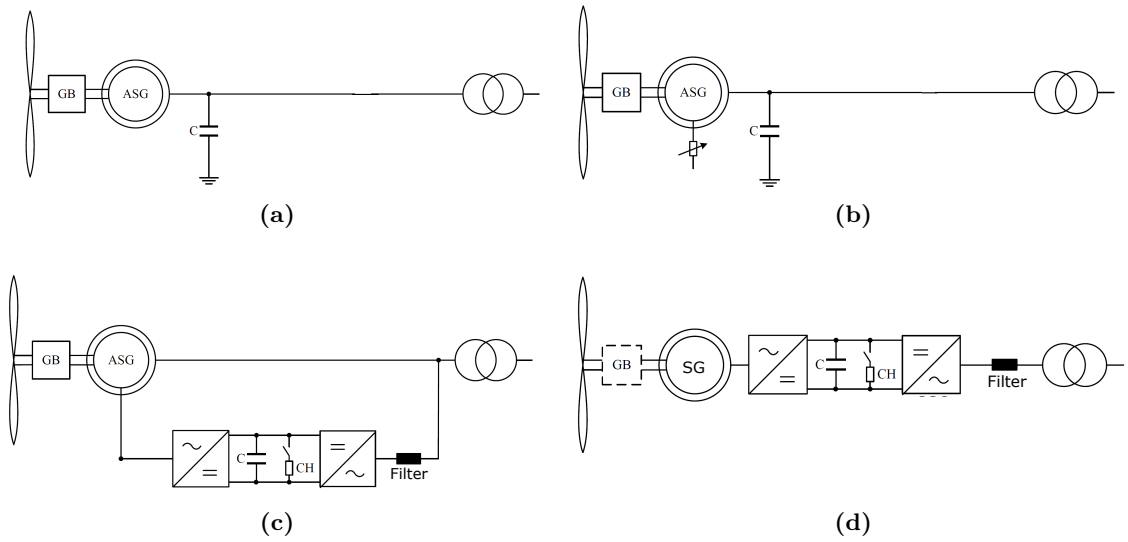

Figure 2.4: Schematic of different types of wind turbine, including: a) Fixed speed, b) Variable slip, c) DFIG, and d) Full converter wind turbines [42].

The next type of turbine developed was the DFIG, which is of primary interest in this study, and the dominate type of turbine used today. Unlike the previous types, a DFIG wind turbine is able to operate over a relatively wide range of turbine speeds, allowing for higher efficiencies. The stator in a DFIG system is connected to the grid directly, while the rotor is connected to the grid through an AC/DC/AC back-to-back configuration of converters. Normally, DFIG wind turbines are designed to operate at ±30% of the synchronous speed. Therefore, the capacity of the power electronic converter is typically 30% of the nominal turbine capacity, which causes the cost of the system to be lower in comparison to full converter type turbines [47, 48]. Arguably the major drawback of the DFIG system is its poor fault ride through capability [49–51].

Finally, the full converter wind turbine has no rotor windings, but rather, the rotor magnetic field is created by using permanent magnets [43, 44]. The generator is decoupled completely from the grid by using converters that improve the performance of the system during a fault in the power system. However, due to the comparatively high costs, this type of wind turbine is yet to be deployed extensively in power systems around the world.

Doubly Fed Induction Generator (DFIG) wind turbines are the dominant type of wind turbine in the global wind market, having a share in 2015, of approximately 50% and 75% of the installed wind capacity in Europe and North America, respectively [52]. In 2013, in the Australian National Electricity Market (NEM), the DFIG wind turbine's share was 35% of the total wind installed capacity, which is anticipated to reach up to 45% in 2020 [53]. This explains the importance of studying and modelling this type of wind turbine, which is the focus of this study.

2.3.2 Modelling of the DFIG wind turbine

Many studies have developed models of the DFIG wind turbine for assessing the technical aspects of their integration into the power system. These models can be classified into full models and reduced order models.

2.3.2.1 Full model

A full model of a DFIG wind turbine considers the mechanical and electrical subsystems, as well as the power electronics. A typical configuration of a DFIG wind turbine was shown in Figure 2.4c, from which it can be seen that the stator windings are connected to the grid directly, while the rotor windings are connected through the power electronics.

The aerodynamic component of a wind turbine model simulates the conversion of the kinetic energy of the wind to the rotational energy of the wind turbine rotor. The blades of the wind turbine are the key element to this aerodynamic conversion of energy. The power extracted from the wind by the blades is calculated as,

$$P_m = \frac{1}{2}\rho C_P A V_w^3, \tag{2.2}$$

where ρ is the air density, A is the blade swept area, V_w is the wind speed and C_P is the turbine power coefficient. C_P indicates the extent to which the kinetic energy in the wind can be extracted with a maximum limit of 59%, known as *Betz'* limit. Various expressions for C_P have been proposed and which relate it to the pitch angle of the blades (β) and their tip-speed ratio (λ) [47, 54].

The rotational energy of the blades is transferred to the generator through the drive-train. Various models of the wind turbine drive-train, ranging from six-mass to two-mass models, have been investigated [55]. The one-mass model has been found to be sufficiently accurate for dynamic modelling and control of a DFIG wind turbine in most instances [56–60].

$$2H_t \frac{d\omega_t}{dt} = T_m - T_e, \tag{2.3}$$

where H_t and ω_t are the inertia constant and rotational speed of the turbine. Also, T_m and T_e denote the mechanical and electromagnetic torques.

The electrical subsystems include the generator and the power electronics. Figure 2.5 shows the equivalent circuit of the rotor and stator of an induction generator where v is the voltage, R is the resistance, i is the current, L_l and L_m denote the leakage and

the mutual inductances and the subscripts r and s correspond to the rotor and stator, respectively [47]. The space vector method is used to simplify the dynamic modelling of an induction generator [43, 47]. In this method, the 3-phase quantities (abc) are stated as a vector with the real and imaginary parts. The stator and rotor voltages are then modelled by the following,

$$\vec{v_s} = R_s\vec{i_s} + \frac{d\vec{\psi}_s}{dt}, \tag{2.4}$$

$$\vec{v_r} = R_r\vec{i_r} + \frac{d\vec{\psi}_r}{dt}, \tag{2.5}$$

where ψ is the flux which can be calculated as,

$$\vec{\psi}_s = L_{ls}\vec{i_s} + L_m(\vec{i_r} + \vec{i_s}), \tag{2.6}$$

$$\vec{\psi}_r = L_{lr}\vec{i_s} + L_m(\vec{i_r} + \vec{i_s}). \tag{2.7}$$

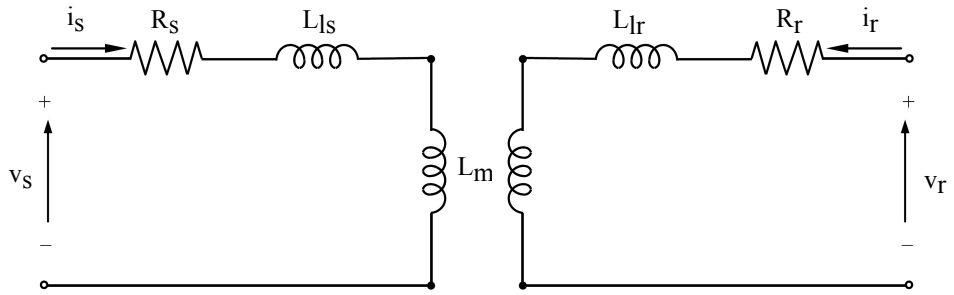

Figure 2.5: Equivalent circuit of stator and rotor of a DFIG wind turbine [47].

The d-q reference frame is commonly used to map abc quantities to a two dimensional reference frame which rotates with synchronous speed (ω_{sync}). The d component corresponds to the real part whilst the q component corresponds to the imaginary part of the vector model. For mapping, the following transformation matrix is used [43].

$$\begin{bmatrix} x_d \\ x_q \end{bmatrix} = \frac{2}{3}\begin{bmatrix} cos\theta & cos(\theta - 2\pi/3) & cos(\theta - 4\pi/3) \\ -sin\theta & -sin(\theta - 2\pi/3) & -sin(\theta - 4\pi/3) \end{bmatrix}\begin{bmatrix} x_a \\ x_b \\ x_c \end{bmatrix}, \tag{2.8}$$

where x is the desired parameter (voltage or current) and θ is the angular position of the rotating frame.

The stator active (P_s) and reactive (Q_s) power in d-q frame can be calculated as,

$$P_s = \frac{3}{2}(v_{ds}i_{ds} + v_{qs}i_{qs}), \tag{2.9}$$

$$Q_s = \frac{3}{2}(v_{qs}i_{ds} - v_{ds}i_{qs}). \tag{2.10}$$

The steady-state rotor active power is,

$$P_r = P_m - P_s = T_m\omega_r - T_e\omega_s = -sP_s, \tag{2.11}$$

where s is the slip of the generator which is typically $\pm$ 30% in DFIG wind turbines. This determines the size of converters to be 30% of the wind turbine's capacity.

The control system comprises the controller of the Rotor Side Converter (RSC) and Grid Side Converter (GSC). The RSC controls the active and reactive power injected to the grid through the stator, while the GSC controls the DC-link voltage and the reactive power. Different approaches have been used for controlling a DFIG wind turbine, among which vector control is very common and is based on the space vector model of the generator. Stator Voltage Oriented Control (SVOC) and Stator Flux Oriented Control [43, 47] have been used extensively in the literature for controlling a DFIG turbine. In these control methods, the d-q reference frame is aligned to the stator voltage or field, depending on the method. The vector control allows the independent control of the active and reactive power by controlling the d and q component of the rotor current [61].

The pitch angle controller is another component of the control system, which is activated at high wind speed. With adjustments of the blade pitch angle, the power extracted from the wind is able to be controlled and overspeeding of the wind turbine can be prevented.

2.3.2.2 Reduced order model

Since detailed modelling of a DFIG wind turbine is computationally demanding, different reduced order models of the DFIG wind turbine have been proposed [57, 62–64]. The results showed that the performance of the reduced order model is similar to the full model except for the fast stator transients that occur in response to a disturbance in the grid. These models are generally suitable for analysing the transient behaviour of a wind farm in response to a disturbance in the grid.

Sorensen et al. [65] presented several reduced order models of DFIG wind turbines. In these reduced order models, the electromagnetic characteristics of the turbine were represented with steady-state relationships, which is considered valid because of the much slower dynamics of the turbine's mechanical systems, relative to the dynamics of its power electronics and generator. It was shown that under normal operating conditions, the reduced order models demonstrated good agreement with the full model in simulating the power generation.

2.3.3 Wind farm modelling

Wind farms are usually comprised of several individual turbines spaced hundreds of metres to kilometres apart. Given the typical length scales in atmospheric boundary layers, individual turbines can therefore have very different instantaneous wind speeds and power generation, even if all turbines experience similar, average wind conditions. This can include periods in which some turbines in a given farm are stationary whilst others are generating.

These dynamics have several consequences, particularly when considering how all turbines in a wind farm might be collectively modelled or controlled, or when considering how other complementary technologies – such as energy storage – might be integrated to improve wind farm operation. Even when only considering aero- and mechanical dynamics, without considering electrical power system dynamics, modelling the dynamic, aggregated power output of all turbines in a wind farm is a non-trivial problem.

Several published works approach the dynamic modelling of wind farms in different ways [66–77]. These range from detailed models that consider the aero-, mechanical and power system dynamics of every turbine with an associated high computational cost, to aggregated models that represent a wind farm with fewer, representative turbines with simplified dynamics. These aggregated models even include cases where the entire wind farm is represented by a single wind turbine. However, with any aggregated wind farm model, an assessment of the validity of the simplifications and assumptions based on field data is required.

2.3.3.1 Detailed model

Detailed modelling of wind farms requires consideration of every single wind turbine, which can result in intractable computational effort. Various studies have used a detailed model of wind farms for validation of a simplified model that aggregates the mechanical and/or the electrical subsystems of turbines [78–80]. However, detailed wind farm models are not appropriate for use in assessing the impact of the wind farm's performance on a large-scale power system [75]. Therefore, there is a requirement of reduced order models for this purpose.

2.3.3.2 Aggregated model

To address the need for models that are computationally less intensive than detailed wind farm models, various aggregated methods have been proposed. These can be classified

into three main groups: single machine, multi-machine and compound equivalent models [81].

The single machine model of a wind farm represents the whole wind farm as a single aggregated turbine with equivalent parameters (e.g. capacity, electrical specifications, etc.) receiving an equivalent wind speed [67, 68, 75]. However, this method is not suitable for cases where the wind speed varies significantly across the wind farm. To address this drawback of single machine modelling, the multi-machine model has been proposed, in which the wind turbines are clustered, with each cluster represented as an aggregated turbine [75, 82]. In the compound equivalent model, the mechanical subsystem of each turbine is modelled individually, and the aggregated torque is fed into an equivalent generator [70, 78, 80, 82, 83]. Studies conducted on wind farm modelling showed that aggregated models can simulate the dynamics of a wind farm with reasonable accuracy while reducing the computation time dramatically.

One of the complexities of implementing aggregated models is determining the equivalent parameters and equivalent wind speed to represent the aggregated group. Studies of the impact of calibrating the equivalent parameters of the aggregated machine and the equivalent wind speed on model accuracy [71, 79] showed that the accurate determination of these parameters can improve the model accuracy significantly and reduce the need for a greater number of machines in the model.

In the multi-machine method, different approaches have also been used for grouping individual turbines into aggregated models and identifying representative turbines. For example, one approach is to assume that all turbines in the same row of a given farm receive a similar wind speed and can therefore be aggregated [67]. However, this method is only suitable for simulating a wind farm for a short period of time in which the wind direction does not change significantly. More complex approaches include the use of machine learning techniques and probabilistic analysis for grouping turbines based on measured wind or power data [69]. These more complex approaches may provide a closer representation of the real wind farm's performance, but also require greater computational expense.

In all of these cases, as individual turbines are aggregated into groups, the partial correlation of each turbine's dynamics to others in the same group results in smoothing of their aggregated power output. Nanahara et al. [84] found that this smoothing effect is significant for time scales of 10 minutes or less. This smoothing can be modelled in various ways using the cross-correlation between the turbines' power generation inside a wind farm [62, 84–90]. This ranges from the coherence spectral analysis performed on the measure wind farm data, as well as adding Gaussian noise to a single wind turbine

power output. Similarly, the aggregation of power generation from a number of dispersed wind farms in a region diminishes the ramp rate in total power, which is an important consideration for the power system operators [90–92].

To validate the accuracy of the various wind farm modelling methods explained above, large amounts of field data for the operation of wind farms is required. These data, however, are usually hard to acquire and are, therefore, used in relatively few studies, e.g. [93, 94]. Hence, further development of aggregated models of wind farms should seek to validate the model's performance with such real performance data.

2.3.4 Wind farm frequency control

Frequency control challenges resulting from a large-scale integration of wind in a power system can potentially be addressed by changing the turbines' control system so that they are more dispatchable and can provide frequency control ancillary services. Generally, DFIG wind turbines can provide frequency control services by either curtailing their generation or providing a synthetic inertial response using kinetic energy stored in their rotor [53, 95–97].

2.3.4.1 Deloading

Deloading refers to the operation of a wind turbine below the Maximum Power Point Tracking (MPPT) curve, which provides headroom for the turbine to increase its power generation if required. The feasibility of this method to provide frequency control services to the power system has been studied widely and can be achieved by two methods: turbine blade pitch control or turbine rotational speed control. For the case of pitch control, the wind power generation of the turbine is curtailed by changing the blades' angle of attack to the incoming wind, while for speed control, the turbine's operating point is shifted along the power-speed curve away from its optimal point to a lower power generation [98–100]. These two deloading methods can be represented by shifts in the operating point on a wind turbine power-speed curve, as shown in Figure 2.6. It can be seen that the same headroom is possible by shifting to the three different operating points, which can be reached by underspeeding, overspeeding or changing the blade pitch.

An evaluation of these two control methods demonstrated that turbine rotational speed control has inferior performance compared with pitch angle control, due to the limitation of the operating speed of the turbine [101]. The feasibility of the pitch angle control method has been proved practically in the Australian National Electricity

Market [10]. Therefore, in the present thesis, the pitch angle control method is used for implementing frequency control capability in wind turbines.

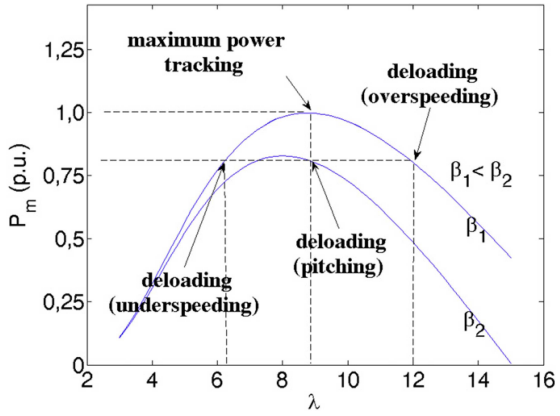

Figure 2.6: Typical wind turbine mechanical power extracted from the wind, P_m, as a function of turbine tip speed ratio(λ) for two different values of blade pitch angle (β). Various deloading set-points that can be achieved by speed control (underspeeding or overspeeding) and pitch control [98].

2.3.4.2 Synthetic inertia

Synthetic inertia is a temporary and fast response of a wind turbine to a frequency deviation that is achieved by using the kinetic energy of the rotating mass of a wind turbine to provide additional power if required. It should be noted that this is a form of Fast Frequency Response (FFR) and is not the same as the natural synchronous inertial response of conventional thermal generators. In the case of synthetic inertia, there is also usually a small delay in the response of the power electronics to the frequency deviation [31, 97, 102]. However, the inertia constant of a variable speed wind turbine is comparable to conventional generators, therefore, their synthetic inertial response can have a significant influence in controlling system frequency. Typically, a synthetic inertial response enables the wind turbine to increase power generation by up to 5-10% of the turbine capacity for 5-10 seconds, which is followed by a recovery period of approximately 30-40 seconds, in which the wind turbine speed returns to the normal operating condition [95, 103].

Figure 2.7 shows a block diagram of a typical control system of a wind turbine with inertial response capability. Since in this controller the power set-point (P_{ref}) changes according to the rate of change of frequency, once the frequency reaches steady-state, regardless of the value of steady-state frequency, the wind turbine returns to normal operation. To help the power system to return to the nominal frequency, a supplementary control loop known as droop control is used, which adjusts the power set-point according to the difference between the frequency and the nominal value [96].

Synthetic inertia has its limitation because there is a trade-off between increasing power and reducing the speed of the turbine, which increases time for speed recovery. In addition, DFIG wind turbines must operate within a specific range of rotational speeds, which constrains the usage of kinetic energy stored in the turbine's rotor [95, 104].

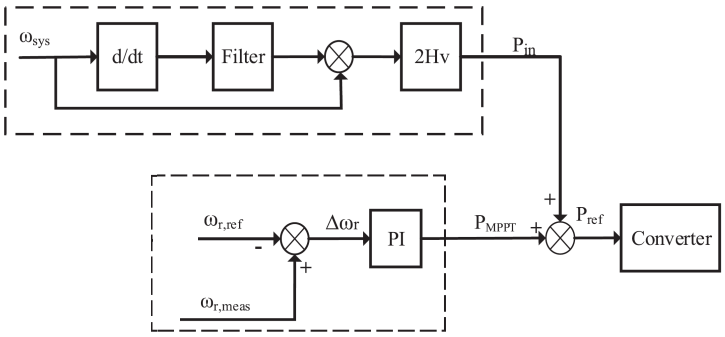

Figure 2.7: Block diagram of a typical control system for a variable speed wind turbine with synthetic inertia capability [96].

A combination of deloading and synthetic inertia has been shown in several studies to be an effective mean of improving both the ROCOF and the frequency nadir of a disturbed system [101, 105, 106]. As an example, Figure 2.8 presents a comparison of various frequency control methods in responding to a 10% load increase in a system with 30% wind penetration. It can be seen that the combination of inertia control and pitch angle control demonstrates better frequency response characteristics than any response of a single technology.

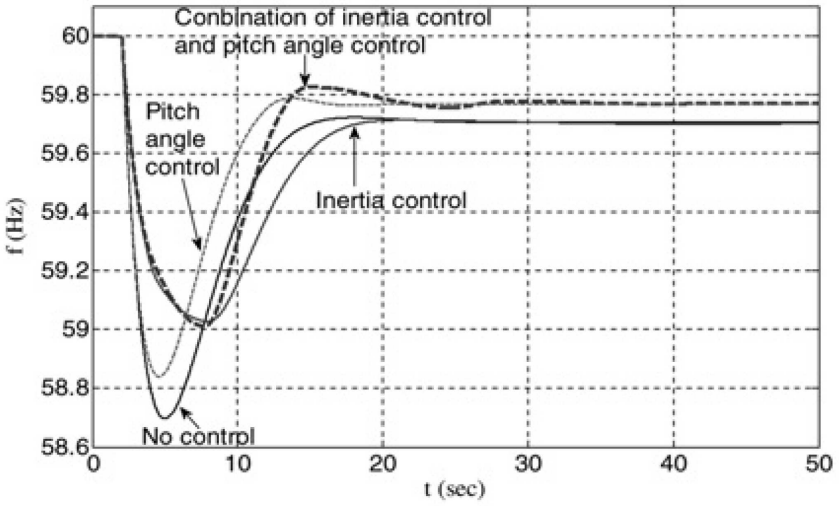

Figure 2.8: Impact of different wind turbine frequency control methods on the ROCOF and frequency nadir in a system with 30% wind penetration after 10% load increase [101].

Many studies have examined the technical performance of a wind farm with frequency control capabilities, while relatively few studies have considered the optimal financial

performance of such a system [107–110]. Such studies have found that the provision of frequency regulation services can increase system revenues by 5-30%.

Furthermore, wind turbines can be controlled in various ways, ranging from the aggregated to distributed control, to provide ancillary services [111–113]. However, these studies did not consider the significance of the financial impact of such control strategies on the performance of the wind farm. Therefore, it is important to investigate the wind farm frequency control capabilities not only from a technical point of view but also from an economic perspective.

2.4 Integration of energy storage

Energy storage technologies can be used to mitigate the variability of wind power generation and its impact on grid security and reliability. Various storage technologies with different technical and cost specifications have been studied to integrate into wind power plants or power systems with large penetration of wind.

2.4.1 Technologies

Energy storage technologies can be classified based on the relevant form of energy into five main groups: mechanical, electrical, electrochemical, chemical and thermal energy storage [114, 115]. Figure 2.9 presents this classification and lists the most common technologies, the specifications and services of which have been reviewed in [116–118]. Figure 2.10 presents a maturity curve of these technologies, which shows that pumped hydro, compressed air, flywheel and batteries are among the most mature and have been deployed most widely [115]. This section reviews the current understanding of these technologies.

2.4.1.1 Pumped hydro

Pumped Hydro Energy Storage (PHES) is the most mature storage technology and contributes to 97% of the global capacity of installed energy storage [119]. PHES comprises two reservoirs with different elevation levels, which allows energy to be stored as gravitational potential energy when water is pumped to the upper reservoir during periods of low demand, and energy to be released when demand is greater than supply [120]. The lifetime of this technology is typically about 30-50 years [121, 122] and its Round Trip Efficiency (RTE) ranges from 65-85%. The main drawbacks of this technology include

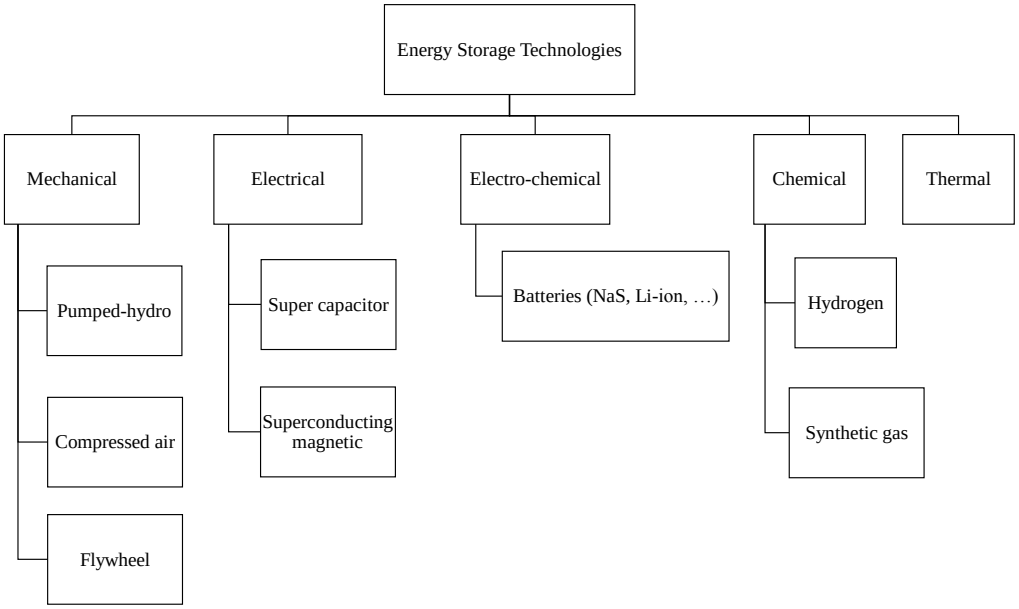

Figure 2.9: The classification of the most common energy storage technologies according to the form of stored energy.

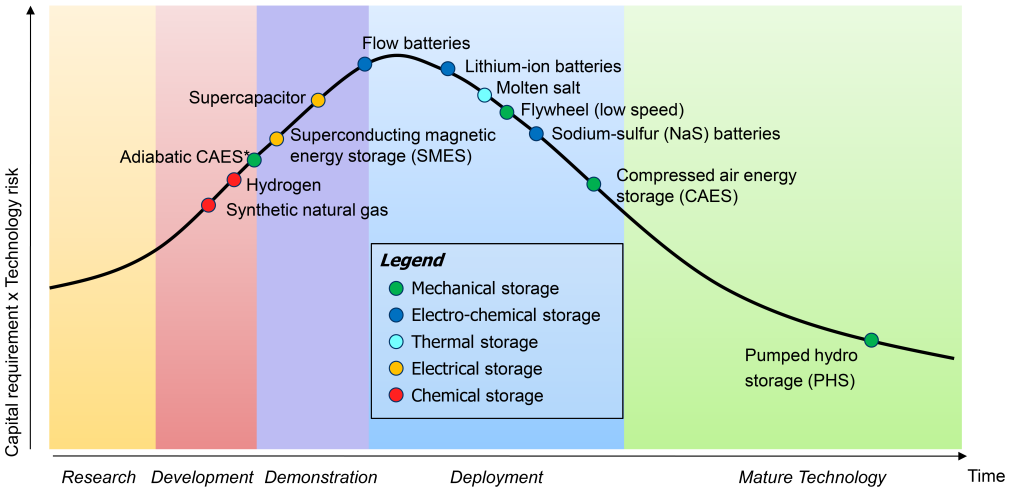

Figure 2.10: Maturity curve of different storage technologies [115].

its intensive capital cost and environmental impacts, as well as the specific geographic needs of the plant. Research has addressed this geographical limitation by proposing underground pumped-hydro energy storage (UPHES). However, this technology is only in the early stages of research and development [114, 120].

2.4.1.2 Compressed air

Compressed Air Energy Storage (CAES) is typically large-scale energy storage that is not yet used widely. CAES consumes electricity to compress air and inject it into a

cavern of hard rocks, an aquifer, or a depleted gas field. During peak demand hours with a relatively higher price, or when the system operator requests, the compressed air is mixed with natural gas and combusted. The expansion of the compressed air and combustion gases rotates a turbine, which is connected to a generator to produce electricity [114, 119, 121]. The lifetime of CAES is about 40 years with an RTE of 50-70%. It should be noted that this technology is not emission free and requires fuel to use the stored energy. However, some studies investigated emission free CAES, which uses the thermal storage to heat the compressed air for power generation [123]. Moreover, the high capital cost and the geographical requirement of a suitable storage cavern are further drawbacks of this technology [121, 124].

2.4.1.3 Flywheel

Flywheels store energy in the form of rotational kinetic energy. Flywheels can be classified as either low speed, operating at the order of 1000 rpm, or high speed, operating at the order of 10000 rpm. The high speed flywheels are suitable for long term applications, which requires the energy storage to provide service for a period ranging from a few minutes to a few hours, whilst the low speed flywheels are appropriate for short term applications, which requires the energy storage to provide a fast and short response ranging from less than a second to a few seconds [114, 121]. Low maintenance cost, long lifetime, robustness in harsh condition and negligible environmental issues are the advantages of this technology [120, 121].

2.4.1.4 Batteries

Batteries store energy using reversible chemical reactions. A battery comprises a set of cells that are connected in series and parallel to provide the desired electrical specifications. Each cell consists of two electrodes together with solid, liquid, or viscous electrolyte. During the electrical discharge from a battery, reactions occur at both anode and cathode, so that electrons flow from anode to cathode in an external circuit while the ions in the electrolyte are exchanged [121, 125, 126]. Battery costs consist of the cost of the storage module, Power Conditioning System (PCS) including the power electronics and protection system (switches, breaker, etc.), and balance of plant that includes the construction, engineering and procurement [121, 127, 128].

Lead-acid

Lead-acid batteries are the oldest and most mature battery technology, having been used for more than 130 years. Lead-acid batteries are classified into two categories: 1) flooded and 2) valve regulated batteries. Flooded lead-acid batteries require periodic water maintenance; an issue that precipitated the introduction of the valve-regulated type. Reactions occurring at the electrodes result in their degradation and reduce the lifetime of lead-acid batteries. This lifetime is approximately 2000-4500 cycles, which might correspond to 5-15 years of use, depending on the application and operation conditions (e.g. depth of discharge, temperature, etc.). Such batteries have a round trip efficiency of 75-80% [121]. The low cost of this technology makes it popular, especially for long period applications due to low cycle lifetime and low daily self-discharge ($< 0.2\%$). The low specific energy and power density dissuade their use in mobile applications [118, 121, 129]. Also, the environmental impact due to leakage of lead is another disadvantage of this technology [114].

Lithium-ion

Lithium-ion (Li-ion) batteries have traditionally been used widely in small scale applications such as personal electronic devices, however, recently their use has progressed to large-scale stationary applications as well. Li-ion batteries have a high energy density, making them ideal for portable applications. Moreover, they can be charged/discharged rapidly with high RTE of approximately 90%. These characteristics make them more appropriate for short term applications. The drawbacks of this technology include its relatively short lifetime and the use of flammable materials in the electrolyte, which makes it hazardous for the environment [118, 119, 121, 130].

Flow batteries

Flow batteries consist of two different electrolytes stored in two separate tanks that are circulated through an electrochemical cell with two electrodes and a separator [127]. The energy and power capacity of flow batteries are independent. The power capacity can be improved by increasing the number of the cells and the size of electrodes, while the energy capacity can be increased by simply increasing the size of the tanks [121]. Since the electrolytes are kept in two separate tanks, the self-discharge is negligible, and therefore they are suitable for long term applications. The most prevalent flow batteries are vanadium redox and zinc-bromine flow batteries. This technology has a lifetime of approximately 10 years with more than 1000 cycles at 100% depth of discharge and

efficiency of 60-70%. The low energy density is one of the drawbacks of this technology [121, 126].

Sodium sulphur

Sodium sulphur (NaS) batteries are a relatively new technology with promising characteristics such as high energy density, high RTE and relatively low capital cost. Furthermore, NaS batteries have low self-discharging characteristics and low maintenance requirements with a lifetime of approximately 10-15 years [114, 121]. The flammability of the sodium, particularly with water, makes NaS batteries hazardous [121, 122].

Table 2.1 summarises the main technical specifications, as well as the capital cost of the aforementioned storage technologies. However, whilst the PHES and CAES are the cheapest technologies, they are large-scale storage and the geographical requirements and environmental footprint limit their widespread deployment. On the other hand, batteries have a smaller footprint due to their significantly higher energy density, and they are modular.

Table 2.1: Technical characteristics and capital cost of different storage technologies [114, 117, 122, 131, 132].

Technology	Power rating (MW)	Efficiency (%)	Energy density (Wh/kg)	Power density (W/kg)	Capital cost ($/kWh)	Lifetime (yrs)	Life cycle
PHES	10-5000	65-85	0.5-1.5	-	5-100	40-60	20000-50000
CAES	5-400	50-70	30-60	-	2-100	20-40	>13000
Flywheel	<20	85-95	20-80	400-1500	1000-5000	15-20	20000-100000
Lead-acid	<50	80-90	30-50	75-300	450	10-15	2000-4500
NaS	0.05-8	75-90	150-250	150-230	300-500	10-15	>2000
Li-ion	<100	85-95	150-350	50-2000	460-560	10	>2000
Flow battery	0.05-2	60-70	30-85	45	150-300	10	5000-10000

Many studies have reviewed the use of different forms of energy storage in a power system and pointed out that the high capital cost of Li-ion batteries prevents the large-scale deployment of this technology for grid applications. Relatively cheaper battery technologies, such as NaS and flow batteries were considered more economic [125, 131, 133, 134]. However, the price of Li-ion technology has reduced significantly over the past few years due to the learning rate and the increasing economies of scale [135]. Recently, the largest Li-ion battery in the world has been installed in South Australia (SA) and shown to have a significant impact on the power system operation and the regulation market [9]. Therefore, there is a need to investigate the cost-effectiveness of this Li-ion

technology using the most recent capital costs while considering various conditions that generate optimal financial performance, especially in integration into a wind farm.

2.4.2 Services

Figure 2.11 presents services, for which various forms of energy storage technologies are most suited for, based on their typical power rating and energy capacity [115]. It can be seen that technologies with short discharge durations such as batteries and flywheels are suitable for short term applications such as ensuring power quality and providing reserves. Since the focus of the present study is on the use of energy storage in the energy and frequency control ancillary services markets, the next sections describe these services.

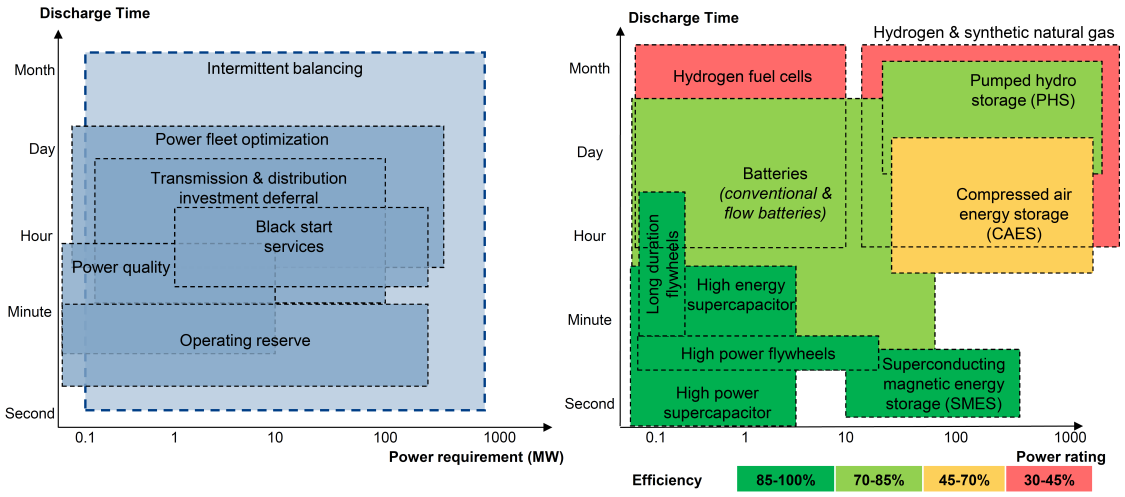

Figure 2.11: Typical rated power and energy capacity of different energy storage technologies and their potential application in the power system [115].

2.4.2.1 Arbitrage

Arbitrage service involves using energy during the off-peak periods to charge the storage when the electricity price is low, and then discharging the storage to sell energy during peak demand periods when the price is high. Energy storage technologies with a high power rating and large storage capacities (hours to days of storage) such as PHES, CAES and batteries, are suitable for this application. In arbitrage, the RTE of energy storage plays an important role because an inefficient technology can result in significant energy and financial loss [122, 125, 126, 136].

2.4.2.2 Frequency control

Frequency control services refer to the use of energy storage to balance demand with generation and cover a range of response times. Regulation reserves are used over a short time frame (a few seconds) to maintain the system frequency within the non-critical band [122, 137]. When a contingency occurs and the frequency is outside the nominal band, spinning reserves are the first reserves that respond. These reserves are online, unused generation capacity that can respond within a few minutes of the contingency. Non-spinning reserves are the generation capacity that is off-line but can be available within 10-30 minutes [119, 121, 122, 137].

Fast Frequency Response (FFR) is similar to regulation services, but is required to have a shorter response time ($< 1s$) [97, 102]. Therefore, storage technologies with a high ramp rate and faster response time are suitable for FFR such as flywheels, batteries and super-capacitors [121, 122]. Since most variable speed wind turbines do not provide frequency control services, energy storage can be employed to support the security of a power system with a large penetration of wind energy [125, 136]. An energy storage system is also technically capable of providing inertial and primary frequency response and of improving frequency control [28]. However, economic aspects of the use of energy storage technologies, especially batteries, for the provision of frequency control ancillary services require further research.

2.4.3 Optimal use of energy storage

Studies of the integration of energy storage technologies into wind farms and systems with high wind penetrations have had various objectives, such as determining the optimal size, control, location and technology type [125, 133, 138]. These studies can be classified into non-market and market studies.

In non-market studies, the objective is to examine the optimal performance of energy storage in an isolated small-scale grid or to meet a specific technical requirement, such as reducing wind generation fluctuations to a certain level. On the other hand, market studies examine the participation of the energy storage system in wholesale electricity markets, while considering the technical and market constraints. These market studies can be further divided into two groups: participation in the energy-only market and participation in the energy and ancillary services markets. The following sections review these different groups of studies and their main findings.

2.4.3.1 Non-market studies

Many non-market studies have been conducted on the optimal use of energy storage as a stand alone system or in integration into a wind farm [139–147]. For example, Luo et al. [139] investigated the optimal sizing and scheduling of a sodium sulphur battery integrated into a wind farm in an isolated network to minimise the annualised cost of the system. Brown et al. [140] studied the optimal sizing of a PHES in an isolated grid with high wind penetration. In this study, energy storage was used to meet the reserve requirement. Brekken et al. [141] and Luo et al. [142] studied zinc-bromine and Li-ion batteries, respectively, integrated into a wind farm to minimise fluctuations and deviations of the wind farm from the scheduled power. Alanazi et al. [143] investigated the optimal sizing of a battery to minimise the wind curtailment due to the transmission congestion. These studies showed that the use of energy storage is an effective way to resolve some issues of variable wind generation.

Various studies also examined the optimal location of an energy storage system. For example, Atwa et al. [144] studied the optimal location of a stand-alone, fixed-capacity battery in a power system with high penetration of wind to resolve the transmission congestion and reducing the wind spillage. Wogrin et al. [145] studied the optimal allocation of various forms of storage technologies in a power system. They found that technologies with more hours of storage such as PHES tend to be allocated at the location of main demand, while technologies with short storage duration, such as flywheels are placed near wind farms to provide regulation services and to reduce wind generation curtailment.

Different configurations of battery energy storage integrated into a wind farm have also been studied [146, 147]. In these studies, the size of energy storage was determined to mitigate fluctuations of the plant's generation and to meet a ramp rate requirement. Li et al. [146] showed that the required power rating of an aggregated energy storage system is approximately 30% less than that for a distributed configuration to achieve the same level of smoothing, due to the smoothing effect of aggregated wind power generation. In their distributed configuration, the size of the battery was determined to achieve a specific smoothing level in each turbines' power output while in their aggregated configuration the battery was used to achieve the same level of smoothing in total power output of the wind farm. Khalid et al. [147] studied three different configurations of energy storage in a wind farm to achieve a specific level of smoothing and ramp requirement, as shown in Figure 2.12. It was shown that their proposed semi-distributed configuration of energy storage requires a slightly smaller (5%) battery compared with the aggregated configuration. However, this study did not consider the additional cost

that their proposed battery configuration may impose on the system due to the increased number of control systems and their coordination. Nevertheless, there are significant potential benefits to aggregated configurations of energy storage, which is the focus of the present thesis.

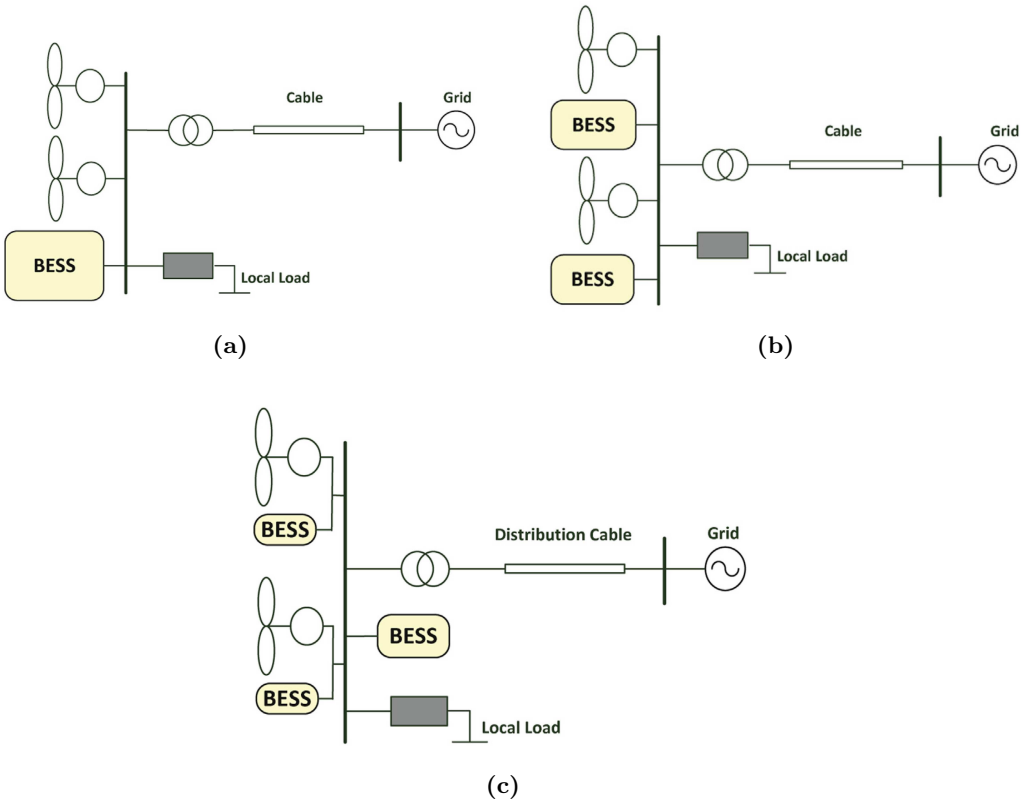

Figure 2.12: Different integrated configurations of Battery Energy Storage System (BESS) into a wind farm, including: a) aggregated, b) distributed, and c) semi-distributed configurations [147].

2.4.3.2 Energy-only market studies

The participation of energy storage in the energy-only market has been studied widely. The general formulation of the objective function minimising the cost of energy storage providing arbitrage is,

$$\min \left\{ C_{ES} + OM_{sys} + \sum_{t} \underbrace{\pi_t \left(E_t^{imp} - E_t^{exp} \right)}_{Arbitrage} \right\}, \tag{2.12}$$

where C_{ES} is the capital expenditure of energy storage system, OM_{sys} is the operation and maintenance cost of the system and the third summation term is the total profit that the system earns by exporting (E_{exp}) and importing energy (E_{imp}) from the energy market over a time period (t). In the formulation of an energy storage system model,

various constraints must be taken into account, such as the technical constraints of the battery, power balance, transmission limit, etc. One of the limitations of some studies is that the size of the battery is determined based on its energy capacity, and the power rating is calculated using fixed hours of storage. However, the power rating and battery capacity of the battery technologies can be optimised simultaneously. This has been addressed by splitting the capital expenditure of the battery into two components: one related to the power; and the other related to the energy capacity [148–150] .

Some studies investigated the performance of stand-alone energy storage in the energy market. For example, McConnell et al. [151] studied the benefits of PHES in the energy-only wholesale market of the Australian National Electricity Market (NEM). They considered perfect and imperfect price forecasts and showed that imperfect price forecast has an adverse effect on the value of the battery, but as the hours of storage increases, this effect becomes weaker. Sioshansi et al. [152] studied the arbitrage value of energy storage in the Pennsylvania-Jersey-Maryland (PJM) market. They investigated the impact of hours of storage on the arbitrage revenues and found that these revenues do not increase significantly for more than 8 hours of storage. Bradbury et al. [148] conducted a comprehensive study on the economic viability of different energy storage technologies providing arbitrage in the US electricity market. The results showed that PHES and CAES are most cost-effective and that 4 hours was the optimal storage duration for most technologies.

Other studies investigated the integration of energy storage into a renewable plant such as a wind farm. For instance, Gill et al. [153] examined the optimal performance of a sodium sulphur battery with fixed capacity integrated into a wind farm and concluded that, for the case considered, it was not an economically viable investment. Castronuovo et al. [154] studied the optimal operation and sizing of a PHES, which is integrated into a wind farm and showed that the storage unit increased the system annual profit by 10% compared with the wind farm-only case. Hessami et al. [155] compared CAES, PHES and thermal storage for integration into a wind farm in the energy market and found that CAES was the optimal technology for their case study. While the studies reviewed in this section identified the benefits of a battery energy storage system operating in the energy-only market, there are significant possible benefits of participating also in the ancillary services market, which need to be evaluated.

2.4.3.3 Energy and ancillary services markets studies

The objective function presented in the previous section can be extended to include the participation of an energy storage system in ancillary services markets also,

$$\min \left\{ C_B + OM_{sys} + \sum_t \underbrace{\pi_t \left(E_t^{imp} - E_t^{exp}\right)}_{Arbitrage} + \underbrace{\mathcal{P}_t - \pi_t^{res} P_t^{res}}_{Ancillary} \right\}, \tag{2.13}$$

where $\mathcal{P}_t$ represents the penalty cost of the system for deviating from the scheduled power in the regulation market and the final term accounts the revenue in the reserve market by providing P_t^{res} MW power.

Again, studies have examined the performance of stand-alone energy storage in the energy and ancillary services markets. For example, Akhavan et al. [156] studied the operation of a stand-alone large-scale battery with fixed capacity under the uncertainty of wind generation, while Das et al. [157] assessed the benefits of a fixed capacity CAES for different levels of wind penetration in a power system. These studies have shown that with more wind in the grid, the energy storage benefits more from providing ancillary services than from providing arbitrage. Berrada et al. [158] and Walawalkar et al. [159] used optimisation techniques to quantify the benefit of different energy storage technologies in the energy and regulation market with the main finding that the high capital cost of batteries makes them unprofitable.

The optimal performance of energy storage integrated into a wind farm without frequency control capability was investigated in various studies. Berrada et al. [160] examined optimal sizing and operation of energy storage using a simple model of the regulation market in which it was assumed that 10% of enabled regulation capacity is always used by the power system. The results showed that participation in the regulation market provided greater financial benefit than the participation in the energy market. Korpaas et al. [161], Garcia-Gonzalez et al. [162] and Ding et al. [163] studied the optimal performance of an energy storage system with fixed capacity integrated into a wind farm. In these studies, the wind farm-energy storage plant did not provide ancillary services but was penalised based on its deviation from the scheduled power in the regulation market, and showed that the energy storage could significantly reduce the penalty costs. A similar study was conducted in Ref [164], which used energy storage to support the large-scale integration of renewables into the power system. Different wind generation scenarios were considered, and the results showed that energy storage reduced the wind curtailment significantly and replaced the thermal units in the ancillary services markets as the requirement of regulation and reserve increased, due to the large penetration of renewable generation.

The optimal performance of energy storage integrated into a wind farm with frequency control capability has been examined in a few studies. For instance, He et al. [165] studied the optimal operation of a flow battery with fixed capacity integrated into a wind farm with frequency control capability in the energy and regulation market of the PJM. In this study, the wind power generation was uncertain, and it was assumed that the prices are known perfectly. Rodrigues et al. [166] used the same approach, but they considered the participation of the system in the spinning reserve market with fixed prices and uncertain energy prices. These studies showed that energy storage can provide considerable benefits for the wind farm. However, they did not investigate the simultaneous participation of the energy storage system in different frequency control ancillary services markets including regulation, spinning and non-spinning reserve.

The impact of different forecasting systems and their accuracy on the optimal battery investment has also not been addressed comprehensively. Wu et al. [167] and Bludszuweit et al. [168] modelled persistence forecast error and its impact on the optimal performance of an energy storage system to avoid payments in the regulation market due to deviations from the scheduled power. They studied various distributions of forecast error, including Gaussian, Laplace, beta and mixed distributions to model the forecast error, and found that the normal distribution has the worst performance in modelling the forecast error despite its widespread use in the Auto Regressive Moving Average (ARMA) based forecasting methods. It was shown that the beta and mixed distribution, which is based on Laplace and Gaussian distributions, has a superior performance and provides higher economic benefits by more optimally sizing the energy storage capacity. Similarly, Tewari et al. [170] investigated statistical modelling of wind forecast error and its impact on the wind farm penalty costs in the electricity market. They showed that the Gaussian distribution is not accurate for modelling the forecast error for a single wind farm; however, it is suitable on a system level because the forecast error of several wind farms is likely to be uncorrelated.

Various studies considered the uncertainty in wind using a stochastic framework to optimise the size of energy storage. In these studies, wind uncertainty was modelled by a simulation of various wind scenarios. Different methods have been used to generate these scenarios, such as ARMA [169] and the Monte-Carlo method [163]. Yuan et al. [171] showed that with a better forecasting system the profit of energy storage in decreasing the wind farm's penalty payments in the regulation market reduces, due to fewer opportunities to reduce regulation payments. Therefore, it is necessary to investigate the impact of improving forecast accuracy on the performance of wind power plants and energy storage investments.

2.5 Summary and research aims

This review showed that the optimal combination of a battery energy storage system integrated into a wind farm with the frequency control capability has not been studied comprehensively. Furthermore, economic considerations of the Li-ion battery energy storage system have been identified as the main challenge for their deployment in power systems. However, as mentioned, its capital cost has decreased significantly over the past few years, and therefore it is necessary to study the impacts of reduced capital costs, and of participation in ancillary services markets on the investability of this energy storage technology. Finally, the impact of wind generation forecast accuracy on the optimal performance of a frequency responsive wind farm with and without energy storage has not been addressed.

Given this summary of the current literature, the following research aims of this thesis are proposed.

1. **To develop a hierarchical and data driven reduced order model of a wind farm.**

   Studying the optimal integration of a wind farm with energy storage into a power system requires an understanding of the wind farm dynamics. Several published works approach wind farm modelling in different ways, ranging from detailed models to aggregated models. Detailed models consider the aero-, mechanical and power system dynamics of every turbine and have an associated, relatively high computational cost. On the other hand, aggregated models represent a wind farm with fewer, representative turbines with simplified dynamics and significantly less computational cost. A feature of these studies to date is their reliance on a relative lack of measured data from an operating wind farm. The accuracy of these models is therefore not clear.

   This thesis therefore presents a new method to model the power output of a wind farm using large amounts of measured data. This method first relates the cross-correlation of the power output of all individual turbines in an operating wind farm to the convective length-scales in the incoming wind. These cross-correlations then suggest a hierarchy of wind farm models that feature a trade-off between the model accuracy and complexity.

2. **To study the optimal techno-economic performance of a wind farm with frequency control.**

Various studies have investigated the technical aspects of wind turbine frequency control capabilities, which require the wind farm to curtail wind generation and can result in significant financial loss in the energy market. Relatively few studies have investigated the economic impact of a wind farm's ability to provide ancillary services on its financial performance. However, these studies did not consider the provision of different frequency control ancillary services simultaneously. In addition, the impacts of wind generation forecast accuracy and the degree of wind farm controllability on its financial performance have not been addressed.

Therefore, this thesis examines the optimal performance of a wind farm-only system in the energy and frequency control ancillary services markets. For this purpose, different wind farm models developed in response to Aim 1 are used to find a reduced order model that is sufficiently accurate for conducting the financial analysis. It further examines the impact of different degrees of controllability on the financial performance of the wind farm. Finally, the impact of wind forecast accuracy on the performance of the wind farm with and without frequency control capability is examined.

3. **To study the optimal techno-economic performance of a lithium-ion battery storage system integrated into a wind farm with and without frequency control capabilities.**

Many studies have been conducted on the optimal use of battery storage with a wind farm in the electricity market. These include studies on the participation of the system in the energy and ancillary services markets. However, there is a lack of research on the optimal integration of battery energy storage into a wind farm with frequency control, taking into account the dynamics of both of these subsystems and unifying this analysis financially. Furthermore, the impact of wind generation forecast accuracy on the optimal performance of the wind farm-battery system participating in the energy and frequency control ancillary services has not been addressed comprehensively.

This thesis therefore investigates the impact of wind farm and battery control on the optimal financial performance of a wind farm-battery system with and without wind farm frequency control. The system dynamics and cash flows associated with the energy and FCAS markets are considered for different combinations of wind farm and battery to understand how each performs when integrated. Finally, the impact of the wind generation forecast accuracy on battery investment is also investigated.

Chapter 3

A hierarchical and data driven approach to wind farm modelling

3.1 Introduction

This chapter presents a hierarchical approach to modelling the dynamics of a wind farm using large amounts of measured data. This starts with modelling a single wind turbine, and extends this to the whole wind farm. A reduced order model of a doubly fed induction generator (DFIG) wind turbine is used in this study, which neglects the fast dynamics of the power electronics and generators, and reduces the computation time dramatically. In order to model the wind farm with a reduced number of wind turbines, spectral analysis is used to investigate the correlation between the power output of turbines. This analysis provides a physical basis for clustering the wind turbines. Different turbine clustering methods are studied and finally, a hierarchical approach to modelling an entire wind farm is proposed and analysed, which incorporates the cross-correlation between the power output of turbines in a cluster.

3.2 Data

This study uses data from the Mt Mercer wind farm in Victoria, Australia. This wind farm is owned by Meridian Energy Australia Pty. Ltd. and is comprised of 64 Senvion MM92, DFIG wind turbines of 2.05 MW capacity, and 2 meteorological (met) masts that are approximately 7.5 km apart. The distance between two adjacent turbines in a row is approximately 400 m while the spacing between two turbine rows is approximately 700 m (Figure 3.1a).

One full year of data from each of the 64 turbines and the 2 met masts was collected for this study. The sampling frequency of the turbines' power output and rotational speed, as well as the met mast wind speed and direction, was 1 Hz. The blade pitch angle, wind speed and wind direction at each turbine were also sampled every 10 minutes. The wind speed at each turbine was modelled at 1 Hz by using the historical power output of each turbine and the manufacturer's power curve (Figure 3.2a). The results of this approach agreed closely with the measured, 10-minute average wind speed at each turbine. Whilst there is no unique wind speed when the turbine generates at its rated capacity, Figure 3.2b shows that these conditions occur for less than 10% of the year, suggesting that the use of the power curves is reasonable.

Figure 3.3 shows the wind rose for the Mt Mercer wind farm using the yearly met-mast data. According to this figure, the prevailing wind direction is from the west and north-west.

(a)

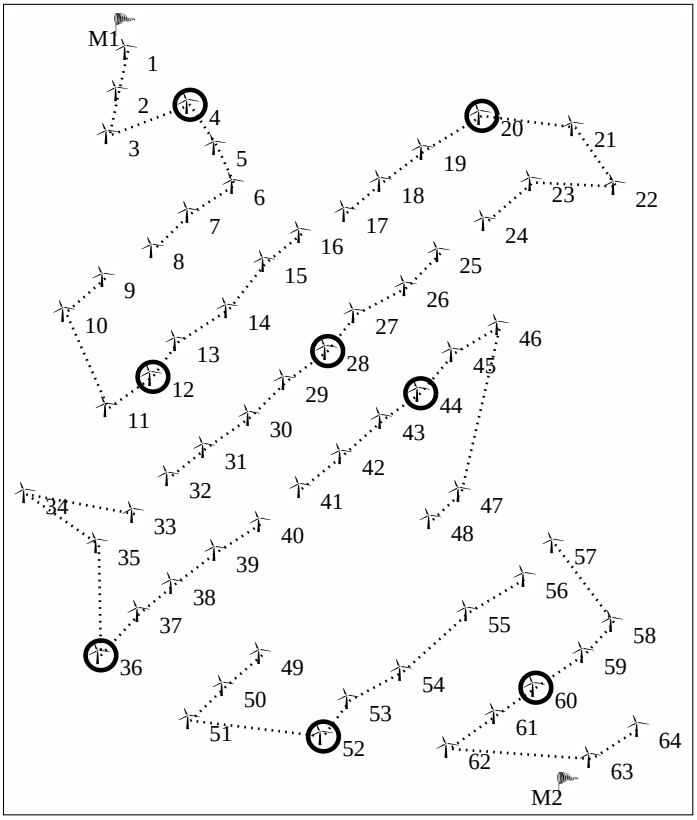

(b)

Figure 3.1: a) Satellite view of the Mt Mercer wind farm and b) line-based clustering of the farm with 8 reference wind turbines.

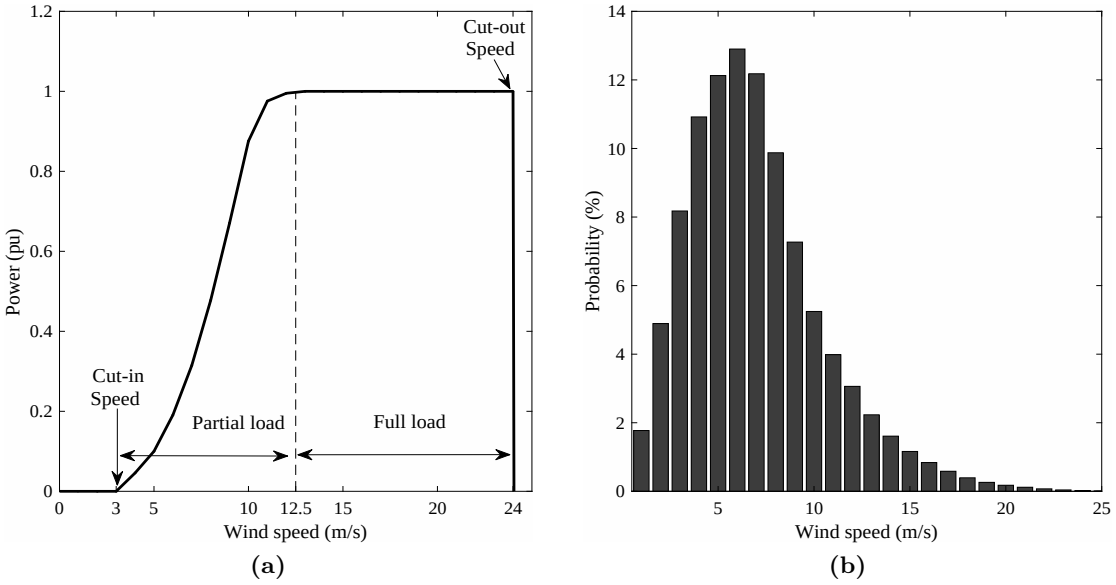

Figure 3.2: a) The power curve of the Senvion MM92 wind turbine [172] and b) the annual distribution of wind measurements at the two met masts at the Mt Mercer wind farm.

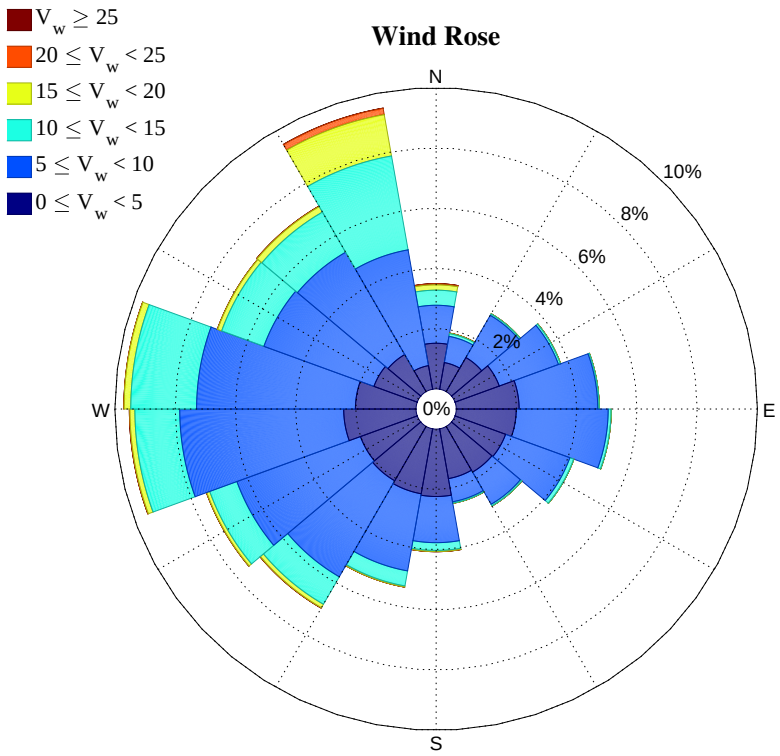

Figure 3.3: Wind rose for the Mt Mercer wind farm.

3.3 Wind turbine modelling

A wind turbine consists of different subsystems, including the rotor, drive-train, generator and control system. Figure 3.4 shows a typical configuration of a wind turbine with a DFIG, as featured in this study. The stator windings are directly connected to the grid while the rotor windings are connected through back-to-back AC/DC and DC/AC converters. The power electronics in these two converters enables the wind turbine to operate over a relatively wide range of wind speeds whilst controlling the active and reactive power separately [43, 54].

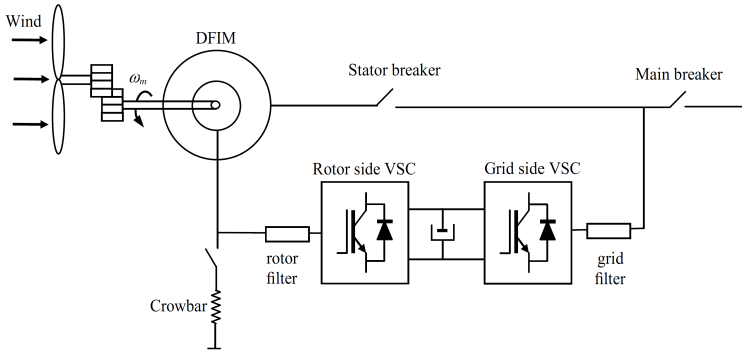

Figure 3.4: Schematic of doubly fed induction generator [47].

3.3.1 Reduced order model

A detailed model of the wind turbine includes the dynamics of the power electronics and generator electromagnetic characteristics. Since the focus of this study is on simulating the power fluctuations of the wind farm due to wind variations and their impact on the financial performance of the plant, a simplified version of the detailed model is required, which only captures the slow dynamics of the turbine [65]. This includes the control system dynamics and the inertial dynamics of the rotor.

The mechanical power that the wind turbine can extract is,

$$P_m = \frac{1}{2}\rho A C_P(\beta, \lambda) V_w^3, \tag{3.1}$$

where ρ is the air density, A is the blade swept area, V_w is the wind speed and C_P is the turbine power coefficient. Different expressions for C_P have been used to relate the turbine power to the blade pitch angle (β) and the blade tip speed ratio (λ). The following equation [47] is used in this study with terms k_1 to k_9 calculated by solving a non-linear optimisation, minimising the Root Mean Square Error (RMSE) to fit candidate curves to the measured data from individual turbines. The fitted values for k_1 to k_9 are shown

in Table 3.1.

$$C_P = k_1(\frac{k_2}{\lambda_i} - k_3\beta - k_4\beta^{k_5} - k_6)e^{(-\frac{k_7}{\lambda_i})},$$
$$\frac{1}{\lambda_i} = \frac{1}{\lambda + k_8\beta} - \frac{k_9}{\beta^3 + 1}, \quad \lambda = \frac{\omega R}{V_w}. \tag{3.2}$$

Figure 3.5 shows the resulting C_p for different β and λ obtained using this equation.

Table 3.1: Parameters of power coefficient (C_P) expression shown in equation 3.2.

k_1	k_2	k_3	k_4	k_5	k_6	k_7	k_8	k_9
0.488	506	1.88	0	0	34.58	27.35	0.108	0.011

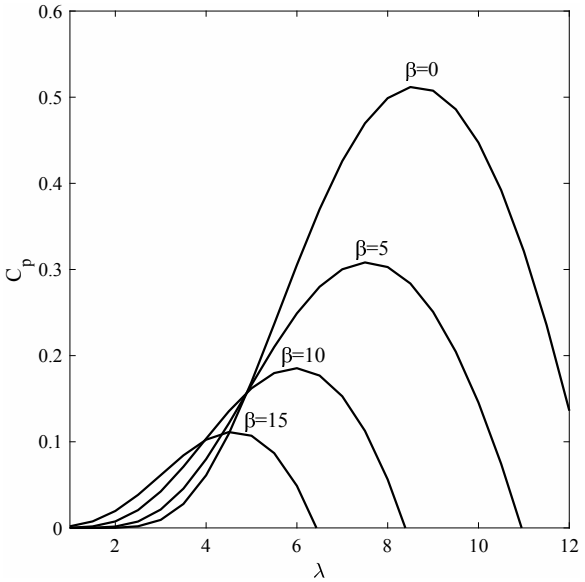

Figure 3.5: Modelled power coefficient (C_p) of the wind turbine as a function of the blade pitch angle (β) and tip speed ratio (λ).

The mechanical power extracted from the wind by the turbine blades is transferred to the generator through the drive-train. Whilst various drive-train models have been developed in the literature (e.g. [55]), a one mass model [57] was used in this study which relates the mechanical torque of the rotor (T_m) and that of the generator (T_{gen}) to the rate of change in rotor speed (ω_{sys}) and turbine's moment of inertia ($J = 9.67 \times 10^6 kg.m^2$),

$$T_m - T_{gen} = J_{sys}\frac{d\omega_{sys}}{dt}. \tag{3.3}$$

The other component of the simplified model is the pitch angle and turbine speed controller. The pitch angle controller is used when the wind speed is higher than the

rated value or to curtail the wind for providing ancillary services. It controls the power extracted from the wind by adjusting the angle of attack for the blades, which results in changing the C_P and consequently the power extraction from the wind. This enables the wind turbine to operate over a wider range of wind speeds efficiently. Since the pitch angle cannot change instantaneously, there is a rate limiter of 7 deg/s imposed [172], as shown in Figure 3.6. In this figure, ω_{ref} and ω_{sys} denotes the reference and measured wind turbine speed, respectively. The reference turbine speed is determined according to the operating curve of the turbine, as shown in Figure 3.7.

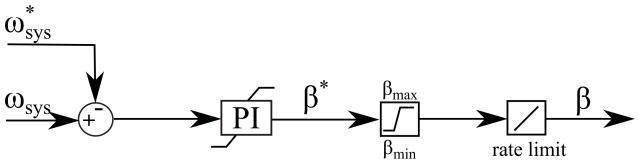

Figure 3.6: Block diagram of pitch angle controller.

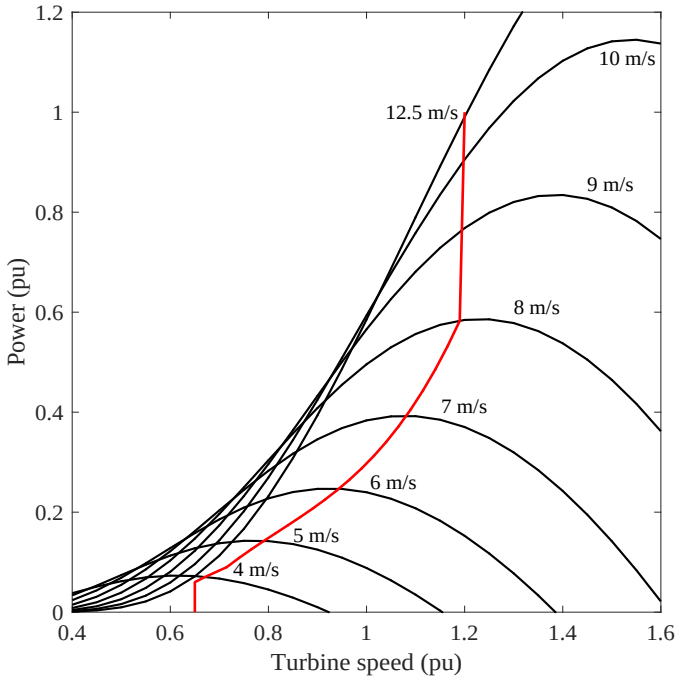

Figure 3.7: Turbine mechanical power versus the turbine speed curves (black) and operation power-speed curve (red).

3.3.2 Model validation

Validation of the present wind turbine model used the historical power and turbine speed data discussed in Section 3.2. The power output and turbine speed were modelled in Matlab/Simulink using a year of wind data, and both showed less than 5% Root Mean Square (RMS) difference with measurements. The measured and modelled quantities for

a single turbine over a period with relatively high wind fluctuations are shown in Figure 3.8. As expected, neglecting the fast dynamics of the power electronics and generator had a negligible impact on the model accuracy.

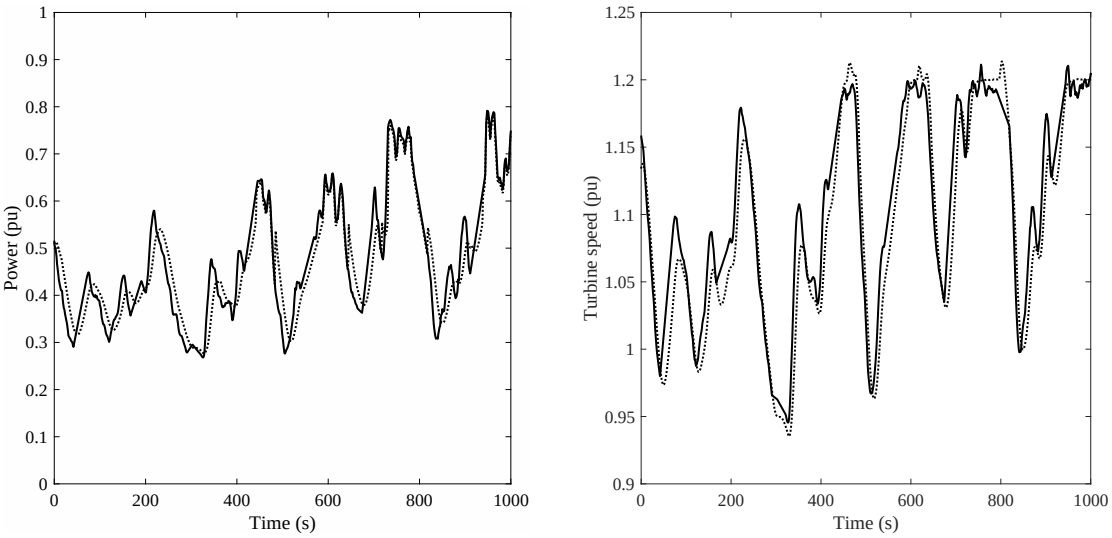

(a) **(b)**

Figure 3.8: Typical measured (solid line) and modelled (dotted line) a) power output and b) rotor speed of Turbine 1 in Figure 3.1b.

3.4 Spectral analysis of wind farm data

Detailed modelling of a wind farm with a large number of wind turbines is computationally expensive. However, different methods can be used to model the wind farm with a reduced number of wind turbines, as discussed in Chapter 2. In the present study, to determine the reduced number of wind turbines that can still accurately simulate the full wind farm power generation, spectral analysis is first used to investigate the cross-correlations between the turbines' power output. For the case in which the turbines of a wind farm are completely correlated, the wind farm's total power can be simulated with a relatively simple scaling of a single turbine's power output to the wind farm capacity. However, in practical wind farms, the correlation between different turbine pairs can vary significantly. In the aggregated wind farm modelling approach, turbines that are highly correlated can be clustered and simulated as a single aggregated machine. This can reduce the computation cost, without sacrificing to a large extent the accuracy of the model.

3.4.1 Coherence

The coherence is a measure of the extent to which two signals are correlated in the frequency domain [173],

$$\gamma_{i,j}(\omega) = \frac{|S_{i,j}(\omega)|}{\sqrt{S_{i,i}(\omega)S_{j,j}(\omega)}}, \tag{3.4}$$

where $S_{i,j}$ is the Cross Power Spectral Density (CPSD) between i and j and $S_{i,i}, S_{j,j}$ are the Power Spectral Density (PSD) of two signals. The cross power spectral density between signal i and j is the Fourier transform of the cross-correlation function $R_{i,j}$,

$$S_{i,j}(\omega) = \sum_{n=-\infty}^{+\infty} R_{i,j}(n)e^{-j\omega n}, \tag{3.5}$$

Figure 3.9a shows scatter plots of the coherence of the annual power output of specific turbine pairs i and j shown in Figure 3.1b. The coherence of all turbine pairs tends towards unity as the frequency tends to zero, whilst it tends to zero at higher frequencies. Figure 3.9b then shows that extending such analysis to all 2016 turbine pairs in this 64-turbine wind farm again shows these two asymptotic behaviours, but with substantial scatter.

The distance between wind turbines plays an important role in their correlation. For example, Figure 3.9a shows that neighbouring wind turbines are more correlated compared to two distant turbines. To account for the impact of the distance between turbines, a *Strouhal* number is defined,

$$St_{i,j}(\omega) = \frac{\omega d_{i,j}}{2\pi\overline{V_w}} = \frac{f d_{i,j}}{\overline{V_w}}, \tag{3.6}$$

where $d_{i,j}$ is the distance between turbine i and j, and $\overline{V_w} = 7.1$ m/s is the annually averaged wind speed measured at the two met-masts.

Figure 3.10 presents the coherence of these same turbine pairs against this Strouhal number. The previously observed asymptotic behaviours of tending to unity and zero coherence at zero and high frequencies respectively are again clear. However, the data now collapses considerably and approaches zero coherence at order $St_{i,j}$=1, *regardless* of the turbine pair. Since $\overline{V_w}/f$ in equation 3.6 is a convective length scale, unity $St_{i,j}$ occurs when this length scale equals the spacing ($d_{i,j}$) between any two turbine pairs. A degree of correlation between the power output of any two turbines, therefore, occurs when perturbations in the wind speed have a sufficiently low frequency such that their

convective length scale is of order or greater than the turbine spacing. Uncorrelated power output occurs when the wind's convective length scales are shorter than the turbine spacing.

Interestingly, the collapse of these coherence functions with the Strouhal number defined in equation 3.6 occurs using each turbines' instantaneous power output over the year, even though the instantaneous wind direction, of course, varies enormously during this period. It can be expected that this is because the transverse and streamwise length scales in the wind are often comparable, and thus the spacing of any turbine pair remains a useful reference scale independent of the turbine pairs' orientation relative to the instantaneous wind speed. Of course, this can only be tested if the instantaneous wind direction at each turbine is known, and unfortunately, this was not available for this study.

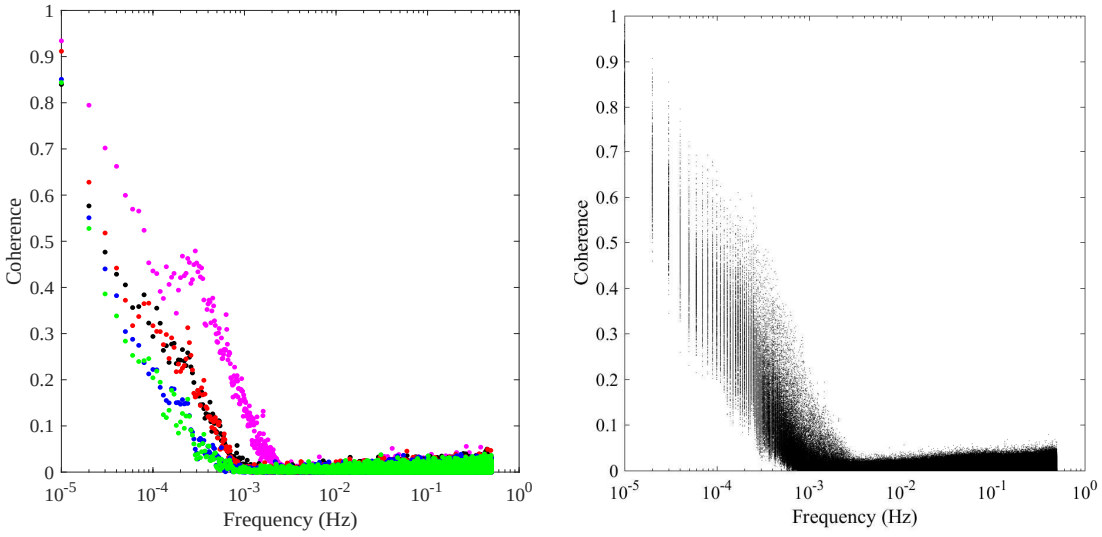

Figure 3.9: Scatter plots of the coherence function of a) turbine pairs 1-2 (purple), 1-16 (black), 1-32 (red), 1-48 (blue), 1-64 (green) in Figure 3.1b and b) all 2016 possible wind turbine pairs in the wind farm versus frequency.

3.4.2 Amplitude and phase

The relationships between all turbine pairs are further examined by considering the spectra of their relative amplitudes and phases of their instantaneous power output. The relative amplitudes and phases are calculated using the Fourier transform of the power output signals.

Since the wind turbines are the same, it is expected that they will have similar amplitude power output at all frequencies, but with instantaneous phase lag or lead

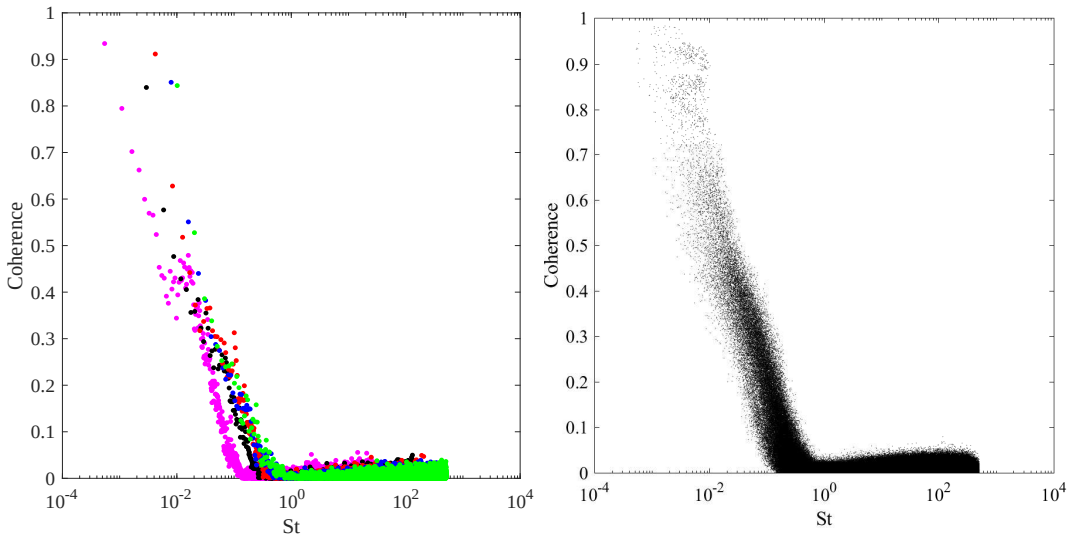

Figure 3.10: Scatter plots of the coherence function of a) turbine pairs 1-2 (purple), 1-16 (black), 1-32 (red), 1-48 (blue), 1-64 (green) in Figure 3.1b and b) all possible wind turbine pairs in the wind farm versus Strouhal number ($St_{i,j}$) defined by equation 3.6.

depending on the dominant wind direction and turbine locations. Figure 3.11a shows a scatter plot of the amplitude ratio of all turbine pairs, with the red line connecting the average ratios at each frequency. This average is close to unity, which agrees with expectations.

Figure 3.11b shows a scatter plot of the relative phase between the power output of all turbine pairs over the year. Consistent with the coherence analysis, signals are always close to being in phase at frequencies well below order unity $St_{i,j}$, but of randomly varying phase at higher frequencies. Once again, the red line represents the average quantity by frequency, and is close to zero for all frequencies. In phase power generation infers zero phase for $St_{i,j} \ll 1$, whilst uncorrelated power generation over the year infers randomly varying instantaneous phase with zero annual average for $St_{i,j} > 1$.

This frequency dependent instantaneous phase between the power output of any turbine pair explains the previously reported 'smoothing' of the power generation of the wind farm relative to that of any individual turbine in the farm [84, 85], since higher frequency content in each turbine's power generation is lost as the power is aggregated. This frequency dependence also now allows a series of simple models of the wind farm power output to be developed, as is presented in the next section.

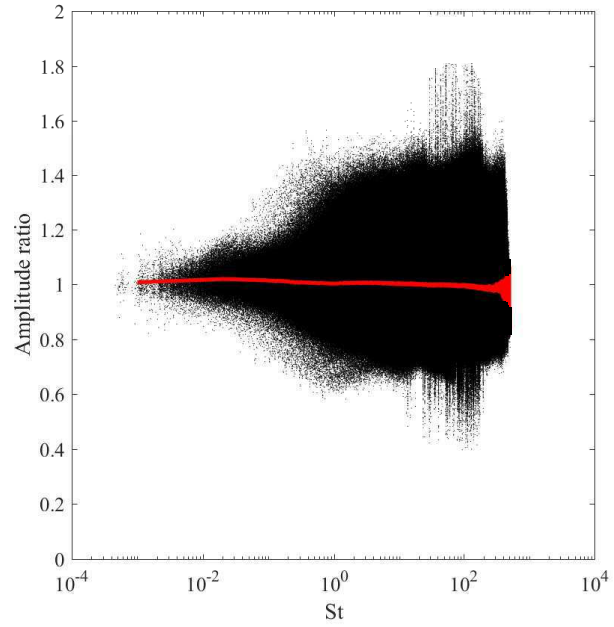

(a)

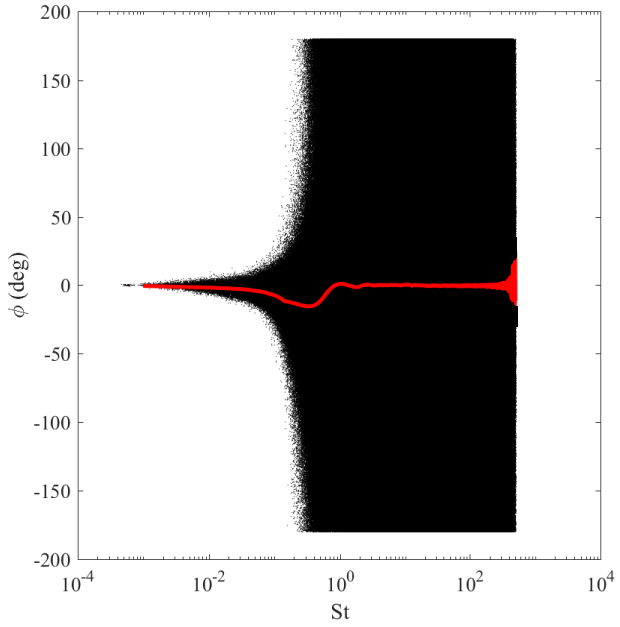

(b)

Figure 3.11: Scatter plots of the relative a) amplitude and b) phase spectra for the power output from all wind turbine pairs versus $St_{i,j}$, where the red line denotes the average quantity by frequency.

3.5 Wind farm modelling

Figure 3.12 shows the block diagram of the proposed model. There are n wind turbines in the farm, aggregated into m groups that are each represented by a reference wind

turbine. The power output of the reference wind turbines is modelled using the model presented in Section 3.3. The power output of all the other turbines in a given group is modelled using the power output of the group's reference turbine and a modelled degree of cross-correlation, represented as transfer functions (H) that depend only on the frequency of the wind disturbance at the reference turbine and the distance of those turbines from the reference turbine.

The contribution of the proposed method for wind farm modelling to the existing literature is that it benefits from the advantages of the detailed and multi-machine methods simultaneously whilst addressing their drawbacks. The similarity between the proposed method and multi-machine is that both methods use a reduced number of turbines to simulate the power generation of a wind farm to reduce the computational effort. Similar to detailed models, the proposed method simulates the power generation of every single wind turbine in a farm separately using the transfer functions that account for the correlation characteristics observed in the spectral analysis.

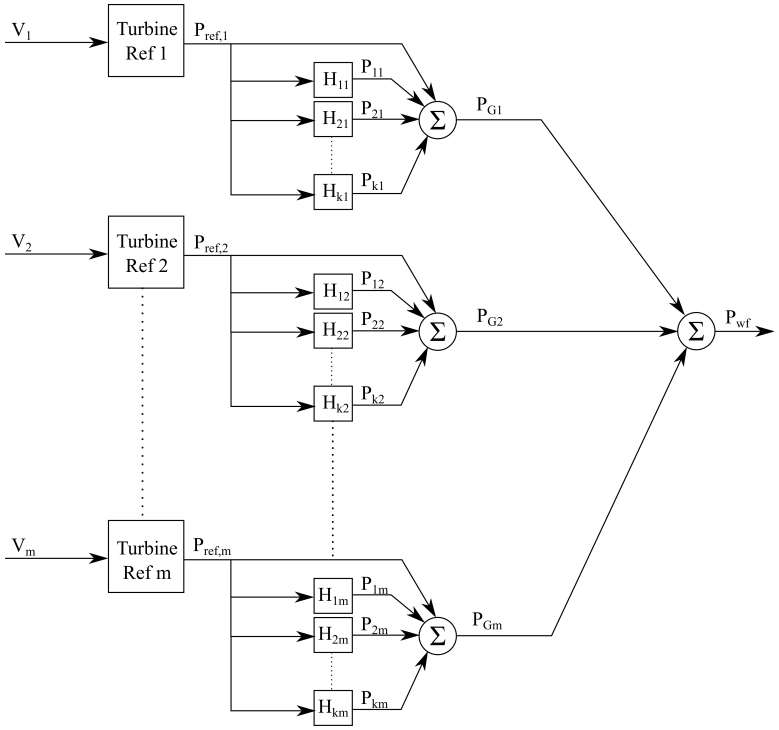

Figure 3.12: Block diagram of the proposed wind farm modelling method.

3.5.1 Clustering wind turbines

The spectral analysis presented in Section 3.4 showed that the correlation between power generation of turbines is strongly dependent on their distance. Therefore, two distance-

based clustering methods are used in this study, which are explained in the following sections.

3.5.1.1 Line-based clustering

Since it is already established that the spacing between turbine pairs is a significant length scale in this problem, a line-based method for grouping wind turbines is an obvious choice. A simple algorithm for aggregating based on proximity is to view the wind farm as a single line of turbines, as shown in Figure 3.1b. The line is then segmented into m groups of turbines. The most central turbine in each group then becomes the reference turbine for that group. Figure 3.1b shows this method applied to 8 turbine groups with the reference turbines circled.

3.5.1.2 Optimal distance-based clustering

To group the turbines optimally, the clustering problem is also formulated as a Mixed Integer Linear Programme (MILP). The objective function is to minimise the total distance between the turbines in groups and the corresponding reference turbines,

$$\min \left\{ \sum_{g} \sum_{j} \sum_{i} \alpha_{i,j,g} d_{i,j} \right\}, \tag{3.7}$$

where $\alpha_{i,j,g}$ is a binary variable, and is equal to 1 if the distance between turbine j and the reference turbine i ($d_{i,j}$) is assigned to group g. Equation 3.8 states that the number of distance elements assigned to each group is equal to the number of turbines in a group. It is assumed that groups have the same number of turbines.

$$\sum_{j} \sum_{i} \alpha_{i,j,g} = \frac{n}{m}. \tag{3.8}$$

Since each group has its own reference turbine, the number of reference turbines is the same as the number of groups, which is shown in equation 3.9. In this equation, $\beta_{i,g}$ is a binary variable which equals 1 if turbine i is selected as the reference turbine of group g. Once turbine i is chosen as the reference turbine for group g, the distances in that group should be in reference to the turbine i and other distance elements between the rest of the turbines must be eliminated. This is achieved using equation 3.10. Equation 3.11 states that if $\alpha_{i,j,g}$ is non-zero, then turbine j is a member of group g. In this equation, $\zeta_{j,g}$ is a binary variable, which denotes whether turbine j is a member of group g or not. Moreover, equation 3.12 ensures that each turbine j can be assigned to

only one group.

$$\sum_{g}\sum_{i}\beta_{i,g} = m, \tag{3.9}$$

$$\sum_{j}\alpha_{i,j,g} = \frac{n}{m} \times \beta_{i,g}, \tag{3.10}$$

$$\zeta_{j,g} \leq \sum_{i}\alpha_{i,j,g}, \tag{3.11}$$

$$\sum_{g}\zeta_{j,g} = 1, \tag{3.12}$$

$$\alpha_{i,j,g}, \beta_{i,g}, \zeta_{j,g} \in \{0, 1\}. \tag{3.13}$$

This optimisation problem was implemented in GAMS [174] and solved for 1 to 32 turbine groups. The results are shown in Figure 3.13, where the reference turbines are shown in circles. It should be noted that in Figure 3.13f, each turbine in a given group can be selected as the reference turbine because there are only two turbines in each group.

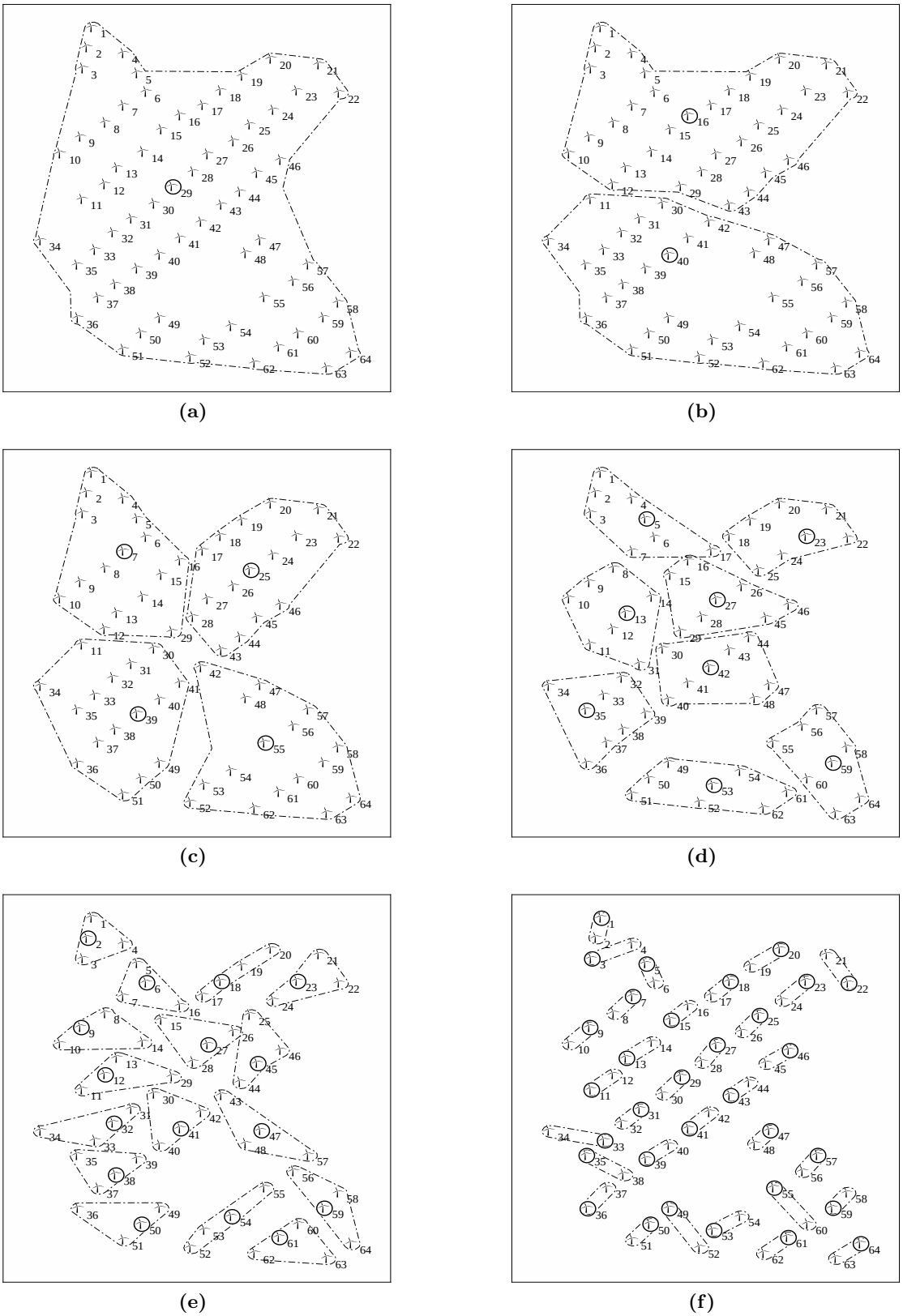

Figure 3.13: Wind turbines optimal distance-based clustering using a) 1, b) 2, c) 4, d) 8, e) 16, and f) 32 turbine groups.

3.5.2 Formulation of proposed method

After clustering the wind turbines, the transfer functions (H) shown in Figure 3.12 are formulated according to the results of Section 3.4. These transfer functions relate the power output of a reference turbine to the rest of the turbines in the same cluster. First, the Fourier transform of the power generation of each group's reference turbine is determined. For group g, this is $\mathscr{P}_{ref,g}(\omega) = \mathscr{F}\{P_{ref,g}(t)\}$. The Fourier transform of the power of the other turbines i in group g is then calculated as:

$$\mathscr{P}_{j,g}(\omega) = H_{j,g}(\omega)\mathscr{P}_{ref,g}(\omega), \tag{3.14}$$

where $H_{j,g}$ is the transfer function between the power output of turbine j and the reference turbine for that group g (Figure 3.12).

Figure 3.11 reveals the amplitude and phase characteristics of the transfer function (H). One idealisation is that $|H(\omega)|$=1, if all turbines have the same power generation, which will only be approximately true given local topology and other effects. However, $|H(\omega)|$ can also be determined from the historical power data, thereby taking into account inhomogeneity present inside the boundary of all wind farms. Since at zero frequency the amplitude ratio of power signals is the same as the ratio of capacity factors, wind turbines' capacity factors are used in order to determine the amplitude characteristics of the transfer functions.

Figure 3.14 shows the capacity factor of wind turbines on the topographic map of the wind farm. The impact of the topology and location of wind turbines on their annual capacity factor can be seen in this figure. Interestingly, the turbines with the highest capacity factors are located on top of hills.

Modelling of the phase of $H(\omega)$ is more involved. One simple method is proposed, by which the phase is zero for $St < 0.2$ and uniformly randomly varying for $St >$0.2. Of course, a more complex phase response could be prescribed, such as one that more closely fits the historical data in Figure 3.11b and better represents the observed gradual transition between correlation and non-correlation with increasing frequency. However, it was found that more complex phase models did not give large benefits, and it was assumed that the transition between perfect correlation and perfect non-correlation occurs at a fixed St instead. It should also be noted that this transition was chosen to occur at St=0.2 because that gave the lowest errors using this simple approach. This transition point is reasonable, given the results in Figures 3.10 and 3.11.

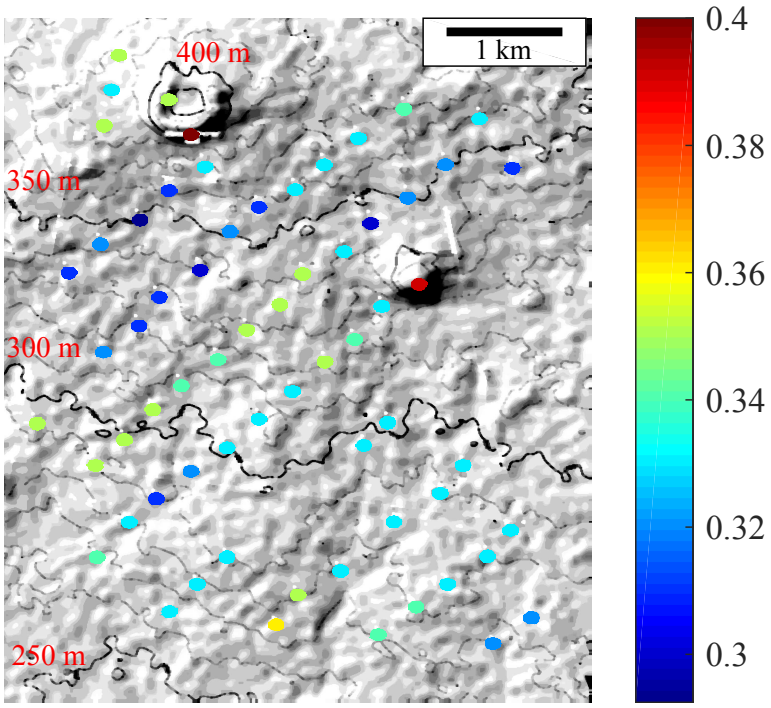

Figure 3.14: Capacity factor of turbines on the topographic map of the Mt Mercer wind farm.

The following equations show the amplitude and phase characteristics of the modelled transfer function (H).

$$H_{j,g}(\omega) = \left| \frac{\mathscr{P}_{j,g}(\omega)}{\mathscr{P}_{ref,g}(\omega)} \right| = \frac{CF_{j,g}}{CF_{ref,g}}, \tag{3.15}$$

$$\angle H_{j,g}(\omega) = \begin{cases} 0 & St_{j,g} < 0.2, \\ \varphi & St_{j,g} > 0.2, \end{cases} \tag{3.16}$$

where φ denotes zero mean random numbers between $-\pi$ to $+\pi$. The time series of the power output of each turbine i in group g is computed by taking the inverse Fourier transform (IFFT), $P_{j,g}(t) = \mathscr{F}^{-1}\{\mathscr{P}_{j,g}(\omega)\}$. The time series of the power output of the whole wind farm is then,

$$P_{wf}(t) = \sum_{g=1}^{m} \left[P_{ref,g}(t) + \sum_{j}^{k} P_{j,g}(t) \right], \quad k = \frac{n}{m} - 1. \tag{3.17}$$

3.5.3 Performance of the proposed method

In this section, the accuracy of the proposed model is investigated for different numbers of turbine groups using both the line-based and optimal clustering methods. Figure 3.15 shows how the Root Mean Square Error (RMSE) and the Mean Absolute Error (MAE) of the modelled wind farm annual power output and its time derivative (the

'ramp rate') both vary with an increasing number of turbine groups. The ramp rate is shown because this is an important quantity when considering the integration of any form of power generation into an electrical power system [23]. The error in power and ramp rate are normalised by the annually averaged power generation and the capacity of the wind farm, respectively.

Increasing the number of turbine groups results in a dramatic reduction in modelling error. This is because more measured information and less modelling are used to calculate the total wind farm power output as the number of turbine groups (m) increases. As Figure 3.12 shows, more turbine groups implies more reference turbines, with the model then performing fewer, imperfect cross-correlations between these reference turbines and other turbines in the wind farm. As equation 3.17 states, with m=64 single turbine 'groups', the 'model' of this wind farm only transforms the measured wind speed at each turbine into its power output, but does not correlate any two turbines in order to determine the wind farm's total power generation.

The proposed method presents a trade-off between the use of measured data and modelling effort, with the use of more measurement, of course, preferable in a given application if that is practical. Figure 3.15 shows that the single group model, which models the 63 other turbines in the wind farm by one reference turbine, has large errors, and that at least 8 turbine groups are required to achieve lower than 10% RMSE. Therefore, it is likely that at least 8 turbine groups with associated measured data will be required in order to have quantitative use.

Furthermore, the performance of the model is comparable using both clustering methods. This suggests that the simple line-based method is a reasonable approach for clustering wind turbines, particularly for wind farms with a large number of turbines. This is because the computational cost increases dramatically by increasing the number of turbines due to the exponential growth of the number of different possible turbine combinations.

Further analysis was performed to investigate the effect of wind speed on the performance of the proposed method. Figure 3.16 shows the average of the absolute instantaneous errors for the wind farm models with 1, 8 and 32 reference turbines. The errors are binned according to the instantaneous wind speed measured at met-mast locations. It can be seen that the model accuracy deteriorates as the wind speed increases from 0 m/s up to rated values in the range 10 - 15 m/s. As the winds speeds increase further, the model then becomes more accurate. The improved model accuracy for the two highest wind speed ranges ($V_w \geq$15 m/s) can be attributed to the wind speed being higher

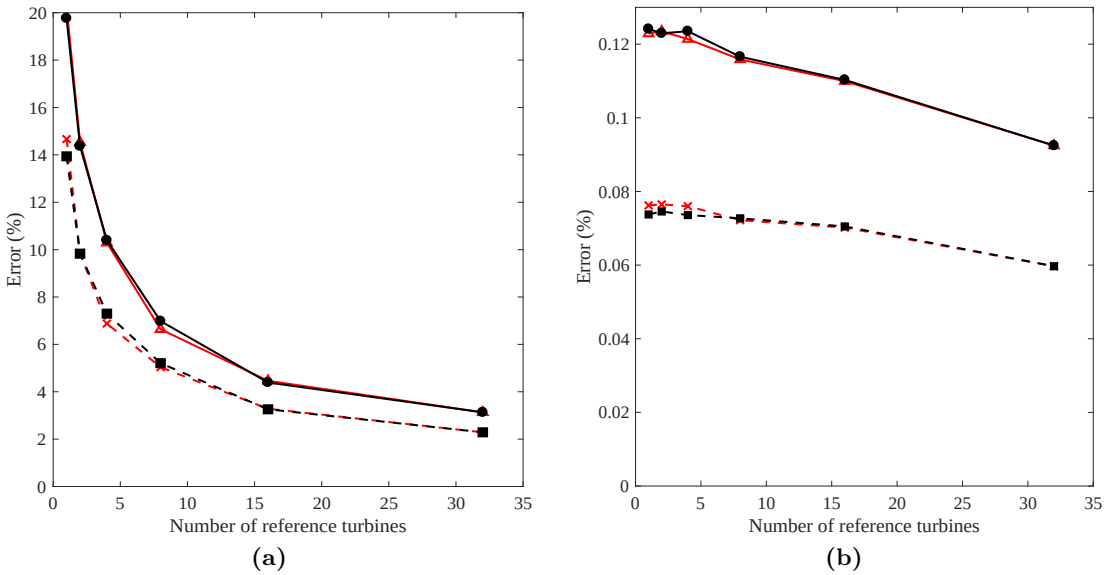

Figure 3.15: Normalised RMSE (solid lines) and MAE (dashed lines) for optimal distance (red) and line-based (black) grouping methods in a) power and b) ramp rate of the modelled wind farm with an increasing number of reference wind turbines.

than the rated value of the turbines, which implies that they are generating power at their rated capacity without significant fluctuation.

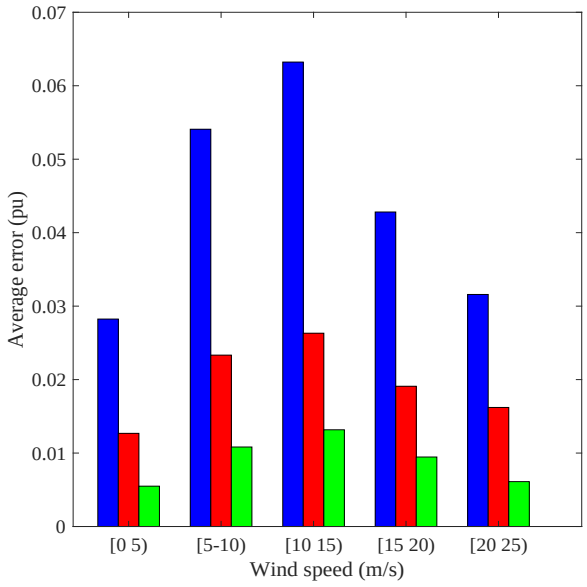

Figure 3.16: Average error for each wind speed range using wind farm models with 1 (blue), 8 (red) and 32 (green) turbine groups.

3.5.4 Analysis of the proposed method

In this section, the spectra of different wind farm models are investigated. The averaging technique and Hanning window are used to attenuate spectral leakage and smooth the spectra [173].

Figure 3.17 shows the spectra of the annual power generation of three wind farm models with different numbers of turbine groups along with the spectra from the measured wind farm. The shaded region in this figure denotes the range of frequencies over which the power generation of each turbine transitions from correlated to uncorrelated. The left boundary of this region has a frequency obtained from the longest length scale in this problem - the distance between the two furthest apart turbines - along with the annually averaged wind speed at the met-masts. Similarly, the right boundary of the shaded region in Figure 3.17 has a frequency obtained from the distance between the two closest together turbines and this same wind speed.

Measurement and *all* models perform very similarly to the left of the shaded region in Figure 3.17 because the wind farm is compact relative to the length scales in the incident wind. In this case, all turbines are in phase and producing similar instantaneous power. To the right of the shaded region, each turbine in the wind farm has power generation that does not correlate with any of the others because the length scales in the wind are much shorter than the spacing between any two turbines. The shaded, transitional region sits between these two extremes, with each turbine in the wind farm on *average* more correlated with closer turbines and less correlated with more distant turbines.

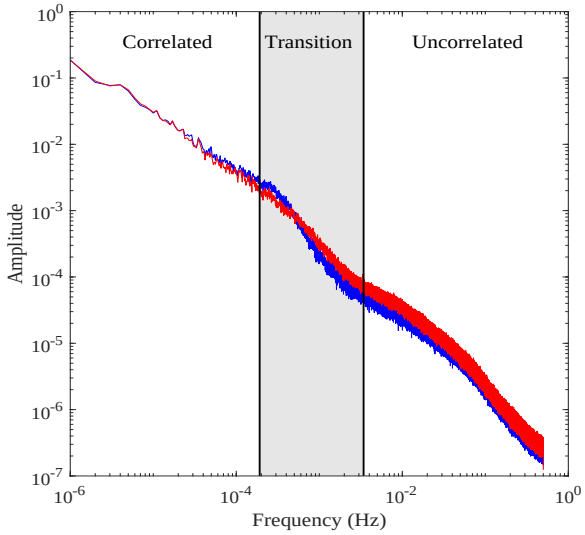

(a)

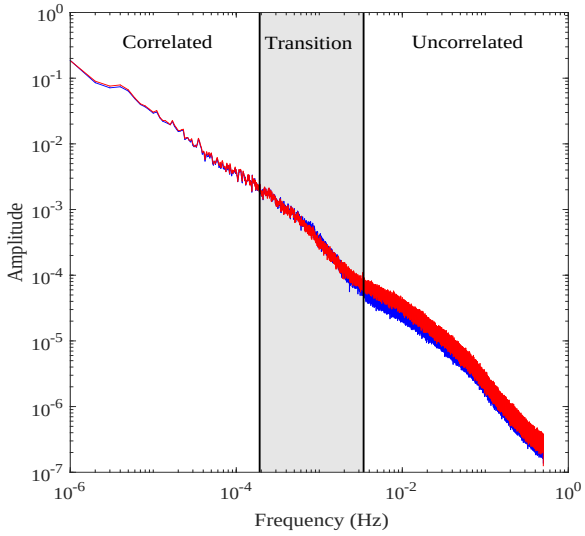

(b)

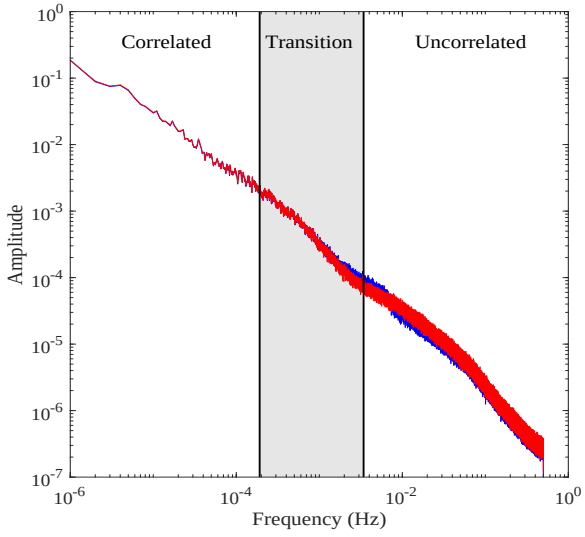

(c)

Figure 3.17: Spectra of actual (red lines) and modelled (blue lines) wind farm power output with a) 1, b) 8 and c) 32 Turbine groups.

As Kolmogorov proposed [175], the energy of a turbulent fluid is proportional to the frequency of the turbulent eddies. Apt et al. [90] showed that the spectrum of a wind farm power generation can be modelled using the Kolmogorov spectrum ($f^{-5/3}$) in the frequency range associated with 30 seconds to 2.6 days. Katzenstein et al. [176] investigated the power spectrum of interconnected wind farms. They found that the power spectrum of a single wind farm follows a Kolmogorov spectrum for time scales of less than 24-hour and with the increasing number of interconnected wind farms the slope of the spectrum becomes steeper due to the smoothing effect.

Figure 3.18 shows that the Power Spectral Density (PSD) of the power generation of our studied wind farm follows the Kolmogorov slope ($f^{-5/3}$) for the time scale of approximately 3 days to 30 minutes before the smoothing effect impacts the power spectrum, after which the slope becomes greater.

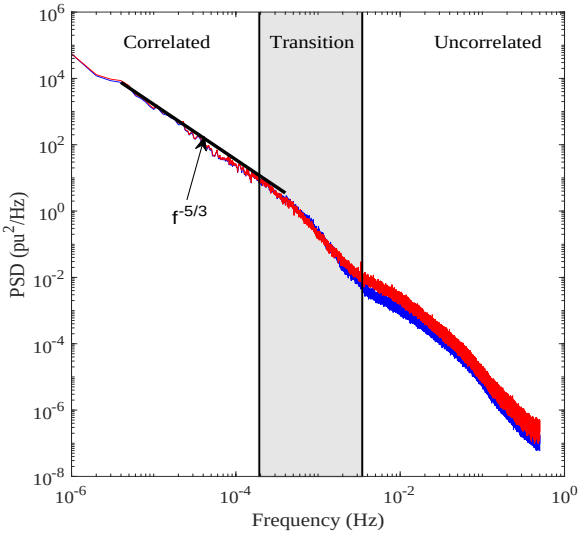

Figure 3.18: Power Spectral Density (PSD) of the actual (red line) and modelled (blue line) wind farm power output with 8 Turbine groups along with the Kolmogorov slope (black line).

Further evidence of the existence of these correlated, transitional and uncorrelated regions in the spectra of wind farm power output is shown in Figure 3.19. This figure shows both the measured wind farm spectra and two scaled spectra of a reasonably central turbine in the farm. If all turbines are highly correlated at the low frequency limit, the power generation of this n=64 turbine wind farm should be close to 64 times that of Turbine 32. Similarly, if all turbines are uncorrelated at the high frequency limit, the fundamental theory of normal Gaussian processes [84, 173, 177] states that the wind farm's power generation should be $\sqrt{n}$ =8 times that of Turbine 32. Figure 3.19 shows that both these high and low frequency limits are observed for the measured total wind farm power generation.

This final result highlights the importance of the transitional region to accurate wind farm modelling. Figures 3.17 and 3.19 together show that reasonable modelling of turbine correlation across the wind farm is important to capture power generation in the transitional region and thus result in lower modelling errors overall. This is likely a general result for modelling any wind farm, even though the proposed wind farm models can be very different.

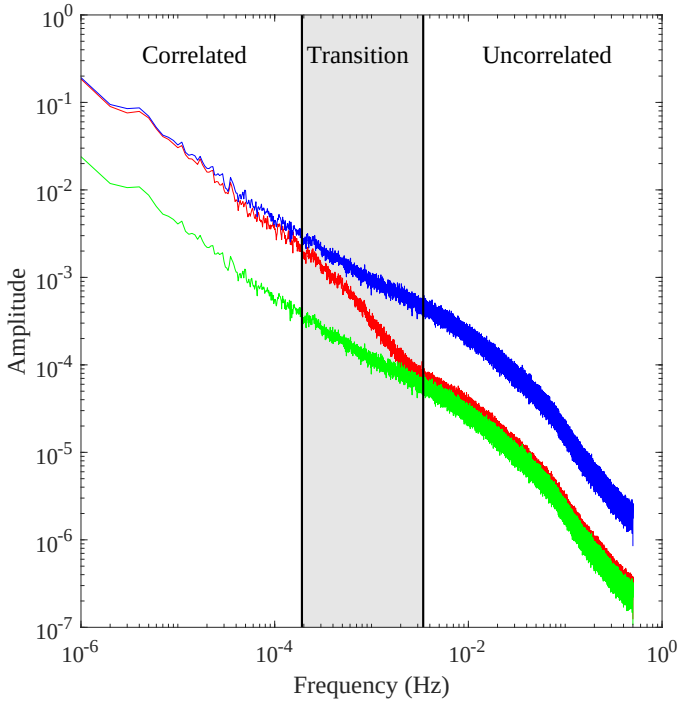

Figure 3.19: Spectra of actual (red line) wind farm power output, 64 times the actual power output of Turbine 32 (blue line) and 8 times the actual power output of Turbine 32 (green line), where Turbine 32 is defined in Figure 3.1b

3.6 Summary

This chapter presented the analysis and modelling of a wind farm using large amounts of measured data. One Hertz data over an entire year from two meteorological masts and each of the 64 turbines in the farm was first used to perform spectral analysis of the relationships between all turbines. A model of the wind farm was then proposed that accommodated these observed relationships.

The spectral analysis showed that the coherence between the power output of any of the 2016 turbine pairs in the wind farm was strongly dependent on the frequency of the incident wind disturbance. The coherence between any turbine pairs tended towards unity and zero respectively as this frequency tended towards zero and infinity. Plotting these coherence functions against a Strouhal number (St) that used the annually

averaged wind speed and the spacing between each turbine then led to the significant collapse of this data, with the coherence function remaining always close to zero for St>0.2. This provided clear evidence that the power generation of any turbine pair is not correlated if the convective length scale in the wind is shorter than the turbine spacing, which was confirmed by further analysis of the relative amplitude and phase of all turbine pairs.

The collapse of the data with this Strouhal number also gave a physical basis with which to model the wind farm's power generation. These models took into account the importance of the spacing between turbines by aggregating turbine groups based on their distance using two different clustering methods: line-based and optimal distance-based. All turbines in a given group were modelled by a reference turbine. The choice of the number of turbine groups was a trade-off, with the use of more groups resulting in higher accuracy but requiring the use of more measured data. Representing the wind farm by one turbine, with the 63 other turbines in the wind farm related to that reference turbine, was found to result in relatively large errors, and at least 8 turbine groups were required to achieve a normalised RMS error of lower than 10%. It was found that the increase of turbine groups to more than 8 does not result in a significant improvement in the model accuracy, however, it increases the computation effort significantly. The results also showed that the simple line-based method is a reasonable approach, especially for large wind farms with a higher computational cost of the optimal distance-based method.

Spectral analysis of the power output of different wind farm models and the measured wind farm power output then revealed three distinct frequency regions. For frequencies lower than that defined by the average wind speed and the spacing between the two, furthest apart turbines, all the models and the measurements performed very similarly. This was because the wind farm was compact relative to the length scales in the wind in this limit, and thus all turbines generated similar instantaneous power. For frequencies higher than that defined by the average wind speed and the spacing between the two, closest together turbines, the turbines' power generation was uncorrelated. A third, transitional region is present between these two limits, with each turbine in the wind farm *on average* more correlated with closer turbines and less correlated with more distant turbines. Since these high and low frequency regimes had relatively simple relationships between all turbines, it is likely a general result that the accuracy of wind farm modelling is most sensitive to the modelled correlation between turbines in this transitional regime.

Chapter 4

Problem formulation

4.1 Introduction

This chapter first presents the formulation of an optimisation model to determine the optimal sizing and performance of a battery energy storage system integrated into a grid-connected wind farm. This problem is formulated as a deterministic linear programme (LP), maximising the Net Present Value (NPV) from a wind farm and a battery, both participating in the energy and Frequency Control Ancillary Service (FCAS) markets. The optimisation problem is modelled with the GAMS [174] software using CPLEX [178] as the solver. The market prices and technical data along with the simulated power generation of the wind farm are used as the input data to the model, and the wind farm is considered to be a sunk cost, i.e. already connected to the grid and operating. The optimiser determines the battery size and the dispatch of the several services offered by the battery and wind farm in different markets.

In order to consider all ancillary service revenues in this LP, a significant part of this chapter also develops and validates a linear model of the FCAS regulation payments, known as Causer Pays Payments (CPPs), which were discussed in Chapter 1. This method uses 4-second dispatch data to evaluate the performance of all units, their impacts on the frequency of the power system and thus the financial penalties that all scheduled assets must pay.

4.2 Optimisation model description and formulation

A schematic diagram of the battery and the wind farm is shown in Figure 4.1. This configuration enables the battery to be charged from either the grid or the wind farm, while the wind farm can dispatch the power directly to the grid or charge the battery. The wind farm also can curtail the wind generation depending on the energy and FCAS prices. Wind farm curtailment can be controlled in various ways, ranging from individual to aggregated control, and in the present instance using the aggregated model developed in Chapter 3.

Figure 4.2 shows the block diagram of the model. The input data that include the wind farm power generation, market data and battery specifications are fed into the optimisation model, which is comprised of five sub-models: the energy market, FCAS markets, a linear version of the Causer Pay Method (CPM, presented later in this chapter), the battery and the wind farm frequency control model. The outputs of the optimisation model are the optimal capacity of the battery and the optimal dispatch of the wind farm and the battery. The optimal dispatch is then used in the full CPM to

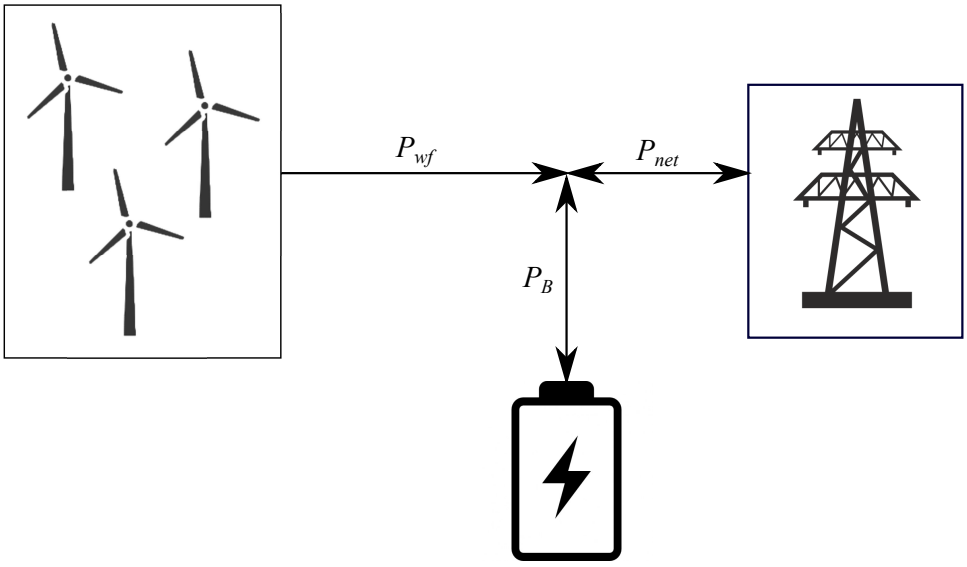

Figure 4.1: Schematic diagram of the wind farm and battery storage.

calculate the exact CPPs. Finally, the optimal revenues and battery costs, as well as the exact CPPs, are used in the financial analysis model to calculate the system's Net Present Value (NPV) and its Internal Rate of Return (IRR).

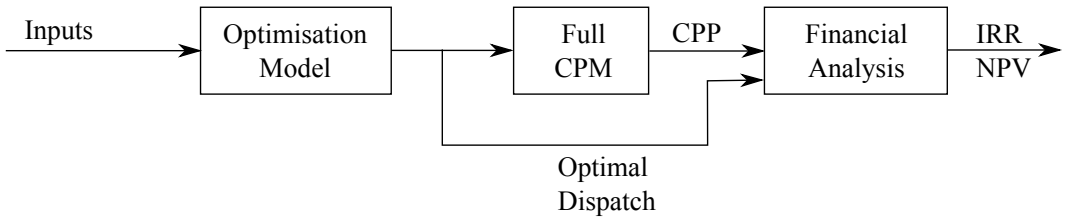

Figure 4.2: Block diagram of the model.

The optimisation model maximises the NPV of the battery and wind farm as they participate in the energy and FCAS markets. In this problem, decisions are made based on the *modelled* power output of the wind farm and the objective function is then corrected according to the wind farm's *measured* power by introducing a penalty cost term, which is explained in the coming sections. Equation 4.1 shows that the objective function has four terms, including revenues in the energy market (R_{Energy}), in FCAS markets (R_{FCAS}), total battery costs (TC_B) and the CPP of the entire wind farm-battery plant. These components will be explained in the following sections.

$$\mathcal{V} = Max\Big\{R_{Energy} + R_{FCAS} - TC_B - CPP\Big\}. \tag{4.1}$$

4.2.1 The energy market

A grid-connected wind farm typically participates in the energy market by dispatching the maximum available wind power. The wind farm can benefit from a battery providing arbitrage by storing electricity at times of low market price and releasing at a higher price. The NPV of the revenue that the plant can earn in the energy market during the battery's lifetime is,

$$R_{Energy} = \sum_{y=1}^{L} \frac{1}{(1+r)^y} \Big[\Delta t \sum_{t=1} P_{net,act}(t)\pi(t) \Big], \tag{4.2}$$

where $P_{net,act}$ is the actual net power injected to the grid. The actual and modelled net power output are related as,

$$P_{net,act}(t) = P_{net,mdl}(t) - \varepsilon(t) + \tau(t), \tag{4.3}$$

where ε is the wind farm model error and τ is the unfulfilled requested curtailment due to the error of the wind farm model at each time interval t. Section 4.2.4 provides a detailed calculation of τ. The wind farm model error is,

$$\varepsilon(t) = P_{wf,mdl}(t) - P_{wf,act}(t). \tag{4.4}$$

The modelled net power dispatched into the energy market ($P_{net,mdl}$) includes the dispatch of the wind farm and battery in the energy market as well as the energy dispatched due to FCAS provision,

$$\begin{aligned} P_{net,mdl}(t) &= P_{wf,mdl}(t) - P_{wf,pcurt}(t) + P_{B,d}(t) - P_{B,c}(t) \\ &+\alpha_{RReg}(t)\Big[P_{B,RReg}(t) + P_{wf,RReg}(t)\Big] - \alpha_{LReg}(t)\Big[P_{B,LReg}(t) + P_{wf,LReg}(t)\Big] \\ &+\rho_{RCont} \sum_{x \in \mathcal{X}_{RCont}} \Big[P_{B,x}(t) + P_{wf,x}(t)\Big] - \rho_{LCont} \sum_{x \in \mathcal{X}_{LCont}} \Big[P_{B,x}(t) + P_{wf,x}(t)\Big], \end{aligned} \tag{4.5}$$

where α_{RReg} and α_{LReg} indicate the extent to which offered FCAS regulation services are used, and the last two terms correspond to the energy dispatched due to contingency services provision. Since the probability of contingency services being required (ρ_{RCont} and ρ_{LCont}) is very small [19], these terms have a minor impact on the optimal dispatch. To calculate α_{RReg} and α_{LReg}, the 4-second Frequency Indicator (FI) data of the National Electricity Market (NEM)'s FCAS market is required [17]. This data, which indicates the amount of FCAS regulation services used in the power system, along with the total FCAS regulation enabled capacity in the Australian Mainland are used

to estimate the plant energy dispatched due to FCAS regulation provision,

$$\alpha_{RReg}(t) = \frac{FI(t)}{D_{RReg}(t)}, \quad FI(t) \geq 0, \tag{4.6}$$

$$\alpha_{LReg}(t) = \frac{FI(t)}{D_{LReg}(t)}, \quad FI(t) < 0. \tag{4.7}$$

4.2.2 FCAS markets

The Frequency Control Ancillary Services (FCAS) markets are comprised of 8 different markets, including 2 for regulation and 6 for contingency. The total FCAS revenue is the sum of the revenues in the regulation and contingency markets minus the penalty cost which considers the excess services that cannot be fulfilled in the actual scenario due to the error of the wind farm model, i.e.

$$R_{FCAS} = R_{Reg} + R_{Cont} - \mathcal{P}. \tag{4.8}$$

Equation 4.9 shows the associated penalty cost, where ϵ is the unfulfilled curtailment due to the wind farm model error if the power system requests for the maximum offered curtailment (equation 4.41). Since the combination of *all* FCAS services contribute to the required amount of curtailment, the provision of multiple offered services may not eventuate due to the wind farm model error. Therefore, the FCAS revenue is penalised in proportion to the wind farm model error,

$$\mathcal{P} = \sum_{t} \epsilon(t) \times \pi^{max}_{FCAS}(t). \tag{4.9}$$

Since FCAS markets are enablement-based markets, providers earn revenues based on the amount of their enablement, even if the power system operator does not call upon them to take action. This important feature of FCAS markets is described and formulated in the following sections.

4.2.2.1 Regulation

The revenues in FCAS regulation markets include the battery's and the wind farm's raise and lower services offered,

$$R_{Reg} = \sum_{y=1}^{L} \frac{1}{(1+r)^y} \Bigg[\Delta t \Bigg(\sum_{t=1} \big[P_{B,RReg}(t) + P_{wf,RReg}(t)\big] \pi_{RReg}(t) + \big[P_{B,LReg}(t) + P_{wf,LReg}(t)\big] \pi_{LReg}(t) \Bigg) \Bigg]. \tag{4.10}$$

In addition to earning revenue in the FCAS regulation markets, the battery can improve the performance of the system and reduce payments by helping the system to follow dispatch targets more accurately. To include this feature in the optimisation model, a linear version of the FCAS Causer Pays Method (CPM), developed later in this chapter in Section 4.3.4, is used to estimate the CPPs,

$$CPP = \sum_{y=1}^{L} \frac{1}{(1+r)^y} \sum_{t=1} K_{CPP}\big(Dev(t) \times FI(t)\big). \tag{4.11}$$

The deviation from the dispatch target is calculated as,

$$Dev(t) = P_{net,act}(t) - DT_{correct}(t). \tag{4.12}$$

FCAS provision by curtailing wind in the NEM requires modification of the dispatch target because the Independent System Operator (ISO) currently sets them based on the maximum available power from a wind farm using the ISO's Australian Wind Energy Forecasting System (AWEFS) [179]. This modification in determining the dispatch target is applied considering the wind farm precurtailment,

$$DT_{correct}(t) = DT_{hist}(t) - P_{wf,pcurt}(t). \tag{4.13}$$

Curtailment is a deliberate reduction in wind power generation during a 5-minute dispatch interval, while precurtailment implies curtailment before the start of a dispatch interval. Historical annual dispatch targets (DT_{hist}) are also determined using the persistence and perfect forecasting methods applied to the historical power generation of the wind farm. This enables assessment of the impact of wind generation forecast accuracy on total system performance, and these forecasting methods are explained later in this thesis. Note also that whilst these forecasts are uncertain in practice, the optimisations performed in this thesis remain deterministic. This is for two reasons. First, the price taking assumption in the energy (Section 4.2.1) and FCAS (Section 4.2.2.3) markets, as well as deterministic wind farm generation make that revenue in these markets deter-

ministic. Second, the calculation of CPPs only requires a 5-minute generation forecast. Given deterministic annual generation, the 5-minute forecast is also deterministic, irrespective of the forecasting algorithm. As with the energy, FCAS and generation time series, the 5-minute AWEFS forecast is historical and known a priori. The 5-minute persistence and perfect forecasts can also easily be calculated from the historical generation prior to any optimisations being undertaken.

4.2.2.2 Contingency

The total revenues earned by the wind farm and battery in different raise and lower contingency markets is,

$$R_{Cont} = \sum_{y=1}^{L} \frac{1}{(1+r)^y} \Delta t \sum_{t=1} \left(\sum_{x \in \mathcal{X}_{RCont}} \left[P_{B,x}(t) + P_{wf,x}(t) \right] \pi_x(t) + \sum_{x \in \mathcal{X}_{LCont}} \left[P_{B,x}(t) + P_{wf,x}(t) \right] \pi_x(t) \right). \tag{4.14}$$

4.2.2.3 A simple FCAS market model

Since the FCAS markets are small relative to the energy market, a single wind farm and battery could dominate them and start affecting FCAS market prices. Determining the FCAS prices and competition between market participants needs a model of the energy and FCAS markets in which many different units can bid, and the market operator decides on their enablement, prices and dispatch targets. Such a model is a large effort and out of scope. Thus, the wind farm and battery are considered as price takers in FCAS markets, implying that they have a small share ($\mathcal{S}$) and so do not affect prices,

$$P_{B,x}(t) + P_{wf,x}(t) \leq \mathcal{S} \times D_x(t), \quad \forall x \in \mathcal{X}. \tag{4.15}$$

4.2.3 Battery model

Equation 4.16 shows the total cost of the battery as the sum of its capital expenditure (CAPEX) and operational expenditure (OPEX) over its lifetime. The CAPEX of the battery has two components that cover storage module costs and power related costs. These comprise the power conversion system, the balance of plant and installation costs [122, 180–183]. The OPEX is further divided into fixed and variable O&M costs that

are calculated by equations 4.17 and 4.18.

$$TC_B = \underbrace{Q_B C_{B,E} + P_{B,max} C_{B,P}}_{CAPEX} + \underbrace{FOM_B + VOM_B}_{OPEX}, \tag{4.16}$$

$$FOM_B = \sum_{y=1}^{L} \frac{1}{(1+r)^y} f_B P_{B,max}, \tag{4.17}$$

$$VOM_B = \sum_{y=1}^{L} \frac{1}{(1+r)^y} v_B \sum_{t=1} |E_B(t+1) - E_B(t)|. \tag{4.18}$$

Different battery constraints should be taken into account to make sure it can provide various services reliably and without significant degradation and damage. Equations 4.19 to 4.22 show the power limit of the battery. It should be noted that the battery can offer raise or lower services in the FCAS markets above the power rating. For example, a 1 MW battery which is charging at full capacity can provide up to 2 MW FCAS raise services by immediately stopping charging and instead discharging at the same 1 MW limit if dispatched. This is reflected in equations 4.21 and 4.22.

Contingency services are complementary to one another and designed to support the system frequency once an extreme event occurs in the power system. This feature was explained in Chapter 1, and is formulated in equations 4.23 and 4.24.

$$P_{B,c}(t) \leq P_{B,max}, \tag{4.19}$$

$$P_{B,d}(t) \leq P_{B,max}, \tag{4.20}$$

$$-P_{B,c}(t) + P_{B,d}(t) + P_{B,RReg}(t) + P_{B,RCont}(t) \leq P_{B,max}, \tag{4.21}$$

$$-P_{B,d}(t) + P_{B,c}(t) + P_{B,LReg}(t) + P_{B,LCont}(t) \leq P_{B,max}, \tag{4.22}$$

$$P_{B,RCont}(t) = max\big\{P_{B,R6}(t), P_{B,R60}(t), P_{B,R5}(t)\big\}, \tag{4.23}$$

$$P_{B,LCont}(t) = max\big\{P_{B,L6}(t), P_{B,L60}(t), P_{B,L5}(t)\big\}. \tag{4.24}$$

The energy level of the battery considering its dispatch in the energy and FCAS markets is,

$$E_B(t) = E_B(t-1) + \Delta t\Big[\eta_c P^{net}_{B,c}(t) - \frac{1}{\eta_d} P^{net}_{B,d}(t)\Big], \tag{4.25}$$

where $P^{net}_{B,c}$ and $P^{net}_{B,d}$ denote the net charging and discharging power, respectively. The battery net power is,

$$\begin{aligned} P^{net}_B(t) &= P_{B,c}(t) - P_{B,d}(t) + \alpha_{LReg}(t) P_{B,LReg}(t) - \alpha_{RReg}(t) P_{B,RReg}(t) \\ &+ \rho_{LCont} \sum_{x \in \mathcal{X}_{LCont}} P_{B,x}(t) - \rho_{RCont} \sum_{x \in \mathcal{X}_{RCont}} P_{B,x}(t), \end{aligned} \tag{4.26}$$

where $P_B^{net} > 0$ is associated with charging while $P_B^{net} < 0$ is associated with discharging.

Equation 4.27 guarantees that there is enough capacity in the battery to charge in the energy market and provide all offered FCAS lower services without violation of the state of charge (SOC) limit. Similarly, equation 4.28 guarantees there is enough energy in the battery to discharge in the energy market whilst providing all offered FCAS raise services, again without violation of the SOC limits. Since operation outside the manufacturer's recommended SOC range can damage the battery, these are conservative constraints,

$$SOC_{up} Q_B \geq E_B(t-1) + \Delta t \eta_c \Big[P_{B,c}(t) + P_{B,LReg}(t) + \sum_{x \in \mathcal{X}_{LCont}} P_{B,x}(t) \Big], \tag{4.27}$$

$$SOC_{low} Q_B \leq E_B(t-1) - \frac{\Delta t}{\eta_d} \Big[P_{B,d}(t) + P_{B,RReg}(t) + \sum_{x \in \mathcal{X}_{RCont}} P_{B,x}(t) \Big]. \tag{4.28}$$

Another technical consideration for a battery is the maximum charging and discharging rate relative to its energy capacity, which is defined as C_{rate} parameter. The constraint on C_{rate} parameter of Li-ion battery is,

$$P_{B,max} \leq C_{rate}^{max} Q_B. \tag{4.29}$$

In addition to the SOC and C_{rate}, the number of charging/discharging cycles plays an important role in the battery degradation. The typical number of cycles for a utility scale battery with 10-15 years life time is one per day [122, 130].

$$\begin{aligned} &\sum_{t=t_i}^{t_{i+1}-1} |E_B(t) - E_B(t-1)| \leq 2 N_{cyc} Q_B \quad \forall i \in \{1, 2, ..., 365\}, \\ &t_i = \delta(i-1) + 1, \quad \delta = \frac{24}{\Delta t}, \end{aligned} \tag{4.30}$$

where δ is the number of time intervals in one day (24 hours period) and t_i denotes the starting interval of day i. Finally, all decision variables associated with the battery in the energy and FCAS markets as well as its capacity and the energy level must be non-negative,

$$\begin{aligned} &P_{B,x} \geq 0 \quad \forall x \in \{c, d, RReg, LReg, R6, R60, R5, L6, L60, L5\}, \\ &Q_B, P_{B,max}, E_B \geq 0. \end{aligned} \tag{4.31}$$

4.2.4 Wind farm frequency control model

Wind turbines can participate in the FCAS lower services markets under normal operating conditions by curtailing their power output. However, for providing FCAS raise services, turbines must operate below the Maximum Power Point Tracking (MPPT) curve or modify their control system to implement synthetic inertia. Operating below the MPPT curve creates a margin for turbines to increase their power output if the power system operator requests raise services. Conversely, synthetic inertia does not require precurtailment, but it is a temporary response of a turbine to locally measured frequency deviations which is followed by a recovery period in which the turbine returns to normal operation. This technology cannot comply with any of the current FCAS services in the NEM because it is a temporary response, whereas participation in FCAS regulation markets requires the turbine to maintain services over a 5-minute dispatch interval. Nonetheless, introducing a fast frequency response (FFR) market can incentivise wind farms to have an inertial response as well [102].

This study focuses on FCAS service provision by curtailing wind power generation. Since the market dispatch interval of 5 minutes is much longer than the time scale of the turbine dynamics, as shown in Chapter 3, the response of the wind farm to a power set-point is assumed to be instantaneous. This enables the use of the wind farm models developed in Chapter 3.

The turbine groups in these wind farm models can be controlled in various ways, ranging from controlling them as a single group to controlling them individually. Index g_c in this chapter denotes the set of controlled groups. It is important to distinguish between the turbine groups in the wind farm models (g) and turbine control groups (g_c). Equation 4.33 shows the relationship between the power output of a controlled group and the power output of the turbine groups in the wind farm model.

$$P_{g,mdl}(t) = \sum_{wt \in g} P_{wt,mdl}(t), \tag{4.32}$$

$$P_{g_c}(t) = \sum_{g \in g_c} P_{g,mdl}(t). \tag{4.33}$$

For instance, all turbine groups in a wind farm model with 8 groups can be controlled as a single group. Of course, increasing the degree of controllability of the wind farm brings more benefits, but it is important to quantify its significance. Additionally, greater controllability introduces more decision variables to the optimisation model, which results in greater computational effort.

Equation 4.34 states that the total FCAS services offered by the wind farm is the sum of all offered services of all controlled groups. These controlled groups are independent, and they can offer different FCAS services.

$$P_{wf,x}(t) = \sum_{g_c} P_{g_c,x}(t), \quad \forall x \in \mathcal{X}. \tag{4.34}$$

Similar to equations 4.23 and 4.24, equations 4.35 and 4.36 show the maximum curtailment required for providing raise and lower contingency services for each group.

$$P_{g_c,RCont}(t) = max\{P_{g_c,R6}(t), P_{g_c,R60}(t), P_{g_c,R5}(t)\}, \tag{4.35}$$

$$P_{g_c,LCont}(t) = max\{P_{g_c,L6}(t), P_{g_c,L60}(t), P_{g_c,L5}(t)\}. \tag{4.36}$$

As discussed, the wind farm must operate below the MPPT curve to provide FCAS raise services, i.e. it must precurtail the wind power generation to have the ability to increase its power output during a 5-minute dispatch interval if required. Equation 4.37 shows the amount of wind farm precurtailment for the provision of raise regulation and contingency services.

$$P_{g_c,pcurt}(t) = P_{g_c,RReg}(t) + P_{g_c,RCont}(t). \tag{4.37}$$

The maximum possible requested curtailment ($P^{max}_{g_c,curt}$) that a controlled group might perform occurs when the power system operator calls upon the total amount of FCAS lower services offered by that group. Therefore, the precurtailment and the curtailment related to the FCAS lower services are aggregated, and $P^{max}_{g_c,curt}$ is,

$$P^{max}_{g_c,curt}(t) = P_{g_c,pcurt}(t) + P_{g_c,LCont}(t) + P_{g_c,LReg}(t). \tag{4.38}$$

Wind turbines cannot continuously provide large variations in power output because this can affect mechanical components, especially in the gear-box. Also, light loading can cause stability issues for the turbine's power controller [184]. Therefore, the maximum allowable curtailment limit ($l^{max}_{g_c,mdl}$) is considered for every controlled group,

$$P^{max}_{g_c,curt}(t) \leq \underbrace{\theta_{curt} P_{g_c}(t) - \sigma_{g_c}(t)}_{l^{max}_{g_c,mdl}(t)}, \tag{4.39}$$

where σ_{g_c} is a parameter that denotes the maximum amount of curtailment that turbines in a given controlled group g_c cannot achieve due to the aggregated control of that group.

For instance, if a wind turbine of a controlled group is not spinning while others are generating power, and they are receiving a signal commanding the same amount of curtailment, σ_{g_c} reduces the $l^{max}_{g_c,mdl}$ to consider the deficit of that stationary turbine. However, if all turbines are controlled separately, i.e. the number of controlled groups is the same as the number of turbines, it follows that $\sigma_{g_c} = 0$.

Equation 4.40 shows the calculation of σ_{g_c}. The first term on the right-hand side is the maximum amount of curtailment divided equally between all turbines of a given controlled group, whilst the second term is related to the individual curtailment limit of each turbine. If the maximum curtailment signal exceeds an individual turbine's curtailment limit, the right-hand side of equation 4.40 becomes positive; otherwise, it is zero. The sum of these values for turbines of the same controlled group constitutes the σ_{g_c} of that group.

$$\sigma_{g_c}(t) = \sum_{wt \in g_c} max\Bigg\{ \underbrace{\frac{\theta_{curt} P_{g_c}(t)}{w_{g_c}}}_{\text{Maximum curtailment signal}} - \underbrace{\theta_{curt} P_{wt,mdl}(t)}_{\text{Individual limit}}, 0 \Bigg\}. \tag{4.40}$$

In order to take into account the error of the wind farm model, I calculate the actual maximum allowable curtailment limit ($l^{max}_{g_c,act}$) using the measured power generation of the farm rather than the calculated limit of the modelled power. In equation 4.41, if the $P^{max}_{g_c,curt}$ exceeds the actual wind curtailment limit ($l^{max}_{g_c,act}$), ϵ becomes positive and the wind farm is then penalised using equation 4.9. This can happen because of the overestimation of the wind turbines' power output. However, if the wind farm model underestimates the turbines' power output, the maximum possible curtailment required for FCAS provision can be fulfilled without violation of the curtailment limit, and therefore there will be no penalty cost.

$$\epsilon(t) = \sum_{g_c} max\Big\{0, P^{max}_{g_c,curt}(t) - l^{max}_{g_c,act}(t)\Big\}. \tag{4.41}$$

It should be noted that ϵ is the unfulfilled curtailment if the power system operator requires the maximum curtailment. However, the actual requested curtailment ($P^{req}_{g_c,curt}$) determines the net power injected to the grid. The following equation shows the requested curtailment, considering the wind farm dispatch due to the provision of FCAS regulation services and ignoring the provision of FCAS contingency services, as they are used rarely.

$$P^{req}_{g_c,curt}(t) = P_{g_c,pcurt}(t) - \alpha_{RReg}(t) P_{g_c,RReg}(t) + \alpha_{LReg}(t) P_{g_c,LReg}(t). \tag{4.42}$$

The amount of requested curtailment that cannot be achieved due to the error in the wind farm model is,

$$\tau(t) = \sum_{g_c} \max \left\{ 0, P^{req}_{g_c,curt}(t) - l^{max}_{g_c,act}(t) \right\}, \tag{4.43}$$

where τ denotes the unfulfilled requested curtailment and must be added to the modelled net power (equation 4.3).

Equation 4.44 ensures that the decision variables associated with the wind farm are non-negative.

$$P_{wf,x} \geq 0 \quad \forall x \in \mathcal{X}. \tag{4.44}$$

Finally, the transmission line to which the wind farm and battery are connected has a fixed capacity which is formulated as equation 4.45. If the transmission line capacity is less than the wind farm's potential power output, the wind farm either needs to curtail or use a battery to store the surplus wind power.

$$P_{net}(t) \leq P_{TL}. \tag{4.45}$$

4.3 Development of a linear model of Causer Pays Payments

Figure 4.3 shows an overview of the procedure to calculate CPFs and convert them to CPPs using the FCAS regulation constraint costs. Since AEMO does not make its code for calculating the CPPs publicly available, a full model of the CPM is first presented in Section 4.3.2 and validated by comparing the results to AEMO's published CPFs for the Mt Mercer wind farm. In Section 4.3.3, the causer pays cost recovery methodology used by AEMO is explained and modelled. Finally, a linear model of these procedures is developed.

4.3.1 Data

The data required to calculate the CPFs and convert them to CPPs include the 4-second dispatch data and the FCAS regulation constraints costs in the NEM dispatch engine (NEMDE), which are explained in the following sections.

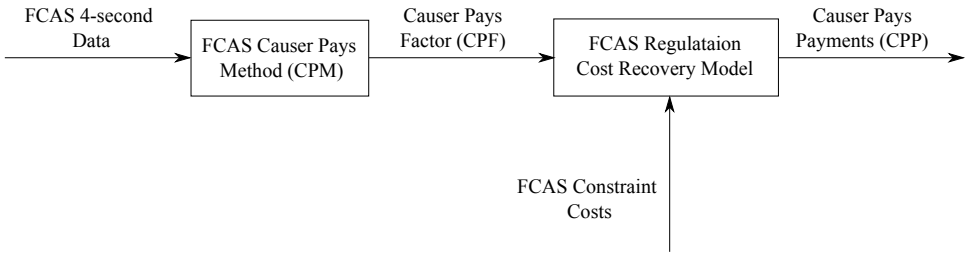

Figure 4.3: Overview of the FCAS causer pays procedure.

4.3.1.1 Causer pays 4-second data

The CPM uses the 4-second dispatch data of all generators and loads in the NEM to calculate their CPFs. This data [185] includes the actual power generation or consumption, dispatch targets, the frequency of the grid and the so-called Frequency Indicator (FI), which quantifies the amount of FCAS regulation services thought required. At each 5-minute dispatch interval, a participant registered in the FCAS regulation market might be enabled to provide FCAS regulation services depending on their offers.

4.3.1.2 FCAS regulation constraint costs

The system operator allocates the FCAS regulation costs to market participants using their CPF and FCAS regulation constraint costs. The market model used by AEMO has various constraints associated with FCAS services. Some of these constraints represent requirements for the whole NEM (global requirements) whilst others represent regional requirements. The costs corresponding to these constraints are updated every 5 minutes and are publicly available [185].

4.3.2 Full model of the causer pays method

AEMO determines a 4-second linear dispatch trajectory connecting two consecutive 5-minute dispatch targets for every participant in the NEM. If a participant deviates from its dispatch trajectory, the CPM then considers the impact of these deviations on system frequency excursions in the normal band (49.85-50.15 Hz). For example, if a participant's deviation from its dispatch target increases the need for regulation services, then it will be assigned a performance measurement factor depending on the size of its deviation. However, if deviations of a participant, except those associated with frequency control response, help the power system to maintain the frequency within the normal band, it does not earn revenues in the FCAS regulation market. AEMO assesses the performance

of all generators and loads every 4 seconds and the final CPFs are calculated based on the average performance over the *sampling period*.

It is important to distinguish between the *sampling* and *application period* in the CPM [18]. The sampling period is a 28-day period for which the CPFs of all participants are calculated, and the application period is a 28-day period in which the previously calculated CPFs are applied to recover the FCAS regulation costs.

4.3.2.1 Model formulation

As discussed, the CPM calculates the deviation from the dispatch target for a given unit and determines the effect of that deviation on the need for regulation services. Since the focus of this study is on wind farms, the CPM is illustrated with a focus on generating units. The deviation for a generating unit is calculated using the following equation every 4 seconds.

$$Dev(t) = P_{act}(t) - DT(t), \tag{4.46}$$

where P_{act} is the actual power generation and DT is the dispatch trajectory. The dispatch trajectory is determined based on the participant categories. In the NEM, participants are classified into non-scheduled, semi-scheduled and scheduled units [186]. A generator is a scheduled unit if the capacity is more than 30 MW and can participate in the central dispatch process managed by AEMO. On the other hand, the non-scheduled units rarely exceed 30 MW power generation, or they have technical difficulties that prevent them from participating in the central dispatch. An intermittent generating unit with a capacity of 30 MW or more is usually classified as a semi-scheduled unit. These units can supply up to their maximum registered capacity, and the system operator can limit their power output in response to network constraints.

Dispatch targets of the scheduled and semi-scheduled units are calculated every 5 minutes. The dispatch target of a semi-scheduled wind farm is determined using the Australian Wind Energy Forecasting System (AWEFS). This system uses the meteorological and wind farm SCADA data to forecast the power output of the wind farm for different forecast horizons ranging from 5 minutes to 2 years [179]. The 5-minute forecast horizon is used to determine the dispatch target of wind farms for the next 5-minute dispatch interval. The dispatch trajectory for scheduled and semi-scheduled units is a straight line connecting two consecutive dispatch targets while for non-scheduled units it is a constant with the value being the initial MW power generation/consumption at the beginning of the corresponding dispatch interval.

To quantify the impact of the deviation on the need for FCAS regulation services, AEMO introduced the Frequency Indicator (FI) parameter which captures the extent to which FCAS regulation services are required to maintain the frequency. The sign of FI indicates the type of the required service (raise or lower). The magnitude of the FI indicates the amount of the required service in MW and is capped at 1560 MW [18].

The registered FCAS regulation providers receive a signal from AEMO through the Automatic Generation Control (AGC) system, which attempts to balance generation and the demand. This signal is updated every 4-second and commands the dispatch of each provider in the FCAS regulation market. The summation of signals transmitted to all FCAS regulation providers gives the FI. Since the Australian mainland and Tasmania are connected through a High-Voltage Direct Current (HVDC) interconnector, AEMO controls the frequency in these regions separately, and therefore the FI values are calculated independently. Since the focus of this study is on the NEM mainland, for the rest of this chapter, FI represents the mainland frequency indicator.

$$FI_{\mathcal{R}}(t) = \sum_{\mathcal{R}} AGC_{Reg}(t), \qquad \mathcal{R} \in \{\text{Mainland, Tasmania}\}. \tag{4.47}$$

The impact of a unit on the frequency of the power system is,

$$PM(t) = Dev(t) \times FI(t), \tag{4.48}$$

where PM is the performance measurement factor. This indicates that the deviation from the dispatch target does not necessarily have a negative impact on the power system frequency. For instance, if a generator is operating below its dispatch trajectory ($Dev < 0$), and the power system frequency is above 50 Hz ($FI < 0$), then the performance of that unit is assessed as positive because it helps the grid to return the frequency to 50 Hz.

According to the required service and the enablement status of a unit, 4-second performance measurements are assigned to different categories shown in Table 4.1. For

Table 4.1: Categories of performance measurement factors.

Category	Condition
Lower enabled factor (LEF)	FI <0
Lower non-enabled factor (LNEF)	FI <0
Raise enabled factor (REF)	FI >0
Raise non-enabled factor (RNEF)	FI >0

most wind farms in the NEM that are not providing FCAS services, only the LNEF and RNEF factors are applicable. At the end of each 5-minute dispatch interval, these factors are averaged separately. Positive factors in each of these categories show that on average, the corresponding unit assisted the power system in the frequency control.

When a contingency event occurs and the frequency for the corresponding dispatch intervals is outside the normal band these factors are excluded from the final CPF calculation. Additionally, if the 4-second FCAS data of a unit in a 5-minute dispatch interval is corrupted, that 5-minute interval must be excluded entirely in the CPF calculation for that specific unit.

At the end of each sampling period, the 5-minute factors are again averaged separately. It is worth noting that this averaging is done for Tasmania and the mainland separately. The averaged factors are then fed into the function f defined as,

$$\begin{aligned} &f(LEF_{4w}, LNEF_{4w}, REF_{4w}, RNEF_{4w}) \\ &= min\Big\{0, \Big[RNEF_{4w} + LNEF_{4w} + min\{0, REF_{4w}\} + min\{0, LEF_{4w}\}\Big]\Big\}, \end{aligned} \tag{4.49}$$

where the subscript $4w$ denotes the 4-week average factor. According to equation 4.49, a positive performance in either LNEF or RNEF category can cancel out the negative performance in the other categories. However, positive REF and LEF factors cannot compensate for negative performance in other categories. Furthermore, if the overall performance of a participant is positive, function f will be zero resulting in zero CPF.

The output of the function f for a scheduled or semi-scheduled unit is denoted as Metered Scheduled or Semi-scheduled Factor (MSF). For non-scheduled units, the Metered Non-Scheduled Factor ($MNSF$) is the output of function f multiplied by a coefficient which magnifies the actual performance of the non-scheduled units to penalise their contributions to the forecast error. The load forecast error (LFE) is computed based on the system deviation factor (SDF) and system forecast error factor (SFF).

$$MSF = f(LEF_{4w}, LNEF_{4w}, REF_{4w}, RNEF_{4w}), \tag{4.50}$$

$$MNSF = (1 + LFE) \times f(LEF_{4w}, LNEF_{4w}, REF_{4w}, RNEF_{4w}), \tag{4.51}$$

$$LFE = \frac{SFF}{SDF}. \tag{4.52}$$

The system deviation factor (SDF) is calculated by averaging the 4-second deviation of the actual demand from a linear trajectory which is determined by fitting a line to the actual demand using the least square method. The system forecast error factor (SFF) is defined as the 28-day average of 4-second deviation of forecast demand trajectory from

that fitted line. The SDF and SFF are calculated as,

$$SDF = f(DLNEF_{4w}, DRNEF_{4w}), \tag{4.53}$$

$$SFF = f(FLNEF_{4w}, FRNEF_{4w}), \tag{4.54}$$

where DLNEF and DRNEF are factors associated with the actual demand deviation from the fitted line and the FLNEF and FRNEF are factors associated with the forecast demand deviation from the fitted line in the lower and raise regulation markets, respectively. These factors are calculated as,

$$DM(t) = FI(t) \times \big[Dem_{line}(t) - Dem_{act}(t)\big], \tag{4.55}$$

$$FM(t) = FI(t) \times \big[Dem_{fcast}(t) - Dem_{line}(t)\big], \tag{4.56}$$

where DM and FM are the 4-second measurement factors and are assigned to the aforementioned raise and lower categories based on the FI sign. The Dem_{fcast} is the demand forecast trajectory connecting two consecutive 5-minute ahead forecast demand.

The aggregated market participant factor ($AMPF$) is used to determine the average performance of each participant as a percentage. The $AMPF$ is,

$$AMPF = \sum_i MSF + \sum_i MNSF + SRF, \tag{4.57}$$

where SRF is the system residual factor and is calculated based on the SDF and SFF.

The market participant factor (MPF) for different participants is determined as,

$$MPF = \frac{MSF}{AMPF}, \qquad \text{for scheduled and semi-scheduled,} \tag{4.58}$$

$$MPF = \frac{MNSF}{AMPF}, \qquad \text{for non-scheduled.} \tag{4.59}$$

To generate a single set of factors for the mainland and Tasmania, the calculated MPFs are normalised according to the average regional demand over the sampling period. The normalised factors are the Causer Pays Factors (CPF) which are published for every 4-week sampling period. Equation 4.60 shows the CPF calculated for a participant located in the NEM mainland.

$$CPF = MPF \times \frac{Dem_{mainland}}{Dem_{Tasmania} + Dem_{mainland}} \times 100. \tag{4.60}$$

If the average performance of a participant is negative, then it is assigned a non-zero CPF; otherwise, the CPF will be zero. The zero CPF implies that the participant's share in FCAS regulation costs recovery for the corresponding application period is zero.

4.3.2.2 Validation

The CPM model is used to calculate the CPFs of the Mt Mercer wind farm for a year and compared to AEMO's published CPFs. Figure 4.4 indicates that the calculated CPFs differ from AEMO's by less than 2% over the year. This small difference is likely due to AEMO excluding certain time intervals from the 28-day period for reasons other than contingency and which is not publicly available.

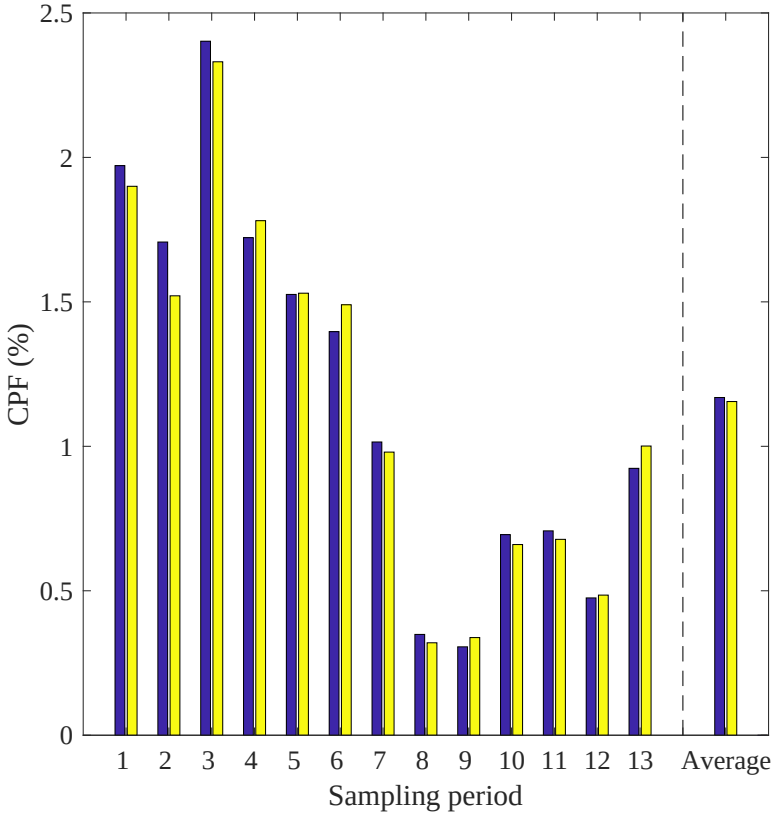

Figure 4.4: Mt Mercer CPFs published by AEMO (blue) and calculated using the full model (yellow) for studied sampling periods along with the annually averaged CPF.

4.3.3 Causer pays costs recovery

AEMO determines a market clearing price for each FCAS service every 5 minutes using the NEMDE. These prices are used to determine the payments to FCAS providers, and these payments are then recovered from the market participants. The recovery method is different for FCAS regulation and contingency services. The FCAS regulation cost,

which is the cost of the binding regulation constraints in the NEMDE, is recovered on the basis of the CPM. To recover this cost from participants in the NEM, the CPFs calculated for the corresponding sampling period are applied. The higher the CPF of a participant in a sampling period, the more it pays in the subsequent application period [16],

$$C_i^X = \Gamma^X \times \frac{MPF_i}{\sum_i MPF_i + \Big(RMPF \times CRMPF\Big)}, \tag{4.61}$$

where C_i^X is the regulation payment of participant i with *MPF* located in the region associated with the constraint X and Γ^X is the costs of that constraint obtained from the NEMDE. In addition, *RMPF* denotes the residual market participant factor, which is scaled to the energy consumption in the related region(s) using the constraint residual market participant factor (*CRMPF*).

$$RMPF = 100 - \sum_i MPF_i, \tag{4.62}$$

$$CRMPF = \frac{\text{Total customer energy in requirement regions}}{\text{Total customer energy in the NEM}}. \tag{4.63}$$

If the global FCAS regulation constraints are binding, then all regions are considered relevant to that constraint and $CRMPF = 1$. However, under special circumstances when the local FCAS regulation constraints are binding, which can happen due to different reasons, such as the loss of interconnectors, the *CRMPF* will be non-unity.

After recovering the cost of binding constraint X from participants with *MPF* in the related region(s), the residual cost is recovered from remaining customers who do not have the MPF. This cost recovery is based on their relative energy consumption,

$$C_j^X = \Gamma_{Res}^X \times \frac{EC_j}{\sum_j EC_j}, \tag{4.64}$$

where C_j^X represents the payment of a participant j without *MPF* for binding constraint X and EC_j is the energy consumption of that participant. Γ_{Res}^X denotes the residual cost of constraint X which is calculated by subtracting recovered costs for participants with *MPF* from the total cost of that constraint,

$$\Gamma_{Res}^X = \Gamma^X - \sum_i C_i^X. \tag{4.65}$$

To calculate CPPs of the Mt Mercer wind farm over the studied period, the costs of FCAS regulation constraints in the NEMDE are used. Since the Mt Mercer wind farm is a participant with *MPF*, the calculated CPFs in the previous section are used in

equation 4.61 to determine the payments for every dispatch interval. The total payments using the AWEFS forecast data, broken down to lower and raise categories, are shown in Figure 4.5. However, the performance of the wind farm in the lower regulation market is superior and on average is positive, but the lower and raise regulation payments are similar. This is because the same CPF, which is calculated based on the average performance in the lower and raise regulation markets, is applied for the cost recovery.

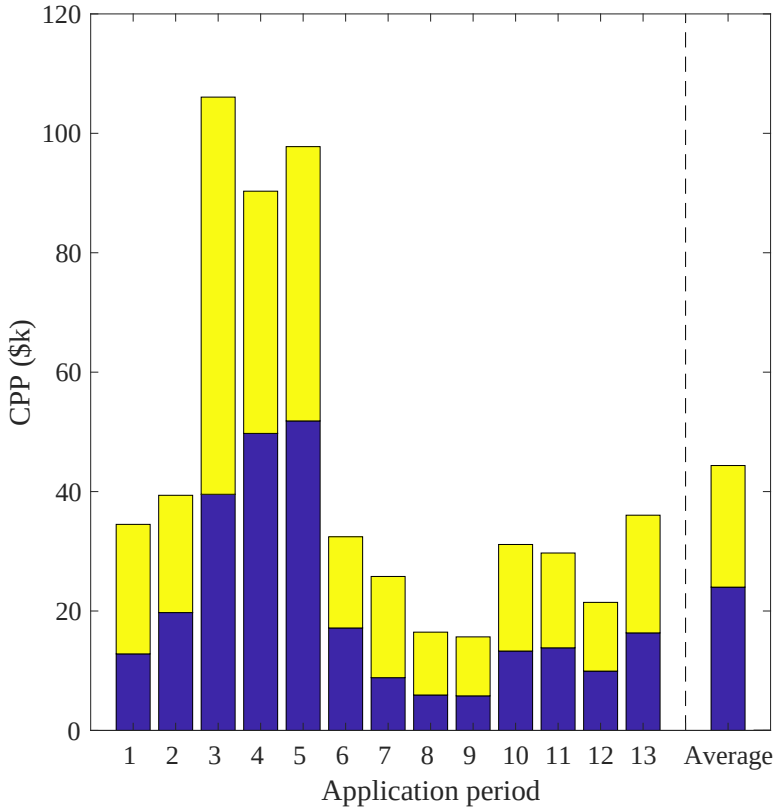

Figure 4.5: Mt Mercer wind farm CPPs in lower (blue) and raise (yellow) FCAS regulation markets in the studied period using the historical AWEFS forecast.

4.3.4 A linear model of the CPM

A simplified, linear model of the CPM is now developed, such that this model can be used in linear programmes, as undertaken earlier in this chapter. The linearisation process involves two phases,

1. A linear model which relates the 28-day performance measurement of a participant to its CPF and
2. A linear model which converts the CPF to the CPP.

For this purpose, the calculated performance measurements and the historical CPFs along with the calculated CPPs are used.

The historical data of two wind farms located approximately 100 km away from each other in Victoria, Australia are used to develop and validate the linear model. Figure 4.6a shows the historical CPFs of the Mt Mercer and Ararat wind farms versus their total 5-minute performance measurements calculated using equation 4.48. Figure 4.6b shows the calculated CPPs using the cost recovery model versus the historical CPFs for each 4-week sampling period. The data points are more scattered in Figure 4.6b, which is due to the large variations in the cost of FCAS regulation. Equations 4.66 to 4.68 show the linear model, which relates the estimated factor (CPF_{lm}) and estimated payments (CPP_{lm}) to the total performance measurement factor.

$$CPF_{lm} = a_1 \times \sum_{28day} PM(t), \tag{4.66}$$

$$CPP_{lm} = a_2 \times CPF, \tag{4.67}$$

$$CPP_{lm} = \underbrace{a_1 \times a_2}_{K_{CPP}} \times \sum_{28day} PM(t). \tag{4.68}$$

The coefficients in these equations (a_1 and a_2) are determined by linear regression. Since the zero performance factor results in zero CPF and CPP, the intercept is set at zero. The values of a_1 and a_2 were calculated as 3.1×10^{-6} and 3.87×10^4, respectively. The fitted lines and the R^2 parameter are shown in Figure 4.6.

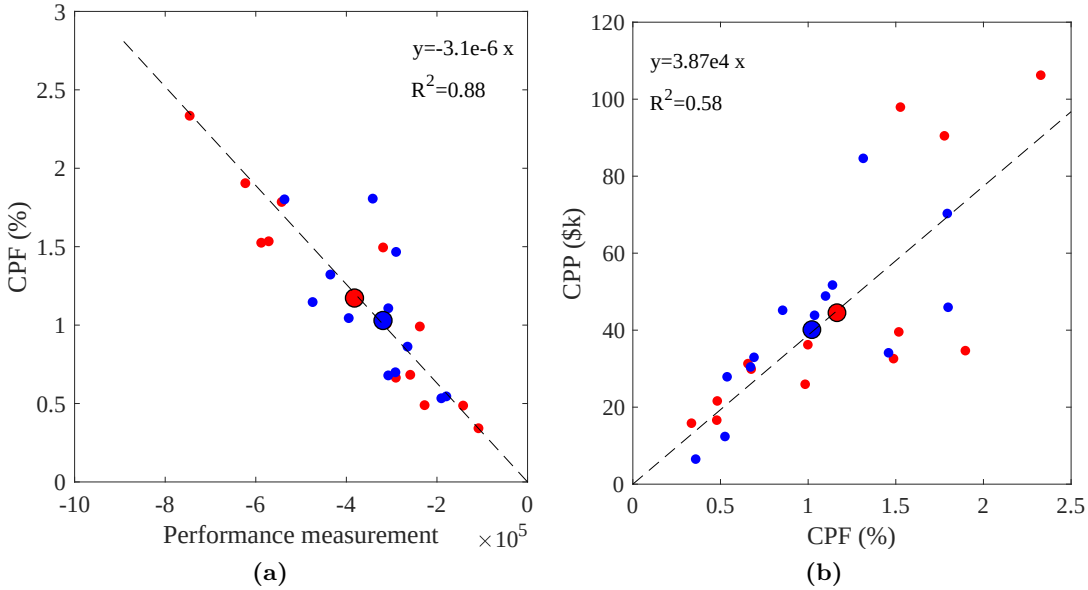

Figure 4.6: 4-week (small dots) and annually averaged (big dots) a) CPF versus performance measurement factor and b) CPP versus CPF for Ararat (blue) and Mt Mercer (red) wind farms.

The linear model is validated against the full annual CPP and average CPF calculated in Sections 4.3.2 and 4.3.3. Table 4.2 indicates that the linear model estimated the annual CPP of the Mt Mercer and Ararat wind farm within approximately 5% of the full model. The yearly average CPF for Mt Mercer and Ararat wind farms differ by approximately 2.5% from the full model. Additionally, the linear model avoids all the non-linearities and complexities in the full CPM and reduces its computation time, being a few minutes for each 4-week period, significantly.

It should nonetheless be noted that the FCAS regulation cost varies for each application period and the performance measurement factors of all participants differ for every sampling period. The coefficients of the linear model must therefore be recalculated for every period investigated.

Table 4.2: The calculated annual CPP and average CPF using the full and linear models.

Wind farm	Parameter	Full	Linear	Difference (%)
Mt Mercer	CPF (%)	1.17	1.20	2.62
	CPP ($k)	576	603	4.72
Ararat	CPF (%)	1.02	1.00	2.40
	CPP ($k)	532	504	5.36

4.4 Summary

This chapter first presented the formulation of a Linear Programme (LP) optimisation model to determine the optimal battery size and dispatch of the wind farm-battery system in the energy and ancillary services markets. In this model, the wind farm was considered as a sunk cost, meaning that it is considered to be already connected to the power system and operating. This optimisation model consists of different sub-models: the energy market, Frequency Control Ancillary Services (FCAS) markets, the battery, wind farm frequency control and a simplified version of the Causer Pays Method (CPM).

The full CPM, which Australia's Independent System Operator uses to calculate the Causer Pays Payments (CPPs) of all participants in the National Electricity Market (NEM) was then described and validated using AEMO's published data. Since these procedures are complex and difficult to integrate into optimisation studies, a linear

model of the full CPM and causer pays cost recovery method was then developed and validated using the actual data of the Mt Mercer and Ararat wind farms.

Chapter 5

Optimal performance of a wind farm when offering energy and ancillary services

5.1 Introduction

Wind farms do not generally optimise their participation in wholesale electricity markets dynamically. However, since a dynamic model of a wind farm has been developed in Chapter 3, this chapter first examines the optimal performance of a wind farm with frequency control capability in the energy and Frequency Control Ancillary Services (FCAS) markets. For this purpose, all terms and constraints related to the battery in the optimisation model presented in the previous chapter are neglected. Different wind farm models, as well as different numbers of controlled turbine groups are studied and, finally, the optimal dispatch of the wind farm is evaluated using the model developed in Chapter 3.

Furthermore, the impact of the wind power forecast accuracy on the performance of the wind farm with and without frequency control is investigated. For this purpose, three different forecasting systems, including the Independent System Operator's Australian Wind Energy Forecasting System (AWEFS) [179], persistence and perfect forecast are used. Unless stated otherwise, the default forecasting system used in this chapter is AWEFS.

5.2 Data

5.2.1 Wind farm power generation

The wind farm's modelled and measured power output are inputs to the optimisation model. The number of turbine groups g in the wind farm model determines the number of time series of the power generation used as inputs, whilst the number of controlled groups g_c determines the number of decision variables associated with wind farm curtailment.

5.2.2 The energy and FCAS markets

In this chapter, the energy and FCAS prices from 2017 are used, as this corresponds to the same period as the wind farm's power output data. Additionally, the yearly data of Victorian enabled capacity for different FCAS services is used. This data is considered as the demand for FCAS services in the region where the wind farm is located.

The yearly Frequency Indicator (FI) data for the FCAS regulation markets is also used. This data is required for the linear model of the Causer Pays Method (CPM) and for estimating the percentage of regulation services used by the power system (α_{LReg} and α_{RReg}).

The Net Present Value (NPV) is calculated using a 6% discount rate over 10 years of the wind farm operation. Table 5.1 presents the input assumptions and parameters used in this optimisation model.

Table 5.1: Input assumptions and parameters used in the optimisation model.

Parameter	Value
r	6%
L	10 years
Δt	5 minutes
$\mathcal{S}$	10%
K_{CPP}	0.12
θ_{curt}	40%
P_{TL}	140 MW

5.3 Performance of the wind farm with frequency control

In this section, the wind farm frequency control is included in the optimisation model to investigate the optimal performance of the wind farm in the energy and FCAS regulation (Reg) and contingency (Cont) markets. The value of avoiding the Causer Pays Payments (CPPs) using the wind curtailment is also calculated, which is denoted as ACPP. I first examine the optimal performance of the wind farm using different numbers of controlled turbine groups, then the different wind farm models developed in Chapter 3 are studied to investigate their performance in the financial analysis of the wind farm.

The optimisation problem was solved using both 5-minute and 4-second dispatch resolution, although the simulations with the finer time resolution are much more computationally demanding. The optimal solutions found with the two different dispatch resolutions had a difference of less than 3%. This is because the prices and enablements are updated every 5 minutes, meaning that once the system is enabled to provide a

certain amount of a specific FCAS service in a 5-minute dispatch interval, it cannot change that amount until the start of next interval. The results presented in the rest of this study are therefore based on 5-minute dispatch resolution.

5.3.1 Impact of wind farm controllability

A wind farm can provide FCAS regulation and contingency services by curtailing its power generation. To achieve this, the wind farm must be controlled, which can be realised in various ways. The 64-group (i.e. each turbine is modelled individually) wind farm model is used here with different numbers of controlled groups to examine the influence of different degrees of wind farm controllability on its optimal performance.

Figure 5.1 shows the changes in revenue by type when the wind farm is optimally controlled as 1, 8 and 16 controlled turbine groups. As a reference, without such forms of participation, the wind farm earns approximately $193M from the energy market only over this same period. It can be seen that the optimal changes in NPV of revenue, broken down into different components, are very similar, suggesting that there is no significant benefit in more distributed control of the wind farm. The main reason for this is that, on average, the amount of FCAS services offered and dispatched by the wind farm is on the order of a few megawatts, which results in only a few hundred kilowatts being assigned to each turbine that can be curtailed without violating its maximum curtailment constraint.

It can also be seen from Figure 5.1 that the wind farm earns less revenue in the energy market due to the curtailment required for the provision of FCAS services, while most of the FCAS revenues are from the FCAS regulation market. The smaller revenue from the FCAS contingency market is because the lower contingency prices are very low, and the raise contingency prices are not high enough most of the time to compensate the wind farm's financial loss in the energy market caused by the precurtailing. The wind farm providing FCAS services also performs better in the CPM, with CPFs reducing, on average, by approximately 25% relative to the wind farm without frequency control. The reduction in Causer Pays Payments (CPPs) is slightly higher for the wind farm with a higher degree of controllability.

5.3.2 Effect of wind farm model accuracy

The different wind farm models developed in Chapter 3 are investigated here to find the reduced order model that is sufficiently accurate for the financial analysis of the wind farm while being sufficiently computationally tractable. Figure 5.2 presents a

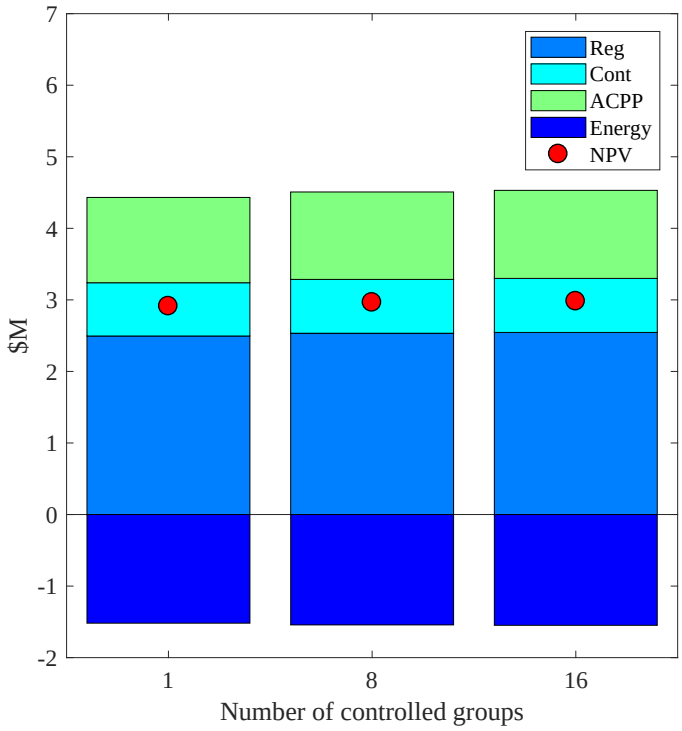

Figure 5.1: Optimal changes in revenue by type for the wind farm with different numbers of controlled groups using the 64-group model of the farm.

comparison of the optimal value of wind farm curtailment using the 1, 8, 16 and 64-group models of the wind farm. The 1-group wind farm model has the lowest NPV, which is due to the large error in the modelled power. As the number of groups in the wind farm model increases, the NPV of optimal performance also increases and tends towards that of the 64-group wind farm model. The difference in NPVs is less than 2% for wind farm models with 8 or more turbine groups, suggesting that the 8-group model is sufficiently accurate for conducting the financial analysis. For the remainder of this thesis, the 8-group model of the wind farm, in which 8 turbine groups are controlled as a single group, is therefore used.

Figure 5.3 shows the wind farm revenue in the FCAS raise and lower regulation markets (RReg and LReg), as well as the FCAS raise and lower contingency markets (RCont and LCont). The wind farm earns most of its FCAS revenue in the lower regulation market. This is because for lower services the wind farm is not required to precurtail the wind generation, hence, the financial loss in the energy market is lower relative to the case of providing raise services. However, the revenue from the lower contingency market is less than that from the raise contingency market, which is mainly due to the significant difference in the prices of these services.

Figure 5.4 shows the dispatch of the wind farm along with offered FCAS services in a 6-hour period with a relatively significant amount of curtailment. Figure 5.4a

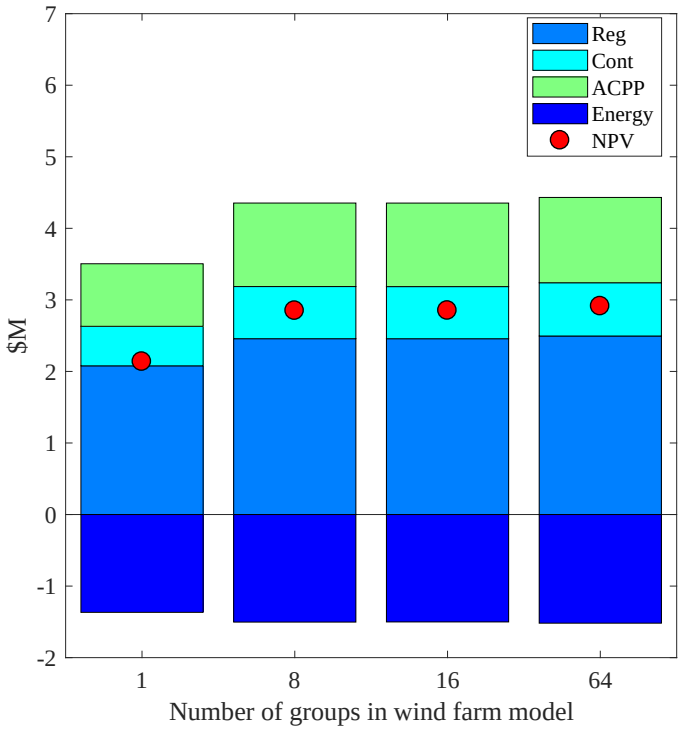

Figure 5.2: Optimal value of wind farm curtailment for different wind farm models, controlled as a single group, in the energy and FCAS markets.

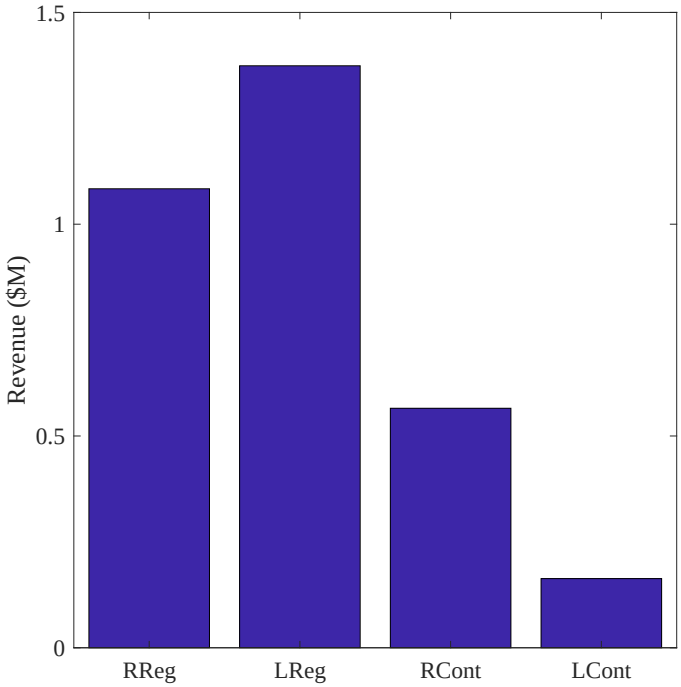

Figure 5.3: Revenues in FCAS regulation and contingency, raise and lower markets using the 8-group wind farm model controlled as single group.

demonstrates the maximum available power generation and the optimal dispatch of the wind farm. It can be seen that the amount of curtailment is high between the fourth and fifth hours when the wind farm is offering a large amount of RReg and RCont services that require precurtailment. Furthermore, the wind farm offers a relatively

small amount of LReg, which is primarily due to the low price. It should be noted that RCont and LCont denote the maximum value of the different types of raise and lower contingency services (6-second, 60-second and 5-minute).

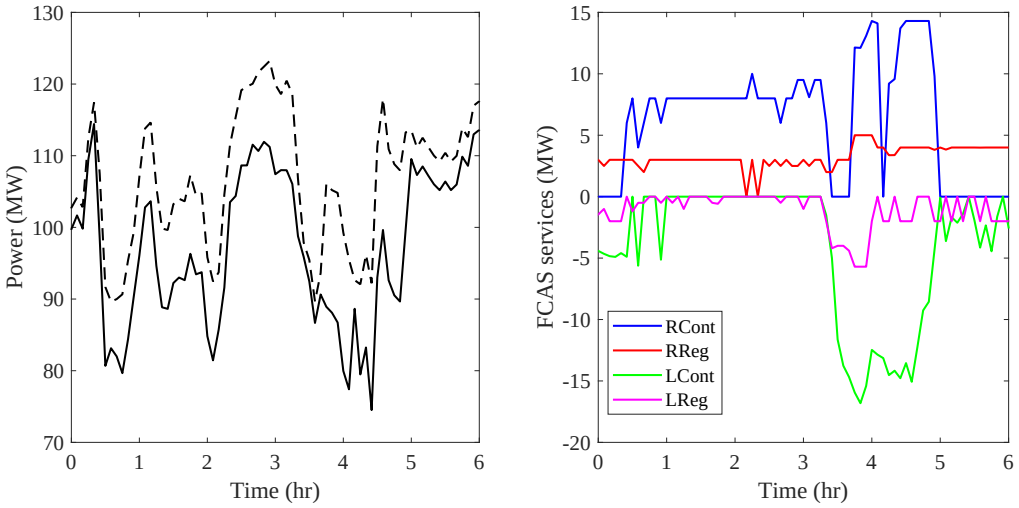

Figure 5.4: a) Wind farm actual maximum available (dashed line) and curtailed (solid line) power generation b) FCAS services offered in a 6-hour period using the 8-group model of the wind farm controlled as a single group.

5.3.3 Technical evaluation of the wind farm optimal dispatch

One of the main concerns about wind farms' FCAS provision is their response time and accuracy in following the Automatic Generation Control (AGC) signal sent by the power system operator. The time resolution of the present optimisation model is 5-minute. However, the wind can change significantly during that 5-minute interval, which could make turbines unable to curtail the correct amount, so that the wind farm would fail to provide the services offered in the FCAS markets. Hence, it is necessary to investigate whether the optimal dispatch obtained from the optimisation model is technically feasible. For this analysis, the curtailment signal sent to turbines is simulated, which requires the information about the amount of precurtailment and the AGC signal received from the power system operator.

To simulate the AGC signal associated with FCAS regulation services, α_{RReg} and α_{LReg} (which represent the amount of raise and lower regulation services used by the power system) are calculated according to the method detailed in the previous chapter. Therefore, the regulation AGC signal received by the wind farm is,

$$AGC_{wf,Reg}(t) = \alpha_{RReg}(t)P_{wf,RReg}(t) - \alpha_{LREG}(t)P_{wf,LReg}(t). \tag{5.1}$$

This approach for simulating the AGC signal has been approved by AEMO [187]. The required wind farm power curtailment at each time instant, considering the precurtailment is,

$$P^{wf}_{curt,cmd}(t) = P_{wf,pcurt}(t) - AGC_{wf,Reg}(t). \tag{5.2}$$

Similarly, the curtailment signal for each turbine ($P^{wt}_{curt,cmd}$) in the wind farm can be calculated. Since the wind farm is controlled as a single group, the total curtailment distributes equally between all the turbines,

$$P^{wt}_{curt,cmd} = \frac{P^{wf}_{curt,cmd}(t)}{w_{g_c}}, \tag{5.3}$$

where $w_{g_c} = 64$ for a single controlled group.

The wind farm model was used to evaluate the optimal dispatch and quantify how well the turbines follow their power set-point. Simulations showed that the wind turbines can follow the power set-point with less than 5% RMSE, thereby confirming that the optimal dispatch of the wind farm is technically feasible without a significant effect on the quality of FCAS services provision in terms of both the response time and the amount of power provided. This also supports the assumption of neglecting the dynamics of the wind farm model in the optimisation model. In fact, the wind turbine pitch angle control system is fast enough to achieve a new set-point which is updated every 4 seconds.

The performance of a single wind turbine during a 30-minute sample period with a relatively high amount of curtailment and wind fluctuations is shown in Figure 5.5. Figure 5.5a presents the maximum available power, power set-point considering the curtailment and simulated power generation over this time period. It can be seen that the simulated power output of the single wind turbine is able to closely follow the power set-point, which is achieved by fine adjustment of the pitch angle of the turbine blades, as shown in Figure 5.5b.

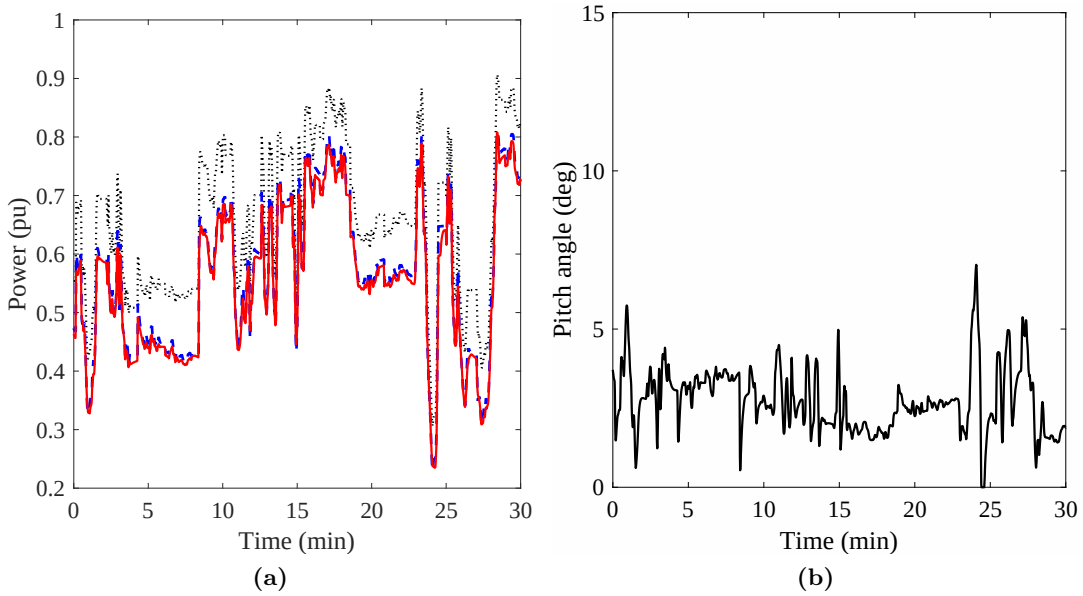

Figure 5.5: a) Maximum available power (black), power set-point (blue) and simulated power (red) b) pitch angle in a 30 minutes sample period.

5.4 Impact of wind forecast accuracy on wind farm's performance

In this section, the impact of the forecast error on the performance of the wind farm without frequency control is examined. Then, the impact of the forecast error on the optimal performance of the wind farm with frequency control is investigated.

5.4.1 Wind farm without frequency control

To examine the impact of the forecasting system on the wind farm's performance in the CPM, persistence and perfect forecast methods are used to determine new dispatch targets based on historical power generation data. The persistence forecast assumes that the power generation of a wind farm at time $t + \Delta t$ is the same as it was at time t. This method can be reasonable for forecasting up to a few hours, and its performance then deteriorates rapidly for longer time horizons [188, 189].

Figure 5.6 shows the calculated CPFs using the AWEFS, persistence and perfect forecast method for determining the dispatch targets of the wind farm over the studied period. The persistence method reduces the wind farm's CPFs significantly, which consequently leads to lower CPPs. Table 5.2 shows the annual Root Mean Square Error (RMSE) and Mean Absolute Error (MAE) of these two forecasting systems. The average performance of the persistence method is approximately 25% better than the

AWEFS, and this results in approximately a 60% reduction in the average CPF. The perfect forecast reduces the CPFs on average by approximately 85%. This highlights the importance of wind forecasting system accuracy and its impact on the financial performance of wind farms in the FCAS CPM.

It should be noted that the dispatch targets in the CPM are updated every 5 minutes and the dispatch trajectory that a wind farm should follow is a line connecting two consecutive dispatch targets. However, the power generation of a wind farm is likely to deviate from the linear trajectory during a 5-minute interval. Therefore, even with a perfect forecasting system, the wind farm's CPFs are not zero.

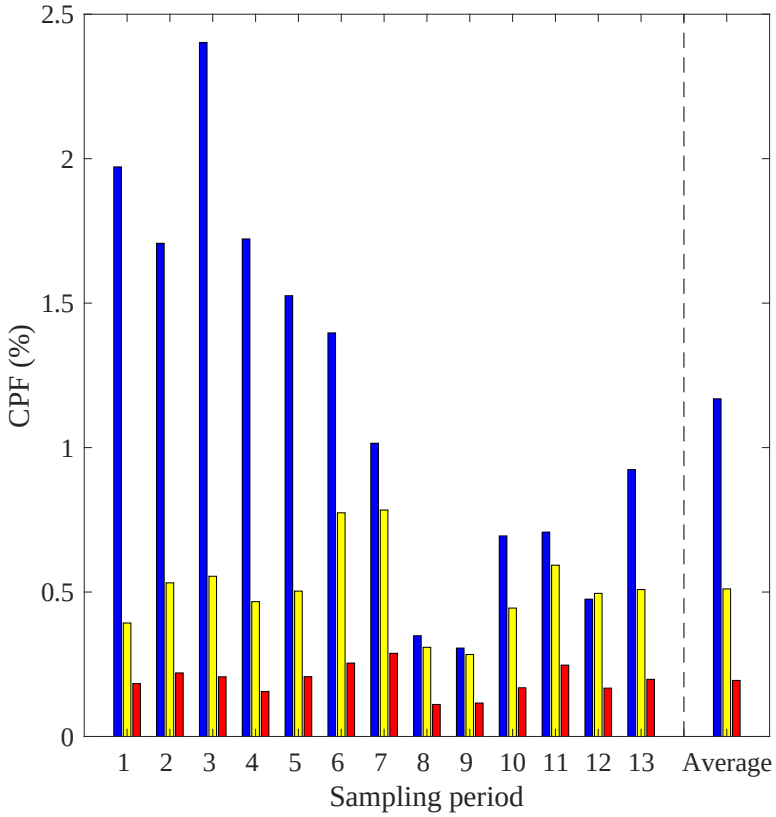

Figure 5.6: Calculated CPFs for the Mt Mercer wind farm over the studied period using AWEFS (blue), persistence (yellow) and perfect (red) forecasting methods.

Table 5.2: The error in the persistence and AWEFS forecasting system.

	RMSE (MW)	MAE (MW)
Persistence	3.94	2.14
AWEFS	5.66	2.76

Figure 5.7 shows the 28-day average RNEF and LNEF factors of the Mt Mercer wind farm using the AWEFS, persistence and perfect forecast systems for the same periods as the calculated CPFs. Interestingly, the performance of the wind farm in the lower

regulation market using the AWEFS is positive for some of the sampling periods. In other words, the wind farm helps the power system when the frequency is above 50 Hz and reduces the need for lower services. Over the year, the performance of the wind farm in the lower market is positive whilst it is more negative in the raise regulation market. This is mainly due to the overprediction of the wind power generation because with a better forecasting system such as persistence, on average, the performance of the wind farm in the raise and lower regulation markets is similar.

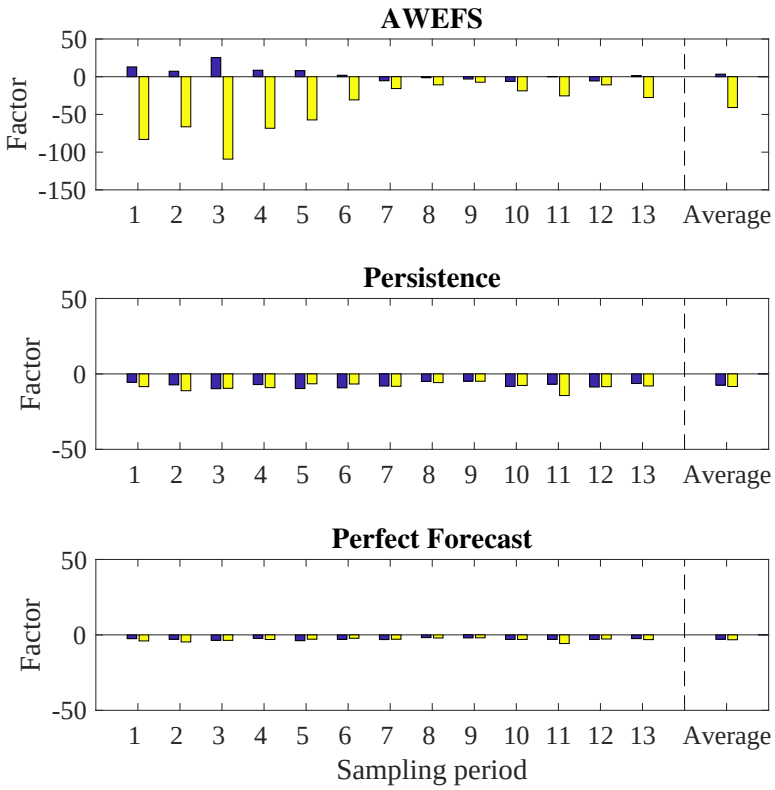

Figure 5.7: RNEF (yellow) and LNEF (blue) factors of the Mt Mercer wind farm over the studied sampling periods along with the annually averaged values using the AWEFS, persistence and perfect forecasting methods.

Figure 5.8 shows the distribution of the 5-minute performance measurement factors using the AWEFS, persistence and perfect forecasting systems. These show that for a large proportion of time the performance measurement factors are close to zero for all forecasting systems. Nevertheless, the factors are slightly high for the persistence and perfect forecasts, relative to AWEFS. In addition, the distribution corresponding to the AWEFS is skewed to the left, which indicates that the extremely negative performance factors occur more frequently compared to extreme positive factors. The main discrepancy between the distributions using these forecasting systems is in the left tail where the performance factor is most negative. These extreme factors occur more frequently using the AWEFS forecast. In other words, the large deviations of the wind farm from its dispatch target determined by AWEFS in relatively few periods of time contributed to a

large proportion of the final CPFs. Therefore, improving the accuracy of the forecasting system in those relatively rare periods will result in considerable financial benefits.

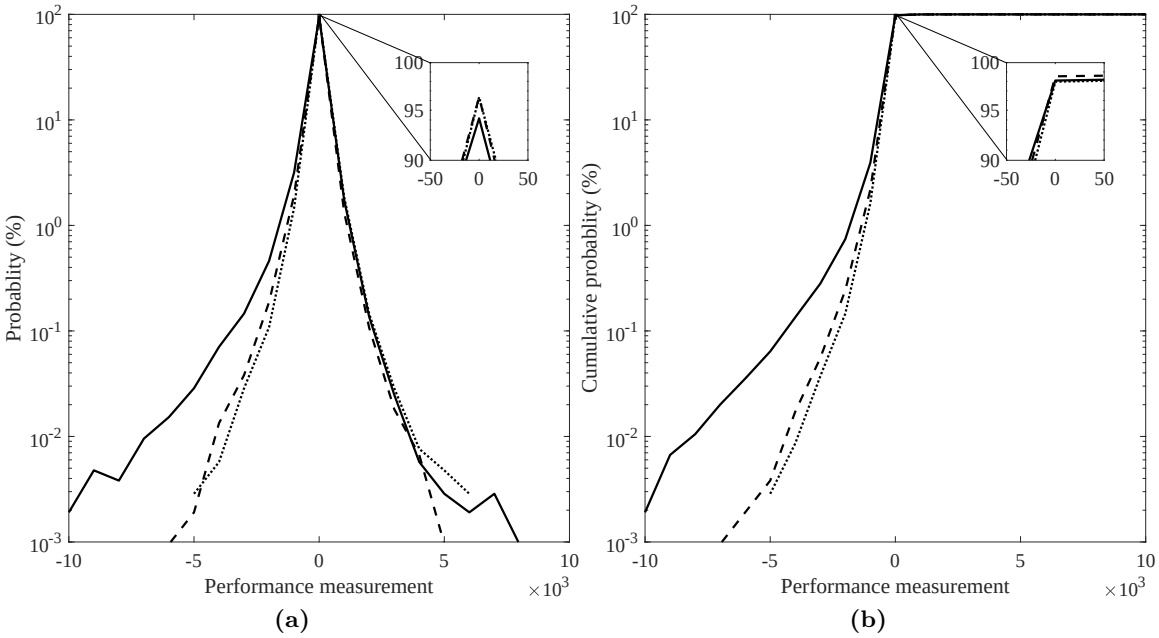

Figure 5.8: a) Probability distribution and b) cumulative distribution of the 5-minute performance measurement factors over the year using the perfect (dotted), persistence (dashed) and AWEFS (solid) forecasting.

The Mt Mercer CPPs using the persistence and perfect forecast are shown in Figure 5.9. On average, the CPPs reduced by approximately 55% and 85% using the persistence and perfect forecasting, respectively. The significant reduction in the annual CPPs with the use of improved forecasting systems also has a considerable impact on the wind farm performance over 10 years. Figure 5.10 shows the NPV of the wind farm without frequency control using the AWEFS, persistence and perfect forecasting system. The revenue in the energy market in all cases is the same and the difference is in the payments in the regulation market. The more accurate the forecasting system, the lower the wind farm's CPPs . The difference between the NPVs resulting from the different forecasting methods indicates the value of improving wind generation forecast.

5.4.2 Wind farm with frequency control

In this section, the impact of forecast accuracy on the optimal performance of the wind farm with frequency control in the energy and FCAS markets is investigated. For this purpose, the persistence and perfect forecast systems are again assessed, and the results are compared with those of AWEFS.

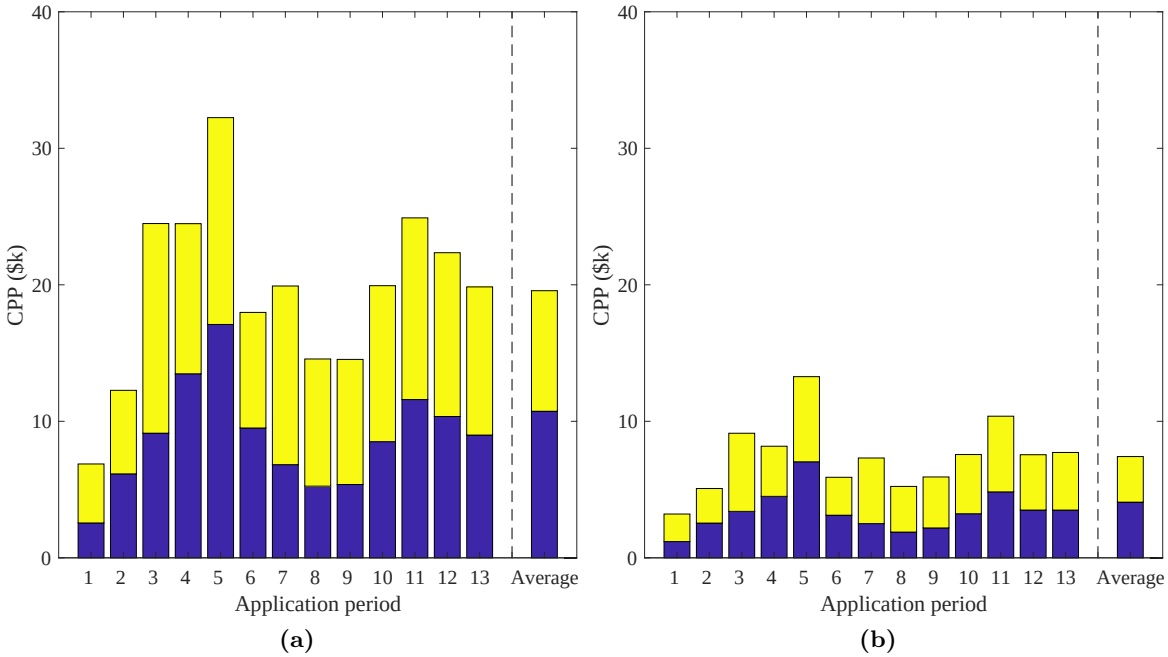

Figure 5.9: Mt Mercer wind farm CPPs in lower (blue) and raise (yellow) FCAS regulation markets in the studied period using a) the persistence forecast and b) the perfect forecast method.

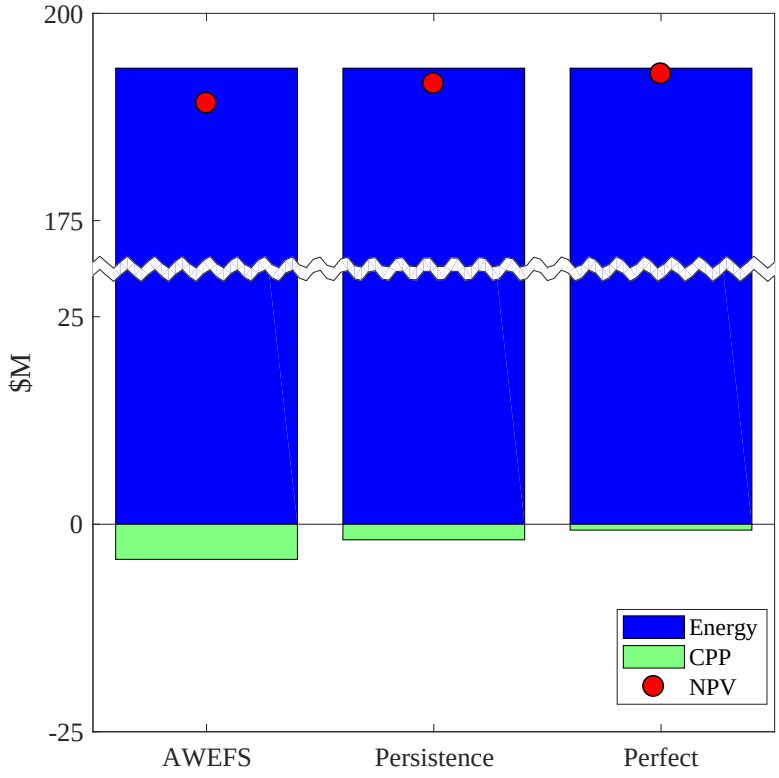

Figure 5.10: Performance of the wind farm without frequency control over 10 years using different forecasting system.

Figure 5.11 shows the NPV of total revenues that the wind farm can earn in the energy and FCAS markets over 10 years. Comparison between Figure 5.10 and 5.11 shows that the effect of implementing frequency control in the wind farm is to increase

its NPV. Again, as the forecast system improves, the performance of the wind farm will also improve, which is mainly due to the reduced payments in the regulation market for deviation from the dispatch target.

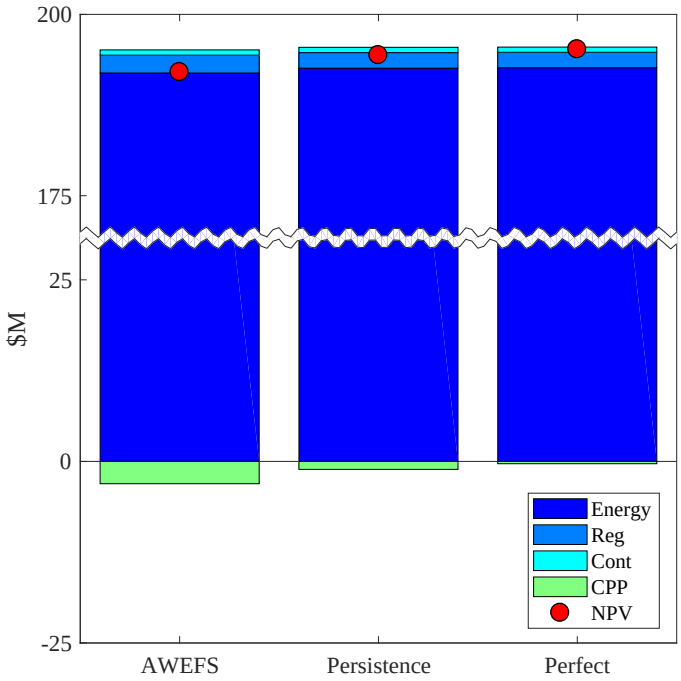

Figure 5.11: Optimal performance of the wind farm with frequency control over 10 years using different forecasting systems.

Figure 5.12 shows the NPV of the wind farm curtailment, which is the difference between the results shown in Figure 5.11 and 5.10. The value of avoided CPPs (ACPP) reduces significantly as the forecasting systems improve. This is because with a more accurate forecasting system the deviation of the wind farm from its dispatch target, and consequently its CPPs reduce therefore there are fewer opportunities and benefits in curtailing the wind generation (Figure 5.13). In fact, the wind farm tends to curtail not only for FCAS provision, but also for improving its performance in the CPM by minimising its deviations from the dispatch target. Comparison of the NPVs of these different forecasting systems reveals that the uncertainty in wind forecasting creates more value for wind farm curtailment.

In a broad view, if the power system operator has perfect information about wind farms generation, it will coordinate the unit commitment and avoid assigning additional reserves to cope with wind uncertainty. Therefore, there are fewer benefits associated with wind generation curtailment to mitigate its fluctuations or provide FCAS services.

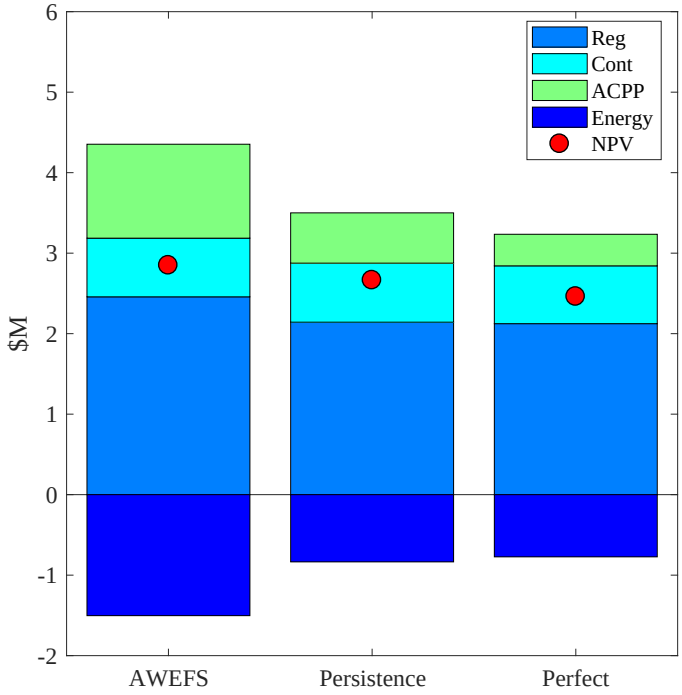

Figure 5.12: Optimal value of wind curtailment using the AWEFS, persistence and perfect forecasting systems.

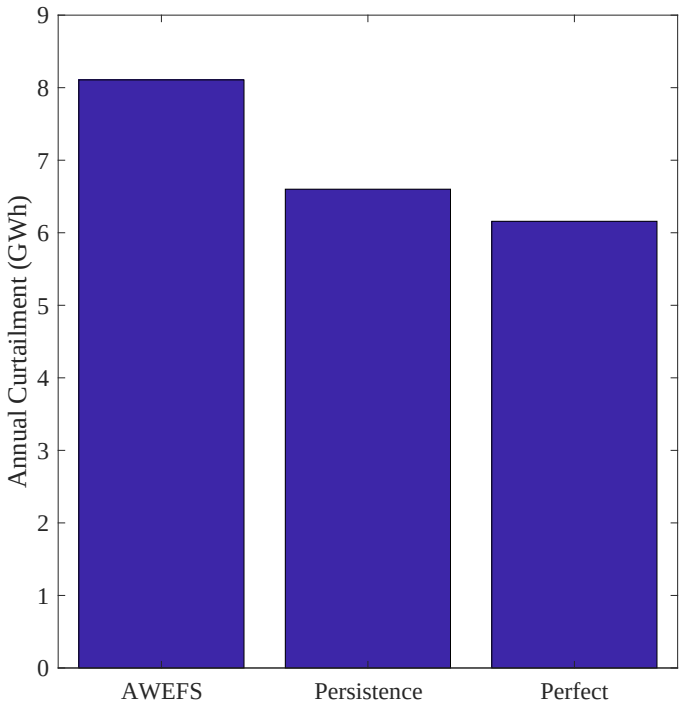

Figure 5.13: Annual wind generation curtailment of the wind farm using the AWEFS, persistence and perfect forecasting systems.

5.5 Summary

This chapter first examined the optimal performance of a wind farm without and with frequency control capability. The problem was formulated as a linear programme (LP),

maximising the Net Present Value (NPV) of the wind curtailment in the energy and FCAS markets. Historical data from the Australian National Electricity Market (NEM) along with the modelled and measured power generation of the wind farm, presented in Chapter 3, were used.

The performance of the wind farm with different numbers of controlled groups was first investigated. The results showed that increasing the degree of controllability of the wind farm curtailment improves its performance only slightly. Additionally, the effect of the wind farm modelling error was studied by comparing the optimal solutions using different wind farm models. It was found that the objective value for models with 8 or more turbine groups was very similar, suggesting that the 8-group model is sufficiently accurate for the financial analysis conducted in this study, while also being computationally tractable.

Further examination of the wind farm's frequency control service provision showed that the wind farm can benefit comparatively more from providing FCAS lower regulation services than from providing other types of FCAS services. This is due to the relatively high price of the lower regulation service in these historical studies and it is not requiring of precurtailing of wind generation. An evaluation of the technical feasibility of wind turbines following the optimal dispatch found that the wind turbines can follow the optimal power set-point with RMSE less than 5%. This small error is likely due to the time delay in the pitch angle controlling system.

The impact of wind forecast accuracy on the performance of the wind farm was then studied using the historical data from the Australian Wind Energy Forecasting System (AWEFS), persistence and perfect forecasting. This analysis showed that the relatively poor performance of AWEFS, which is used by AEMO to determine dispatch targets for wind farms, caused high Causer Pays Factors (CPFs) in some periods, with some of these periods contributing to a large proportion of the final CPFs. Remarkably, a simple persistence forecast was 25% more accurate than AWEFS and reduced CPFs by approximately 60%. This demonstrates the benefits of a better wind forecasting system.

Given this finding, the impact of forecast accuracy on the optimal performance of the wind farm with frequency control was then examined. The results showed that a better forecasting system resulted in superior performance of the wind farm in the electricity market, mainly due to the reduced Causer Pays Payments (CPPs). However, the results also showed that wind generation curtailment has less value in the presence of a better forecasting system. Therefore, as the wind generation forecasting system becomes more accurate, there are fewer opportunities in curtailing wind generation for the purpose of avoiding CPPs and earning FCAS revenue.

Chapter 6

Optimal integration of battery storage into a wind farm

6.1 Introduction

This chapter examines the optimal sizing and performance of a lithium-ion (Li-ion) battery integrated into a wind farm, with both the battery and the wind farm participating in the energy and Frequency Control Ancillary Services (FCAS) markets. First, the performance of the wind farm-battery system without wind farm frequency control is investigated. Then, wind farm frequency control capability is included in the optimisation model to study its impact on the battery investment and the performance of the entire wind farm-battery system. A sensitivity study of the battery's investability under different capital cost and FCAS price scenarios is also conducted. Finally, the impact of wind power forecast accuracy on the battery investment is studied. As in the previous chapter, the Australian Wind Energy Forecasting System (AWEFS), along with the persistence and 5-minute ahead perfect forecasting systems are used.

6.2 Data

As shown in the previous chapter, the 8-group wind farm model controlled as a single group is sufficiently accurate for conducting the present financial analysis, and therefore is used again in this chapter. The FCAS prices data of 2015 and 2017 is used to perform the sensitivity analysis. The technical and cost specifications of the Li-ion battery are also used as input parameters to the optimisation model.

6.2.1 The energy and FCAS markets

As mentioned in Chapter 1, the Australian National Electricity Market (NEM) has experienced a significant increase in FCAS prices since 2015. However, future FCAS market prices will be subject to the supply and demand for regulation and contingency services in the network. For example, greater participation of technologies such as batteries and flexible loads will potentially lead to lower FCAS prices. Furthermore, improving the forecasting of demand and renewable power generation reduces the need for FCAS services and thus will also potentially reduce prices. Two FCAS price scenarios are therefore used in this study to investigate their impact on battery investment. These scenarios are the Victorian FCAS prices for 2015 and 2017, which exhibited the lowest and highest prices in recent years, respectively. Table 6.1 shows the average price of different FCAS services for these years in Victoria. The energy market price of 2017 is also used.

Table 6.1: Average prices of FCAS services ($/MWh) in Victoria for 2015 and 2017 [7].

FCAS service	2015	2017
Raise regulation	1.9	27
6-second raise contingency	1.3	10
60-second raise contingency	1	5
5-minute raise contingency	1.7	6.5
Lower regulation	0.9	20.7
6-second lower contingency	0.05	0.02
60-second lower contingency	0.16	0.05
5-minute lower contingency	0.67	0.24

6.2.2 Battery specifications

The battery cost is usually reported as a price per unit of energy storage capacity ($/kWh). However, for this study, the battery capital cost is comprised of two components, one related to each of the energy and power capacities, since the costs of different sub-systems (battery modules, inverters, balance of plant, installation, etc.) will have different dependencies. Thus, total costs will depend on both the total storable energy (i.e. kWh) and the total power in/out (i.e. kW). These costs for Li-ion batteries, as reported in various studies, are summarised in Table 6.2, and show a large degree of variation. Since the cost of battery modules has fallen significantly in the last decade, whilst that of the balance of plant and installation has fallen to a lesser extent, the more recent studies in Table 6.2 are used to estimate a reasonable reference battery cost for this study. Given the significant variations in Table 6.2, it is appropriate to undertake scenario-based analysis using battery costs as a key input, as this chapter presents.

Table 6.3 shows all the other battery parameters used in this study. A range of Fixed and Variable Operation and Maintenance costs (FOM and VOM) have been reported for utility scale Li-ion batteries from 5-12 $/kW and 0.0011-0.0046 $/kWh, respectively [122, 181, 190]. An average value is therefore used in this study.

Deep charging and discharging of a battery can have an adverse impact on its useful life. Therefore, battery technologies usually have a recommended upper and lower State of Charge (SOC) thresholds to prolong the lifetime of the technology. For example, the recommended SOC range for Li-ion batteries is often 10-90% [180, 181]. Moreover, for Li-ion batteries $C_{rate}^{max} \leq 1$ is a typical rate recommended by manufacturers [181]. The typical lifetime for a utility scale Li-ion battery, operating in the recommended SOC

Table 6.2: Capital cost of utility scale Li-ion batteries.

Source	Energy-related ($/kWh)	Power-related ($/kW)	Year
Sandia [122]	846-1533	492-811	2015
CSIRO [190]	440-560	514-1410	2015
NRECA †[180]	775-1080	-	2017
NYSERDA [191]	490-700	940-1050	2017
Lazard† [128]	540-685	-	2017
IRENA§ [192]	800-1470	-	2017
Bloomberg ‡ [135]	273	-	2017
EIA § [193]	560-1890	-	2018
NREL [183]	300	550-685	2018
PacifiCorp [194]	210-525	868-1470	2018
Reference values	400	600	

*All are in Australian dollar
†Four hours of storage
‡Cost of storage module only
§Two hours of storage

range and with the typical number of daily cycles, is 10 years [182, 190]. It should also be noted that a 6% discount rate is used here to calculate the Net Present Value (NPV) of the system.

Table 6.3: Input assumptions and parameters used in the optimisation model.

Parameter	Value
r	6%
L	10 years
Δt	5 minutes
η_d, η_c	92.2%
$\mathcal{S}$	10%
K_{CPP}	0.12
f_B	9 \$/kW-year
v_B	0.0027 \$/kWh
C_{rate}^{max}	1
SOC_{up}	90%
SOC_{low}	10%
N_{cyc}	1
θ_{curt}	40%
P_{TL}	140 MW

6.3 Optimal performance without wind farm frequency control

In this section, the optimal performance of a wind farm-battery system without wind farm frequency control is examined. Since relatively few wind farms in Australia have frequency control capability, this study investigates whether installing batteries in such wind farms is a financially viable investment. In Section 6.3.1, the optimal performance of the battery in the energy-only market is studied, followed by Section 6.3.2, which considers its participation in FCAS markets as well.

6.3.1 Battery in the energy-only market

To study the optimal performance of the wind farm-battery system in the energy-only market, constraints and terms associated with FCAS markets explained in Chapter 4 are excluded from the optimisation model. The financial viability of the battery in the energy market depends only on the spot price volatility, i.e. the more volatile the price becomes, the more revenue the battery can generate.

Simulations indicate that the Li-ion battery is not investable with its current capital cost and in the absence of subsidy, i.e. its optimal size is zero. Table 6.4 presents the results of a sensitivity study to determine the required capital cost for a Li-ion battery system to achieve a 10% Internal Rate of Return (IRR) in the energy-only market. It can be seen that the Li-ion cost would need to reduce by about 85% of current values to achieve this IRR, or equivalently, an 85% subsidy would be required.

The optimal power capacity of the battery (48.6 MW) shown in Table 6.4 is relatively large compared with the wind farm capacity (132 MW). If the transmission constraint is not binding, the larger the battery, the more profit it earns by providing arbitrage. For example, a 2MW / 2MWh battery earns twice the arbitrage revenue of a 1MW / 1MWh battery, but costs double. Therefore, the NPV of the larger battery is twice that of the smaller, but their IRR is the same. Since the objective function of the present model maximises the NPV, the optimal solution is the larger battery. In addition, the optimal C_{rate} for the battery is approximately 0.38, which is equivalent to 2.6 hours of storage at the rated power. This is because the energy capacity of the battery plays a more significant role than the power rating, due to the need for the battery to store relatively cheap electricity for hours, and then to sell the electricity when the price is higher.

Table 6.4: Required energy ($C_{B,E}$) and power related ($C_{B,P}$) capital cost for the Li-ion battery to achieve an IRR of 10% in the energy-only market.

$C_{B,E}$ (\$/kWh)	$C_{B,P}$ (\$/kW)	NPV (\$M)	Capacity (MWh)	Power rating (MW)
60	90	2.97	125.5	48.6

6.3.2 Battery in the energy and FCAS markets

In this section, the optimal performance of the battery in the energy and FCAS markets is examined. For this purpose, the terms related to the battery's participation in FCAS markets are included in the model while terms corresponding to the wind farm FCAS provision are neglected. Two battery capital cost scenarios are considered: 100% and 50% of the reference values (Table 6.2), together with the two FCAS price scenarios using the 2015 and 2017 market data. This results in a total of 4 scenarios:

- High capital cost-low FCAS prices (HC-LF),
- High capital cost-high FCAS prices (HC-HF),
- Low capital cost-low FCAS prices (LC-LF),
- Low capital cost-high FCAS prices (LC-HF).

These four scenarios are selected to cover an estimated, reasonable future range of market conditions.

As expected, simulations show that the most favourable investment scenario for the battery incorporated into a wind farm participating in the energy and FCAS markets is the LC-HF scenario, while HC-LF is the least favourable. In this case, the battery synergistically benefits the wind farm by not only providing ancillary service revenues but also by reducing the plant's Causer Pays Factors (CPF) (as shown in Figure 6.1) by decreasing the deviations of the wind farm power output from its dispatch target. Therefore, financial analysis of the optimal performance of the battery in the energy and FCAS markets first requires the calculation of the new CPFs and Causer Pays Payments (CPPs) with the full model of the Causer Pays Method (CPM). Figure 6.1 demonstrates a significant decrease in yearly average CPFs of the wind farm with the introduction of the battery and its participation in FCAS markets. These results show that even a small battery (Figure 6.2c) could reduce the CPFs significantly.

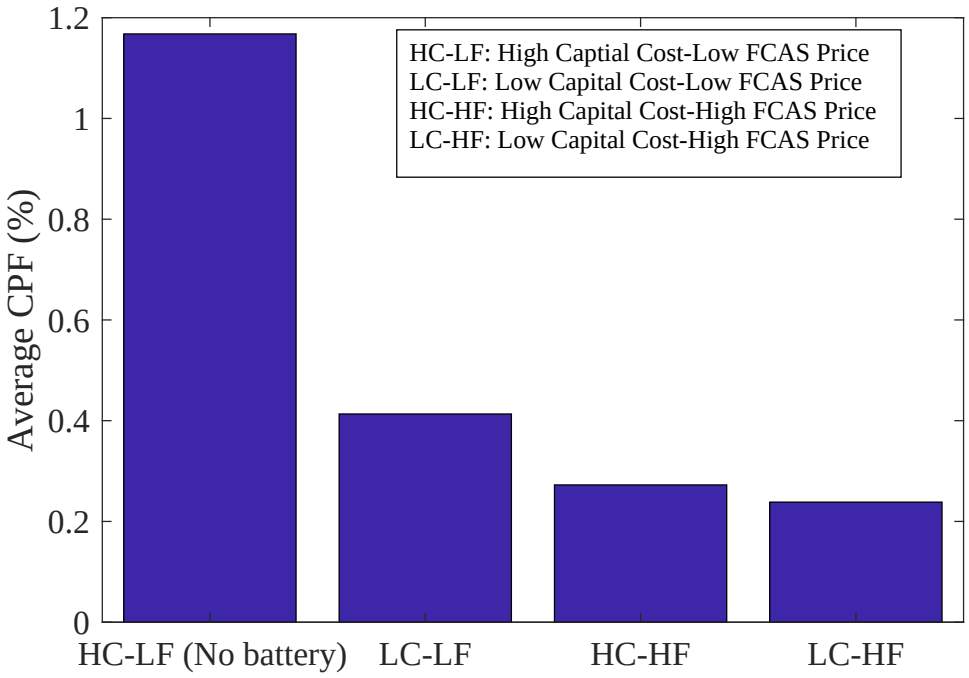

Figure 6.1: FCAS annually averaged CPF before and after battery FCAS provision calculated with the full model of the CPM.

Results of the financial analysis performed for the optimal solution of the four different capital cost-FCAS price scenarios, along with the optimal battery capacity and power rating, are shown in Figure 6.2. Despite the small size of the FCAS markets in comparison to the energy market, they impact the optimal solution significantly, and battery investability is highly sensitive to FCAS prices. For example, a Li-ion battery with the current capital cost was found to be an attractive investment with an IRR of approximately 20% if 2017 FCAS prices data are used. However, if FCAS prices return

to their historically low levels, as seen in 2015, this investment no longer had a positive IRR and the optimal capacity was again zero. However, if the battery capital cost is halved and the FCAS prices return to the 2015 level, an IRR of approximately 6% can be achieved.

These results are thought significant for any investment in batteries because the participation of new entrants into the FCAS markets should reduce FCAS prices, potentially leading to poor financial performance for battery investments throughout the wholesale market. However, the high IRRs for high FCAS price scenarios imply that the battery earns most of its value in the first few years. Overall, these results highlight the importance of modelling the FCAS markets, which are much smaller than the energy market and thus more sensitive to participant entry and withdrawal, in order to better estimate battery investment risk. Such modelling is beyond the scope of this thesis, and thus the price taker assumption stated in Chapter 4 is used.

The results in Figure 6.2a also show that the battery earns more revenue in the FCAS contingency markets relative to the regulation markets. This is likely due to the larger number of contingency markets, including fast, slow and delayed, as well as the fact that the battery offers the maximum possible amount of contingency services most of the time. Additionally, among the four scenarios, the battery always has $C_{rate} < 1$ for the LC-HF and LC-LF, which is likely due to the battery providing more arbitrage in the energy market relative to other scenarios and, as discussed in the previous section, the importance of the battery energy capacity is greater than the power rating for the provision of this service.

Figure 6.3 shows the battery energy level and FCAS services offered during one 6-hour period with large variations in SOC using the HC-HF scenario. Since the contingency services are rarely used, the battery tends to offer the maximum amount that it can provide. It should be noted that RCont and LCont represent the maximum value of the different raise and lower contingency services (6-second, 60-second and 5-minute) offered by the battery, respectively. Despite the battery offering FCAS raise regulation (RReg) between hours 2 to 4, its SOC increases during this time. The reason this occurs is that the battery is charging in the energy market, which provides an opportunity to offer raise services without discharging the battery and only by reducing the amount of charging.

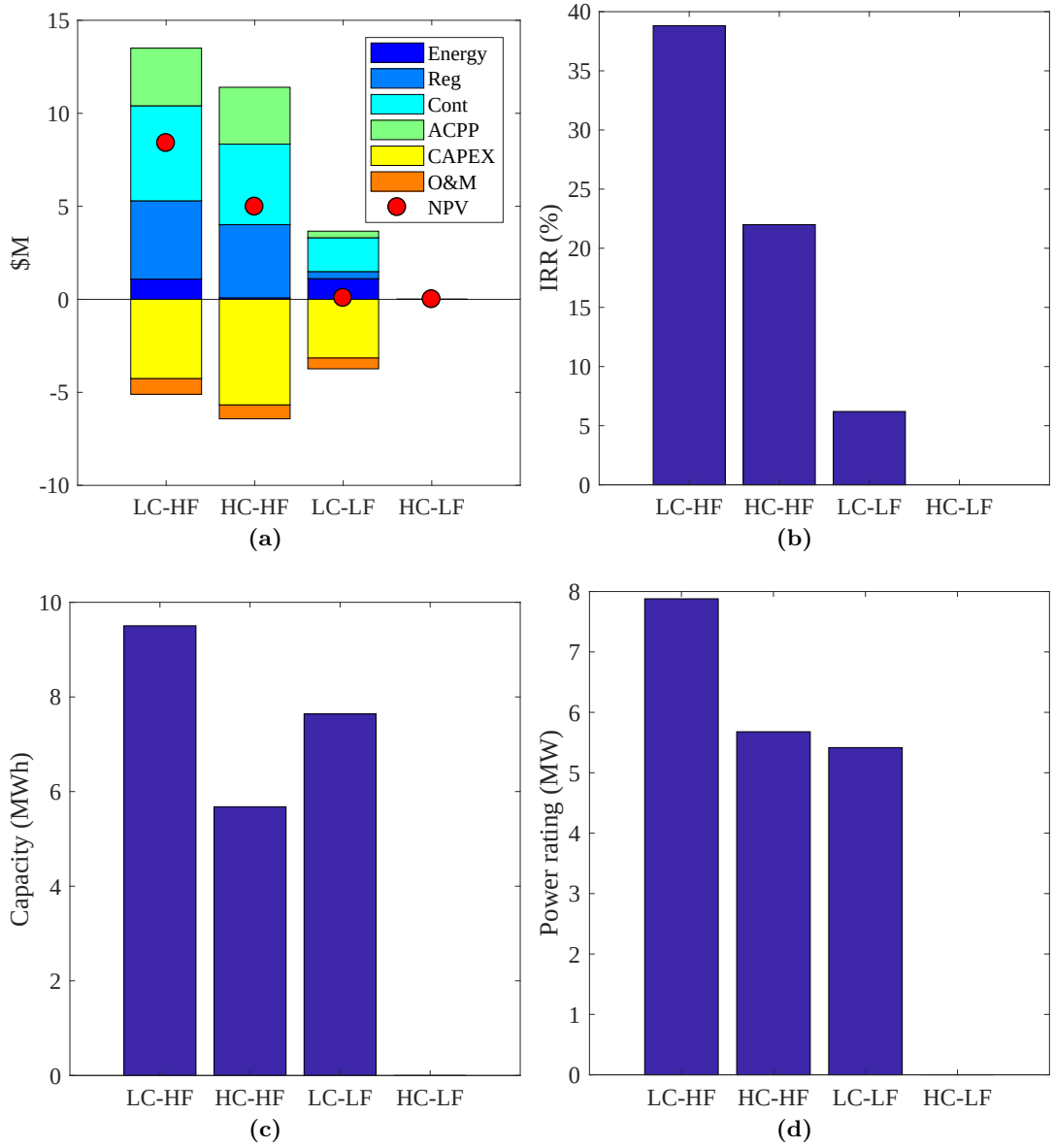

Figure 6.2: Optimal performance of battery, integrated into the wind farm, in the energy and FCAS markets for different battery capital cost and FCAS price scenarios. Results are presented in terms of: a) NPV, b) IRR, c) battery capacity and d) battery power rating.

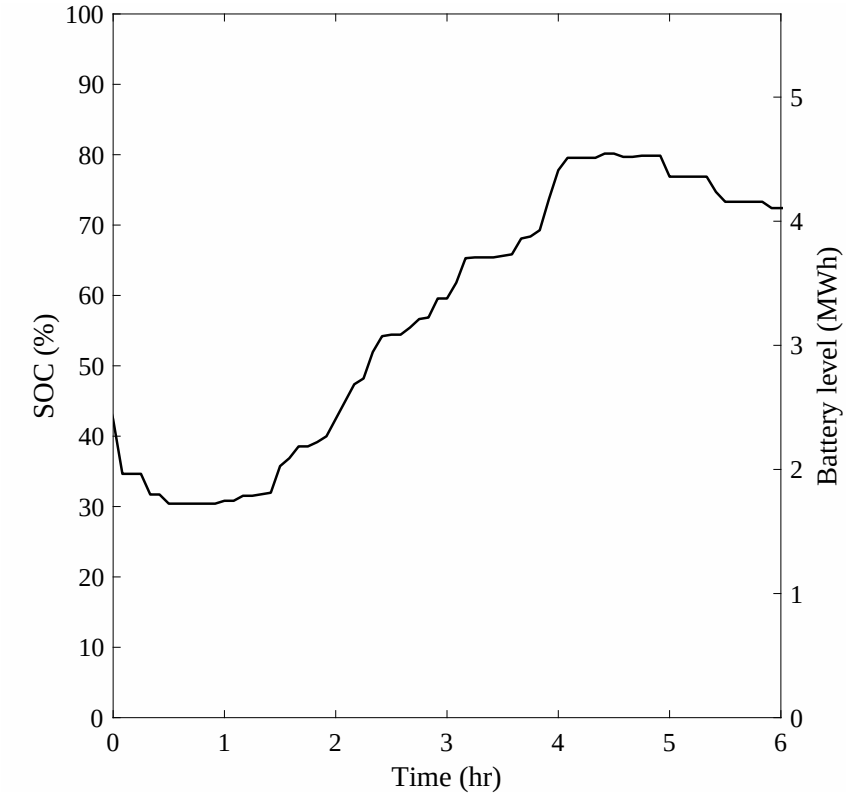

Figure 6.3: a) Battery energy level and SOC, and b) FCAS services offered in a 6-hour sample period with large SOC variations.

6.4 Optimal performance with wind farm frequency control

Thus far in this thesis, the optimal performance of the wind farm and battery storage in both the energy and FCAS markets were studied in isolation. This section examines their simultaneous participation in these markets.

6.4.1 Impact of wind farm curtailment on battery investment

Figure 6.4 shows the financial performance of the wind farm-battery system along with the optimal battery capacity and power rating, for the four capital cost-FCAS price scenarios considered previously. A comparison between the total NPV in Figure 6.4a and 6.2a indicates that the combination of the wind farm frequency control and the battery results in slightly higher NPVs than the case of wind farm-battery without wind farm frequency control, as a system with greater flexibility should. This comparison also reveals that revenues in the energy and FCAS markets, as well as the Avoided CPP (ACPP) of the system with frequency control, is very similar to the one without frequency control, implying that the introduction of frequency control into the system does not provide significantly more revenue and avoided payments. Rather, the improved total performance is largely due to the smaller size of the battery and therefore the reduced CAPEX.

Although the NPV of the entire system is higher when the wind farm frequency control is combined with battery storage, the NPV of the battery itself (Figure 6.4b) is less than for the case of no wind farm frequency control (Figure 6.2a). This shows that in a system where the wind farm itself has frequency control capability, battery storage has less value. Therefore, wind farm FCAS provision impacts battery performance and reduces the optimal battery capacity. Figure 6.4b also shows that installing a battery in a wind farm providing FCAS services has a significant impact on FCAS contingency revenues and a relatively smaller impact on FCAS regulation revenues. This is because the wind farm with frequency control in the absence of energy storage tends to participate mostly in the regulation market, as discussed in the previous chapter. It is also worth noting that the battery has the potential to reduce wind generation curtailment, such that the wind farm loses less money in the energy market. This can be clearly seen in the benefits of the battery in the energy market for the LC-HF scenario in Figure 6.4b. Although the NPV of the battery is lower when the wind farm has frequency control, Figure 6.4c shows that the IRRs are similar to those in Figure

6.2b, which can be attributed to the reduced battery CAPEX as smaller batteries are used.

Figure 6.4d shows that the optimal battery capacity is zero for both low FCAS (LF) price scenarios. This indicates that if FCAS prices come down in the future, and some cheaper alternatives, such as wind farm frequency control are also available, future battery investments, even with 50% of the current capital cost, may still be inferior investments relative to some alternatives. In addition, Figure 6.4a demonstrates that the value of avoided wind curtailment is positive in the energy market for LF scenarios. This is due to the low FCAS prices causing the wind farm to mostly curtail its power when the energy price is negative, and therefore it earns revenue in the energy market while the financial loss imposed by FCAS provision is negligible.

Table 6.5 present a summary of the optimal performance of the battery for different studied cases. It can be seen that in the wind farm with frequency control a battery with $C_{rate} \simeq 1$ is optimal for the LC-HF scenario while a lower C_{rate} is optimal in the absence of wind farm frequency control. This is because the wind farm's participation in FCAS markets diminishes the need for more hours of storage, to provide arbitrage.

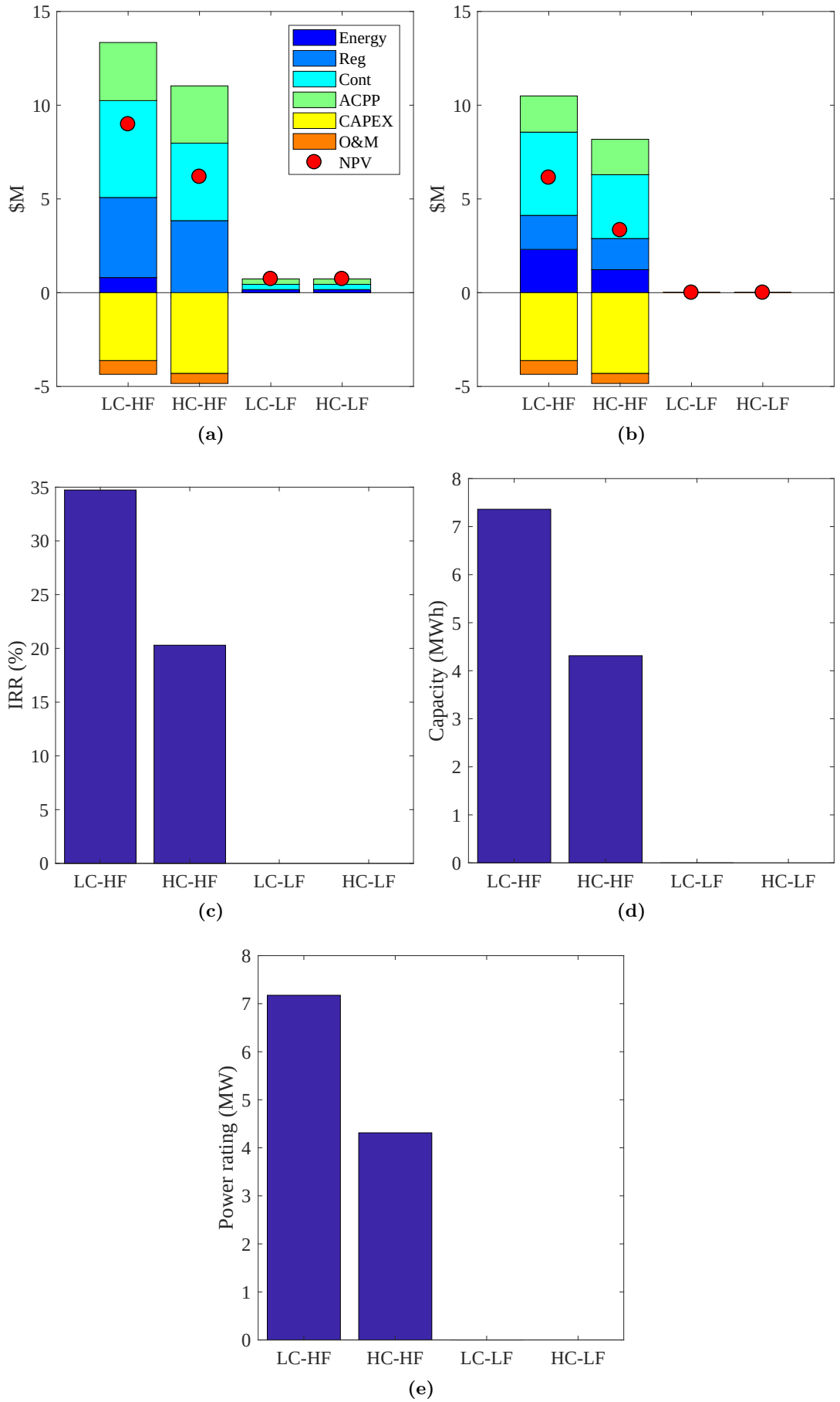

Figure 6.4: Optimal performance of the wind farm with frequency control, and with an integrated battery, participating in the energy and FCAS markets, for different capital cost-FCAS price scenarios: a) NPV of the battery and wind curtailment, b) NPV of the battery-only, c) IRR of the battery, d) battery capacity and e) battery power rating.

Table 6.5: The optimal battery energy capacity (Q_B), power rating (P_B^{max}), C_{rate}, NPV and IRR for different studied cases.

Battery FCAS provision	Wind farm frequency control	Scenario	$Q_B(MWh)$	P_B^{max} (MW)	$C_{rate} = \frac{P_B^{max}}{Q_B}$	NPV ($M)	IRR (%)
No	No	No CAPEX subsidy*	-	-	-	-	-
		85% CAPEX subsidy	125.5	48.6	0.39	2.97	10
Yes	No	HC-HF	5.68	5.68	1	4.98	22
		HC-LF*	-	-	-	-	-
		LC-HF	9.50	7.88	0.83	8.39	38.8
		LC-LF	7.64	5.42	0.71	0.07	6.2
Yes	Yes	HC-HF	4.31	4.31	1	3.33	20.3
		HC-LF*	-	-	-	-	-
		LC-HF	7.36	7.18	0.98	6.14	34.7
		LC-LF*	-	-	-	-	-

* The battery is not investable in these cases.

6.4.2 Effect of the battery on wind farm curtailment

Introducing a battery into a wind farm with frequency control affects the performance of the entire system by reducing the wind generation curtailment and increasing revenues in the FCAS markets. Figure 6.5 shows the annual amount of wind curtailment of the wind farm having frequency control capability with and without the integrated battery. The result of the wind farm-only (WF-only) system is based on the previous chapter in which the high FCAS (HF) price scenario was used. It can be seen that the battery can reduce the curtailment significantly, which results in increased revenue from the energy market. The optimal battery capacity for the low FCAS price scenarios, LC-LF and HC-LF, is zero because the wind farm already participates in the FCAS markets.

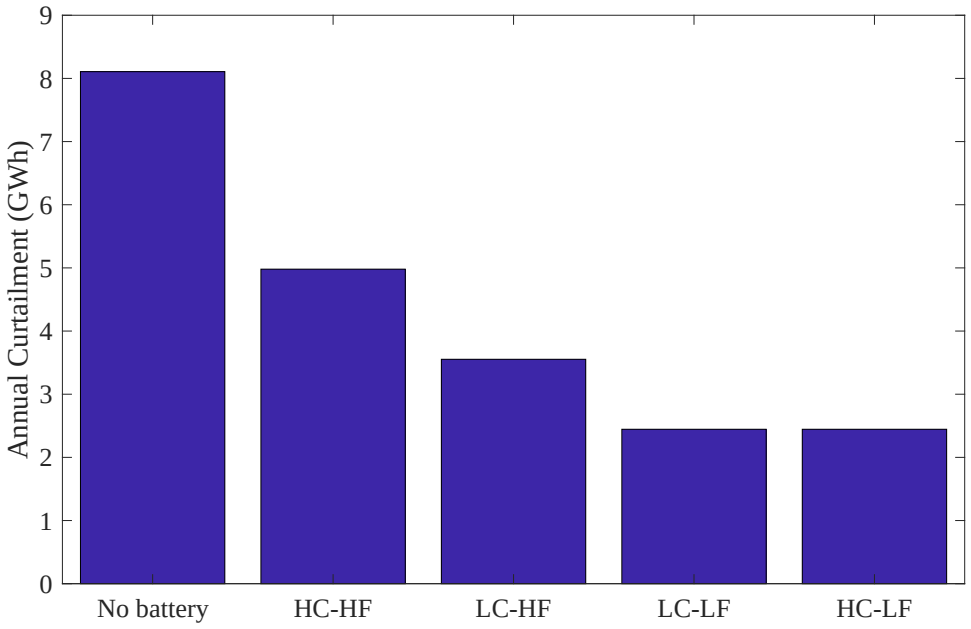

Figure 6.5: Annual curtailment of the wind farm with frequency control, for the high FCAS price scenario without a battery (WF-only), and the four battery capital cost-FCAS price scenarios.

Figure 6.6 shows the dispatch of the wind farm and battery in the same 6-hour period as Figure 5.4 for the optimal solution of the HC-HF scenario. The curtailment is lower in the case with a battery (Figure 6.6a), and consequently, the amount of FCAS services, particularly raise, offered by the wind farm is lower compared with the no battery case (Figure 5.4). However, less curtailment allows the wind farm to offer more lower contingency services, which can be seen in Figure 6.6b, particularly between hours 3 and 5. Figure 6.6d shows that the battery is used more for raise services because the advantage of using the battery in the wind farm with frequency control is to reduce the amount of precurtailment. Since the optimal battery power rating is approximately 4.3 MW, when the offered services are greater than this value, the battery is either charging or discharging in the energy market, depending on the type of offered FCAS services.

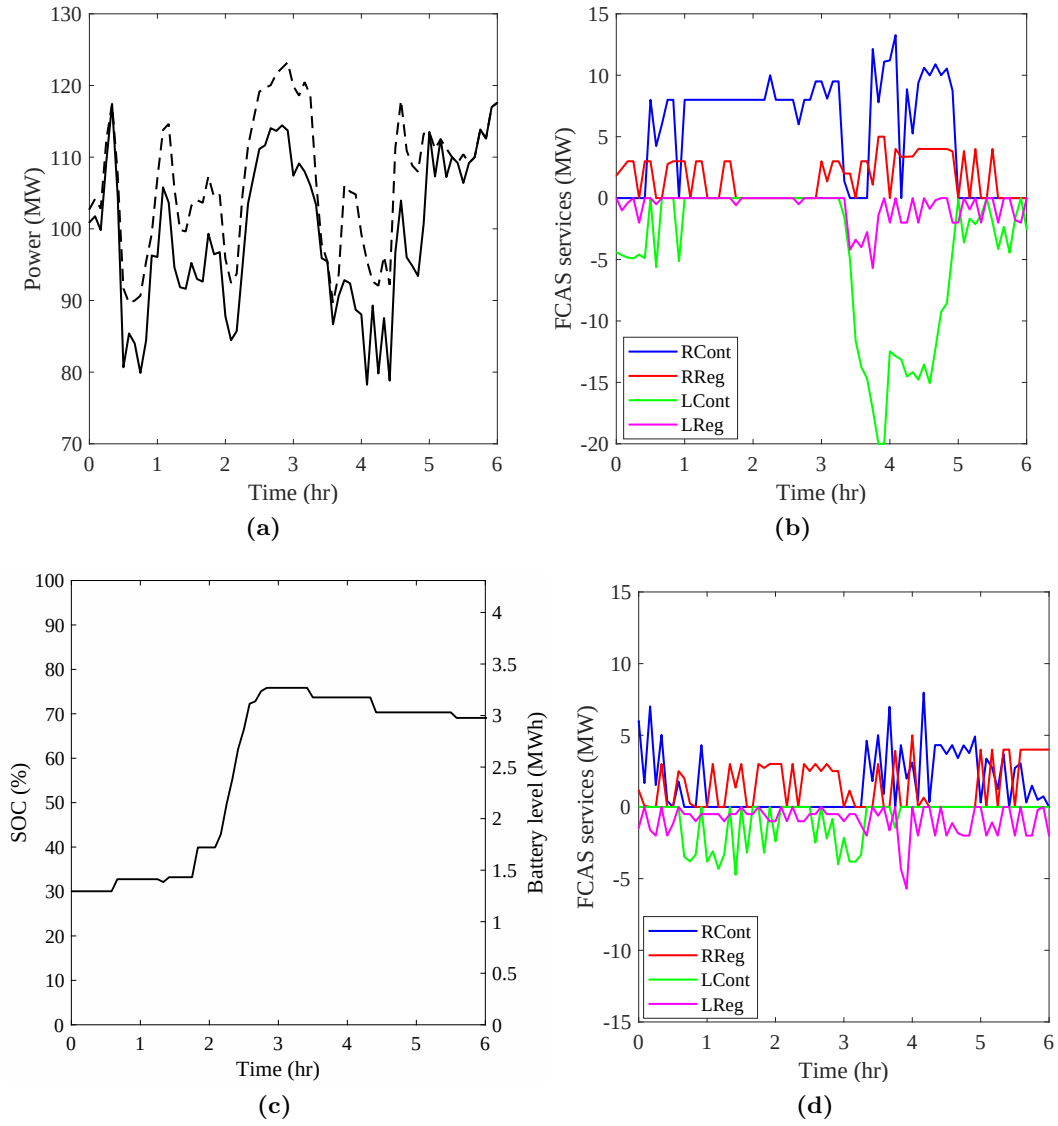

Figure 6.6: a) Wind farm actual maximum available (dashed line) and curtailed (solid line) power generation, b) wind farm FCAS services offered, c) Battery energy level and SOC and d) battery FCAS services offered in a 6-hour period.

6.5 Impact of wind forecast accuracy on battery investment

This section examines the impact of the wind forecasting system on the optimal performance of the Li-ion battery integrated into the wind farm with and without frequency control. To investigate the impact of forecast accuracy on the battery investment, the LC-HF scenario is used because minor changes in the wind farm's dispatch targets have a more observable effect on the optimal battery capacity due to the low battery capital cost. It is also insightful to investigate the impact of more accurate wind generation fore-

casting systems, since any form of improved information that is relevant to the wholesale market should reduce the need for capital investment to achieve a stated objective.

6.5.1 Wind farm without frequency control

Figure 6.7 shows the optimal performance of the wind farm-battery system without wind farm frequency control in the energy and FCAS markets using different forecasting systems. As expected, the system NPV increases with the improvement of forecasting system accuracy. The comparison between different forecasting systems indicates that the revenues are very similar, and the difference in NPVs is mainly due to the lower CPP and battery CAPEX.

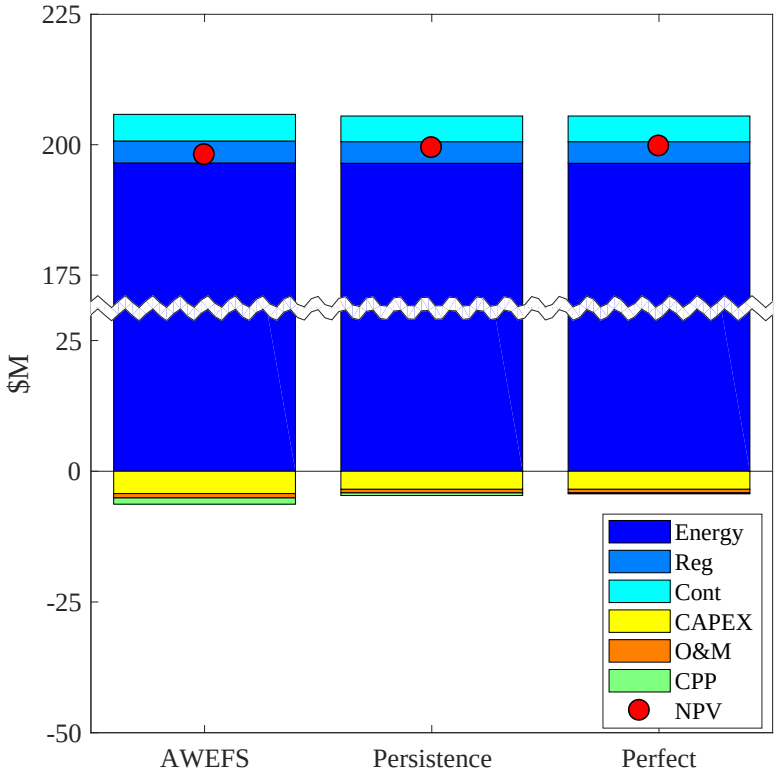

Figure 6.7: Optimal performance of the wind farm-battery system without wind farm frequency control using different forecasting systems.

Figure 6.8 shows the optimal performance of Li-ion battery storage using different forecasting systems. It can be seen that with better forecasting, the battery has a lower NPV. This is due to the reduced ACPP in the persistence and perfect forecasting, whilst the revenues in the energy and FCAS markets are almost independent of the forecasting system. This shows that the uncertainty in the wind forecasting system creates value for battery storage.

Interestingly, Figure 6.8b indicates that the IRR of the battery using the persistence forecast is the highest. This can be attributed to the reduced CAPEX of the battery compared with that of the AWEFS, as well as the higher ACPP relative to the perfect forecast (Figure 6.8a).

According to Figure 6.8c, the battery capacity is reduced by approximately 30% with the improved forecast accuracy of the persistence and perfect forecasting system relative to that of AWEFS. However, there is no significant difference between the persistence and perfect forecasting systems, suggesting that the forecast accuracy has a considerable impact up to a certain point, after which further improvements in the forecast accuracy do not result in significant additional benefits.

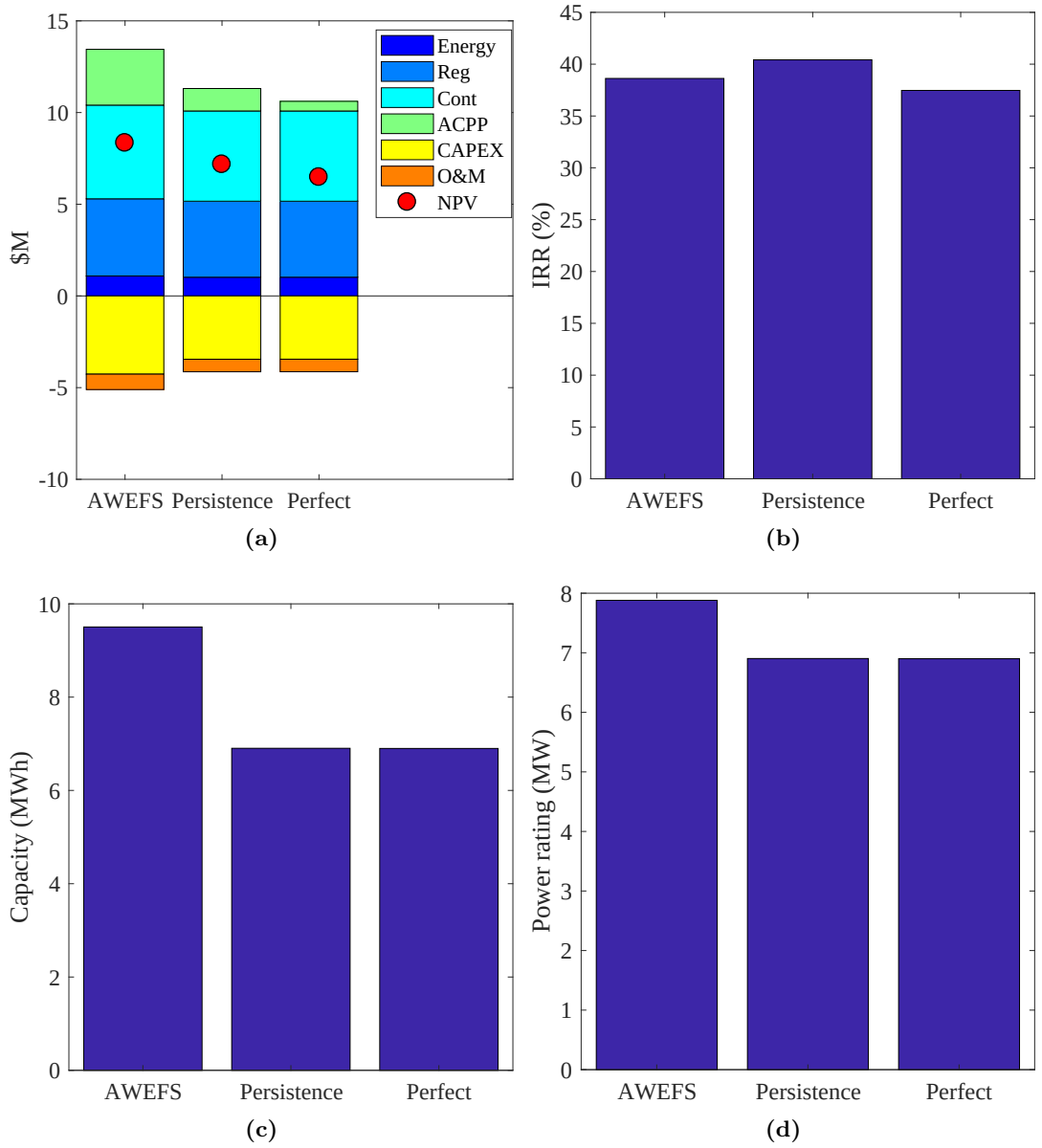

Figure 6.8: Optimal performance of battery, integrated into the wind farm, in the energy and FCAS markets using different forecasting systems: a) NPV, b) IRR, c) battery capacity and d) battery power rating.

6.5.2 Wind farm with frequency control

The impact of forecast accuracy on the optimal performance of the wind farm-battery system is investigated here, with the frequency control capability of the wind farm now included. Figure 6.9 shows the optimal performance of the wind farm-battery system with wind farm frequency control participating in the energy and FCAS markets using different forecasting systems. Again, using a more accurate forecasting system results in a higher NPV, which is mainly due to the reduced CAPEX required for the battery, together with reduced CPPs.

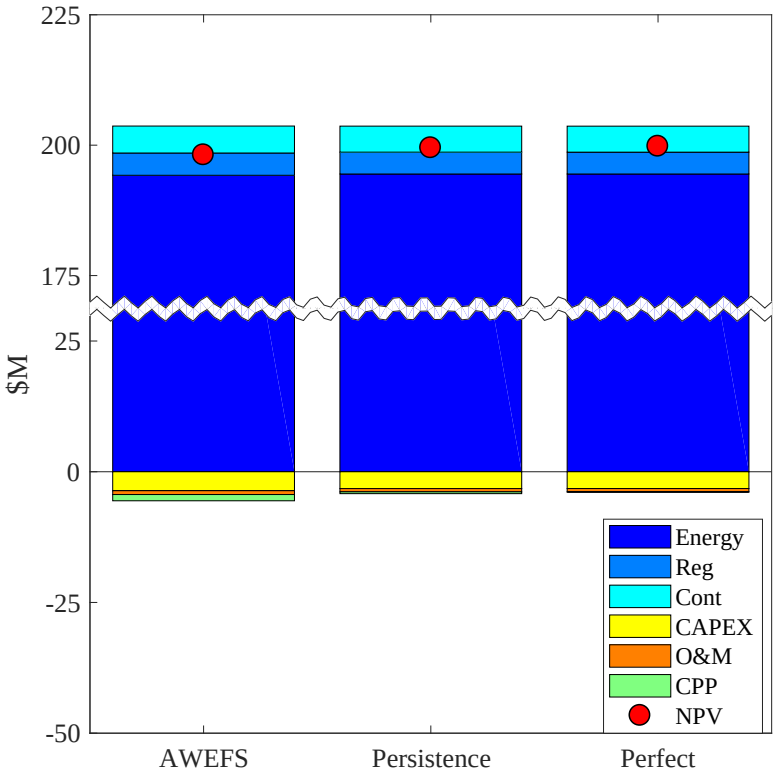

Figure 6.9: Optimal performance of the wind farm-battery system with wind farm frequency control using different forecasting systems

Figure 6.10a shows the total NPV of the wind farm curtailment and battery in the energy and FCAS markets. The wind curtailment and the battery have lower value in a wind farm with a better forecasting system, and therefore less curtailment and a smaller battery are required. As a result of less wind curtailment with better forecasting, the share of the energy market in the optimal financial performance of the system increases.

Figure 6.10b demonstrates the NPV of the battery itself, from which it can be seen that with a better forecasting system, there is again less value in the battery installation. Also, as the forecasting system improves, the battery value in the energy market reduces. The reason for this is that with AWEFS the amount of wind curtailment is higher, and the influence of the battery to decrease curtailment is more significant compared with better forecasting systems. Results in Figures 6.10b-6.10e are consistent with this and previous results, showing that smaller batteries are again optimal when the wind farm has the frequency control capability and that there is little financial benefit in a forecasting system that is more accurate than a persistence forecast.

Table 6.6 summarises the results of the impact of wind generation forecast accuracy on the optimal battery investment for all studied cases.

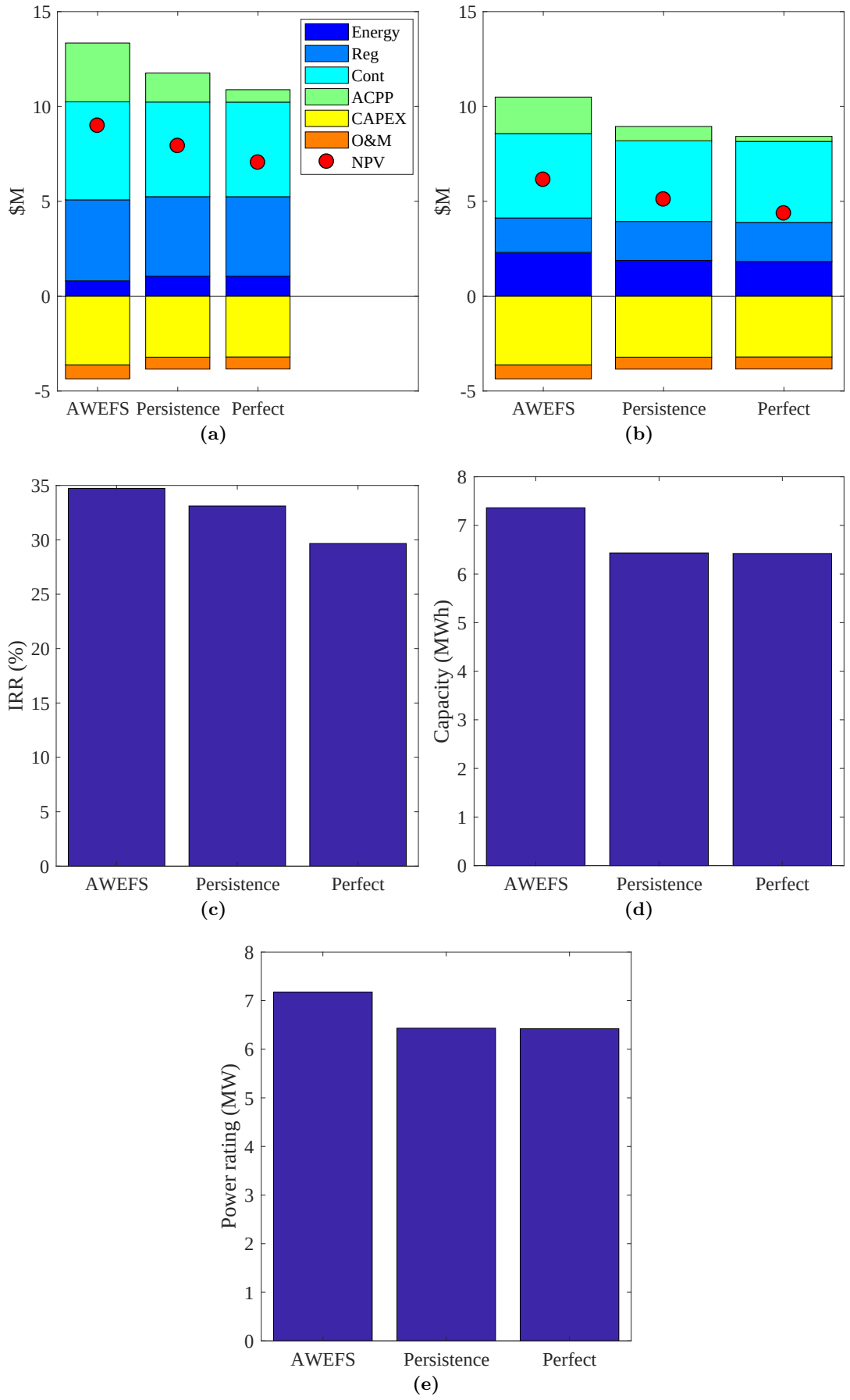

Figure 6.10: Optimal performance of battery and the wind farm with frequency control using different forecasting systems: a) NPV of battery and wind curtailment, b) NPV of battery only, c) IRR of battery, d) battery Capacity and e) battery power rating.

Table 6.6: The optimal battery energy capacity (Q_B), power rating (P_B^{max}), C_{rate}, NPV and IRR for different wind forecasting systems using LC-HF scenario.

Battery FCAS provision	Wind farm frequency control	Forecasting system	Q_B (MWh)	P_B^{max} (MW)	C_{rate}	NPV ($M)	IRR (%)
Yes	No	AWEFS	9.50	7.88	0.83	8.39	38.8
		Persistence	6.91	6.91	1	7.17	40.4
		Perfect	6.9	6.9	1	6.48	37.5
Yes	Yes	AWEFS	7.36	7.18	0.98	6.14	34.7
		Persistence	6.43	6.43	1	5.10	33.1
		Perfect	6.42	6.42	1	4.36	29.7

Figure 6.11 shows the annual curtailment of the wind farm with frequency control and with an integrated battery using different forecasting systems. As mentioned, since the wind curtailment has less value in the wind farm with better forecasting, the amount of curtailment reduces. The annual wind curtailment reduces by approximately 25% relative to the AWEFS if the persistence method is used. Again, the perfect forecasting system does not result in a significant change compared with the persistence method.

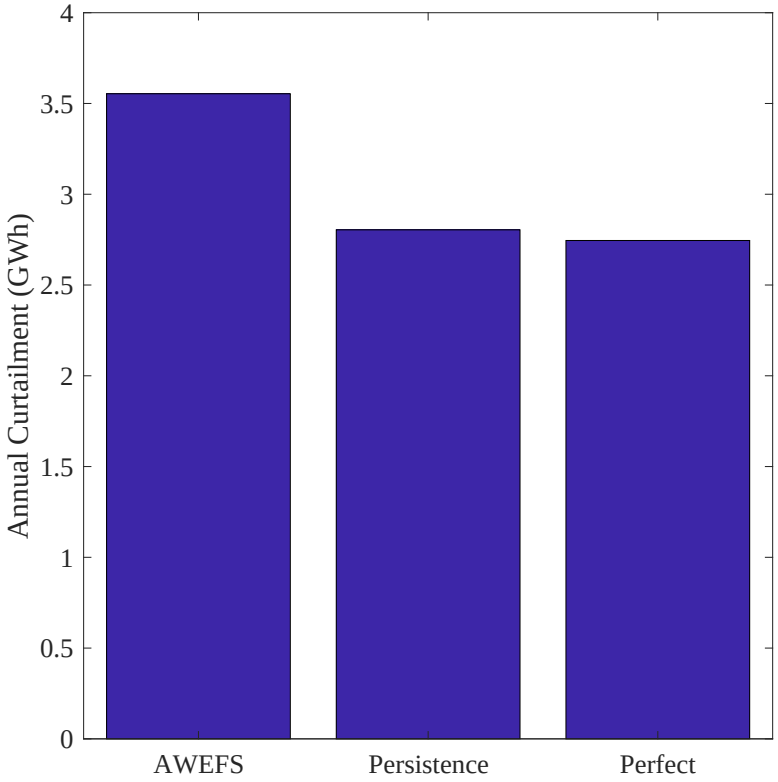

Figure 6.11: Annual curtailment of the wind farm with frequency control and with an integrated battery, for different forecasting systems.

6.6 Summary

This chapter examined the optimal performance of a Li-ion battery storage system integrated into a wind farm participating in the energy and Frequency Control Ancillary Services (FCAS) markets. The Net Present Value (NPV) of the wind farm (as a sunk cost) and the battery was maximised while considering different markets and technical constraints.

The optimal performance of the battery in the energy-only market was first studied. Sensitivity analysis showed that a battery with current costs is not investable without very substantial subsidies. However, despite their small size, participation in the FCAS markets had a significant impact on battery investability. Results indicated that the

battery's financial performance is very sensitive to FCAS prices and that with high prices, such as were seen in 2017 in the Australian National Electricity Market (NEM), the battery can be considered highly investable, even with its relatively high current capital cost. However, the analysis also showed that if FCAS prices return to the historically low levels, such as those experienced in 2015, a battery with current capital cost would no longer be considered investable without subsidy.

The optimal performance of the wind farm-battery storage system with wind farm frequency control capability was then considered. The results indicated that the battery could reduce the wind generation curtailment significantly, allowing increased revenues in the energy market. It was also found that the introduction of wind farm frequency control reduced the optimal size of the battery and its Internal Rate of Return (IRR), which is expected since the wind farm then provides lower cost services that would otherwise be provided by the battery.

Finally, the impact of wind generation forecast accuracy was investigated using the Australian Wind Energy Forecasting System (AWEFS), persistence and perfect forecast methods. As expected, increased forecast accuracy also reduced optimal battery size and its NPV, once again through realising alternative, lower cost means of providing some of the services that batteries can provide. It was also found that the forecast accuracy has a weaker influence on the optimal battery capacity when the wind farm has frequency control capability. No significant difference was found between the optimal system performance for the persistence and perfect forecasting systems, suggesting that in the presence of a sufficiently accurate forecasting system, there is no significant benefit in further increases of forecast system accuracy.

Chapter 7

Conclusions and recommendations

7.1 Conclusions

This thesis has examined different means by which the financial performance of a wind farm participating in the electricity market can be optimised. This optimisation is necessary because the large-scale integration of wind energy into a power system can result in various significant challenges, as were identified in the Literature Review (Chapter 2).

The main findings of this thesis are as follows.

1. **The cross-correlation between wind turbines' power output is related to the convective length scale in the incoming wind and can be accounted for in a hierarchy of reduced order models of wind farms. For these reduced order models, there is an inherent trade-off between accuracy and complexity.**

   Spectral analysis of the cross-correlation between the power output of the wind turbines using large amounts of data found that the coherence between the power output of a turbine pair in the wind farm is strongly dependent on the frequency of the incident wind disturbance. It was also found that the power generation of any turbine pair is uncorrelated if the turbine spacing is greater than the convective length scale in the wind. A hierarchical method for modelling wind farms was then proposed and demonstrated a trade-off between the model accuracy and the complexity.

   Spectral analysis of the power output of different wind farm models and the measured wind farm power output revealed three distinct frequency regions: correlated, uncorrelated and transitional. In the correlated region, which includes frequencies lower than that defined by the average wind speed and the spacing between the two, furthest apart turbines, all the models and the measurements perform very similarly. This is because the length scales in the wind are greater than the wind farm dimensions, and thus all turbines are highly correlated. On the other hand, for frequencies higher than that defined by the average wind speed and the spacing between the two, closest together turbines, the turbines' power generation is uncorrelated. A transitional region exists between these two limits, in which wind turbines in the wind farm *on average* are more correlated with closer turbines and less correlated with more distant turbines. Since these high and low frequency regimes have relatively simple relationships between all turbines, it is

likely a general result that the accuracy of wind farm modelling is most sensitive to the modelled correlation between turbines in this transitional regime.

2. **The introduction of wind farm frequency control capability can improve its financial performance through the provision of Frequency Control Ancillary Services (FCAS). The use of a more accurate wind forecasting can also improve the overall performance of the system.**

   The analysis showed that wind farm participation in the FCAS lower regulation market was the most attractive, due to the relatively high price of this service in the historical studied period and it not requiring precurtailed wind generation. Additionally, wind turbines can accurately follow the optimal power set-point, suggesting that the optimal dispatch found by the optimisation model is technically feasible.

   The impact of wind forecast accuracy on the performance of the wind farm without frequency control was then studied using the historical data from the Australian Wind Energy Forecasting System (AWEFS), persistence and perfect forecasting systems. It was found that a simple persistence forecasting was 25% more accurate than AWEFS and reduced CPFs by approximately 60%. Since the economic impact of the forecasting system on the wind farm was found to be significant, the impact of forecast accuracy on the optimal performance of the wind farm with frequency control was examined. A greater forecasting system accuracy improved the performance of the wind farm in the electricity market, mainly due to reduced Causer Pays Payments (CPPs). However, the results also showed that the curtailment has lower value in the presence of a more accurate forecasting system because it is less valuable to curtail wind generation for avoiding CPPs and earning FCAS revenue.

3. **The investability of a battery integrated into a wind farm is highly sensitive to its participation in frequency control ancillary services markets and the price of these services. The introduction of wind farm frequency control capability and a more accurate forecasting system also reduces the value of the battery investment.**

   Investigation of the optimal performance of a Lithium-ion (Li-ion) battery storage system integrated into a wind farm participating in the energy-only market found that a Li-ion battery is not investable without substantial subsidies. However, allowing the battery to participate in the FCAS markets improved the battery's financial performance significantly. Thus, the economic justification of integrating a battery is highly sensitive to FCAS prices, such that a battery can be considered

highly investable, even with its relatively high current capital cost, if the FCAS prices remain high. However, the analysis also showed that if FCAS prices return to historically low levels, a battery with current capital cost would no longer be considered investable without subsidy.

The introduction of wind farm frequency control into the wind farm-battery system reduces the optimal size of the battery and its value. This implies that for a wind farm capable of providing FCAS services, there is a lower requirement for expensive complementary technologies such as a battery. Also, the use of the battery in a wind farm with frequency control capability reduces the wind generation curtailment significantly, allowing increased revenues in the energy market.

Finally, as the forecast accuracy improves, the optimal battery size and its value decrease, suggesting that wind forecast uncertainty creates value for a battery. The optimal system performance was found to be similar using the persistence and perfect forecasting systems, suggesting that with a sufficiently accurate forecasting system, there is no significant benefit in its further improvement.

7.2 Recommendations for future research

The Mt Mercer wind farm, used in this study, is a typical large-scale operational wind farm in the Australian National Electricity Market (NEM), therefore, the presented optimisation model and wind farm modelling approach can potentially be applied to other wind farms for future research. However, the number of clusters required for modelling the wind farm can vary and must be determined using the proposed approach. Although the methodology used in this study is general, the results cannot be generalised, since various electricity markets around the world have different characteristics and operating conditions. In conclusion, this study suggests the following for future research:

1. **To demonstrate the findings of this study in an operating wind farm.** This study showed that the wind farm can provide Frequency Control Ancillary Services (FCAS) by curtailing the wind generation, which can result in the improvement of the financial performance of the system in the electricity market. The results also indicate that the wind farm is able to follow the power set-point accurately; however, the practical feasibility of the optimal dispatch of a real wind farm providing FCAS services should be investigated.

2. **To develop a model of the energy and frequency control ancillary services markets, in which the wind farm and battery can potentially participate as price setters.**

The present study considered the wind farm and energy storage as price takers in the energy and FCAS markets, which can be considered reasonable, due to their small size relative to the current power system. However, increasing penetration of wind energy into the grid, together with the introduction of wind farms providing frequency control services can affect the price of the FCAS services. Therefore, it is necessary to develop a model of the electricity market in which wind power plants can compete with each other and other technologies for the provision of these services.

3. **To investigate the financial feasibility of investment in other complementary technologies, such as an electrolyser with hydrogen storage.**
   As the penetration of the wind energy in the power system increases the curtailment of wind power generation will become inevitable to stabilise the power system, which will have an adverse impact on the financial performance of the wind power plants. However, instead of wind generation curtailment, there is a growing interest in the storage of excess wind energy generation in alternative forms of energy storage, such as via the electrolytic conversion of electricity to hydrogen. This power-to-gas option has attracted attention in the past few years as one potential component of future clean and emission free energy systems. Therefore, it is potentially worthwhile to investigate the financial performance of integrating this power-to-gas option into a wind farm. In addition, the electrolyser could be used to provide ancillary services as a flexible load by managing its electricity consumption, which can have a significant impact on the financial viability of this storage technology.

4. **To extend the present optimisation model to determine the optimal size of the wind farm.**
   The present optimisation model considers the wind farm as an already built asset and determines its optimal performance with and without energy storage. However, this model can be extended to optimise the investment on the wind farm as well as the energy storage system, considering energy and ancillary services markets. This can potentially facilitate the integration of the wind energy into the power system and benefits the owner of newly built wind farms to maximise their profit while keeping the power system secure.

References

Bibliography

[1] Pavlos S Georgilakis. Technical challenges associated with the integration of wind power into power systems. *Renewable and Sustainable Energy Reviews*, 12(3): 852–863, 2008.

[2] Guorui Ren, Jinfu Liu, Jie Wan, Yufeng Guo, and Daren Yu. Overview of wind power intermittency: Impacts, measurements, and mitigation solutions. *Applied Energy*, 204:47–65, 2017.

[3] Paul Veers, Katherine Dykes, Eric Lantz, Stephan Barth, Carlo L. Bottasso, Ola Carlson, Andrew Clifton, Johney Green, Peter Green, Hannele Holttinen, Daniel Laird, Ville Lehtomäki, Julie K. Lundquist, James Manwell, Melinda Marquis, Charles Meneveau, Patrick Moriarty, Xabier Munduate, Michael Muskulus, Jonathan Naughton, Lucy Pao, Joshua Paquette, Joachim Peinke, Amy Robertson, Javier Sanz Rodrigo, Anna Maria Sempreviva, J. Charles Smith, Aidan Tuohy, and Ryan Wiser. Grand challenges in the science of wind energy. *Science*, 366 (6464), 2019.

[4] Le Xie, Pedro MS Carvalho, Luis AFM Ferreira, Juhua Liu, Bruce H Krogh, Nipun Popli, and Marija D Ilic. Wind integration in power systems: Operational challenges and possible solutions. *Proceedings of the IEEE*, 99(1):214–232, 2010.

[5] Global Wind Energy Council (GWEC). Global wind report 2018. Technical report, 2019. [Online]. Available: https://gwec.net/wp-content/uploads/2019/04/GWEC-Global-Wind-Report-2018.pdf.

[6] British Petroleum (BP). BP Statistical Review of World Energy. Technical report, 2018.

[7] Intelligent Energy Systems, NEO Express. [Online]. Available: http://products.iesys.com/NEO/NEOexpress. [Accessed: 2019-05-26].

[8] Australian Energy Market Operator (AEMO). Black system South Australia 28 September 2016. Technical report, 2017. [On-

line]. Available: https://www.aemo.com.au/-/media/Files/Electricity/NEM/Market_Notices_and_Events/Power_System_Incident_Reports/2017/Integrated-Final-Report-SA-Black-System-28-September-2016.pdf.

[9] Australian Energy Market Operator (AEMO). Quarterly Energy Dynamics Q1 2018. Technical report, 2018. [Online]. Available: https://www.aemo.com.au/-/media/Files/Media_Centre/2018/QED-Q1-2018.pdf.

[10] Australian Energy Market Operator (AEMO). Hornsdale Wind Farm 2 FCAS trial. Technical report, 2018. [Online]. Available: https://www.aemo.com.au/-/media/Files/Electricity/NEM/Strategic-Partnerships/2018/HWF2-FCAS-trial-paper.pdf.

[11] Australian Energy Market Operator (AEMO). Initial operation of the Hornsdale power reserve battery energy storage system. Technical report, 2018. [Online]. Available: https://www.aemo.com.au/-/media/Files/Media_Centre/2018/Initial-operation-of-the-Hornsdale-Power-Reserve.pdf.

[12] Australian Energy Market Commission (AEMC). Frequency Control Frameworks Review. Technical report, 2018. [Online]. Available: https://www.aemc.gov.au/sites/default/files/content/0fd91c30-bc61-4d53-8ee3-249eac0123b5/Issues-paper.pdf.

[13] Australian Energy Regulator. Wholesale statistics. [Online]. Available: https://www.aer.gov.au/wholesale-markets/. [Accessed: 2019-09-24].

[14] Australian Energy Market Operator (AEMO). National Electricity Market. [Online]. Available: https://www.aemo.com.au/Electricity/National-Electricity-Market-NEM. [Accessed: 2019-10-22].

[15] International Atomic Energy Agency (IAEA). Country Nuclear Power Profiles 2018 Edition. [Online]. Available: https://www-pub.iaea.org/MTCD/Publications/PDF/cnpp2018/countryprofiles/Russia/Russia.htm. [Accessed: 2020-02-27].

[16] Australian Energy Market Operator (AEMO). Settlements guide to ancillary services payment and recovery. Technical report, 2015. [Online]. Available: https://www.aemo.com.au/-/media/Files/PDF/settlement-guide-to-ancillary-services-payment-and-recovery-v2.pdf.

[17] Australian Energy Market Operator (AEMO). Guide to ancillary services in the national electricity market. Technical report, 2015. [Online]. Available: https://www.aemo.com.au/-/media/Files/PDF/Guide-to-Ancillary-Services-in-the-National-Electricity-Market.pdf.

[18] Australian Energy Market Operator (AEMO). Causer pays procedure. Technical report, 2017. [Online]. Available: https://www.aemo.com.au/-/media/Files/Electricity/NEM/Security_and_Reliability/Ancillary_Services/20170106-Causer-Pays-Procedure.pdf.

[19] Australian Energy Market Operator (AEMO). Frequency monitoring – three year historical trends. Technical report, 2017. [Online]. Available: https://www.aemo.com.au/-/media/Files/Electricity/NEM/Security_and_Reliability/Ancillary_Services/2017-06-Frequency-Monitoring---Three-Year-Historical-Trends.pdf.

[20] MH Albadi and EF El-Saadany. Overview of wind power intermittency impacts on power systems. *Electric Power Systems Research*, 80(6):627–632, 2010.

[21] Hassan Bevrani, Arindam Ghosh, and Gerard Ledwich. Renewable energy sources and frequency regulation: survey and new perspectives. *IET Renewable Power Generation*, 4(5):438–457, 2010.

[22] Temitope Raphael Ayodele, Adiasa Jimoh, Josial L Munda, and Agee J Tehile. Challenges of grid integration of wind power on power system grid integrity: a review. *International journal of renewable energy research (IJRER)*, 2(4):618–626, 2012.

[23] Thomas Ackermann et al. *Wind power in power systems*, volume 140. Wiley Online Library, 2005.

[24] Robert Passey, Ted Spooner, Iain MacGill, Muriel Watt, and Katerina Syngellakis. The potential impacts of grid-connected distributed generation and how to address them: A review of technical and non-technical factors. *Energy Policy*, 39(10): 6280–6290, 2011.

[25] Ronan Doherty and Mark O'malley. A new approach to quantify reserve demand in systems with significant installed wind capacity. *IEEE Transactions on Power Systems*, 20(2):587–595, 2005.

[26] Hannele Holttinen, Michael Milligan, Brendan Kirby, Tom Acker, Viktoria Neimane, and Tom Molinski. Using standard deviation as a measure of increased operational reserve requirement for wind power. *Wind Engineering*, 32(4):355–377, 2008.

[27] Hannele Holttinen. Wind integration: experience, issues, and challenges. *Wiley Interdisciplinary Reviews: Energy and Environment*, 1(3):243–255, 2012.

[28] Vaclav Knap, Sanjay K Chaudhary, Daniel-Ioan Stroe, Maciej Swierczynski, Bogdan-Ionut Craciun, and Remus Teodorescu. Sizing of an energy storage system

for grid inertial response and primary frequency reserve. *IEEE Transactions on Power Systems*, 31(5):3447–3456, 2015.

[29] Pieter Tielens and Dirk Van Hertem. Grid inertia and frequency control in power systems with high penetration of renewables. In *Young Researchers Symposium in Electrical Power Engineering, Date: 2012/04/16-2012/04/17, Location: Delft, The Netherlands*, 2012.

[30] AM Foley, BP Ó Gallachóir, EJ McKeogh, D Milborrow, and PG Leahy. Addressing the technical and market challenges to high wind power integration in ireland. *Renewable and Sustainable Energy Reviews*, 19:692–703, 2013.

[31] Pieter Tielens and Dirk Van Hertem. The relevance of inertia in power systems. *Renewable and Sustainable Energy Reviews*, 55:999–1009, 2016.

[32] Marshman, Daniel . "Performance of Electricity Markets and Power Plant Investments in the Transition to a Low-Carbon Power System". PhD dissertation, The University of Melbourne, 2018.

[33] Xiaodong Liang. Emerging power quality challenges due to integration of renewable energy sources. *IEEE Transactions on Industry Applications*, 53(2):855–866, 2016.

[34] MHJ Bollen. What is power quality? *Electric Power Systems Research*, 66(1): 5–14, 2003.

[35] Johan Morren and Sjoerd WH De Haan. Ridethrough of wind turbines with doubly-fed induction generator during a voltage dip. *IEEE Transactions on energy conversion*, 20(2):435–441, 2005.

[36] Lori Bird, M Milligan, and Debra Lew. Integrating variable renewable energy: Challenges and solutions. *National Renewable Energy Laboratory*, 2013.

[37] Juha Kiviluoma, Mark O'Malley, Aidan Tuohy, Peter Meibom, Michael Milligan, Bernhard Lange, Hannele Holttinen, and Madeleine Gibescu. Impact of wind power on the unit commitment, operating reserves, and market design. In *2011 IEEE Power and Energy Society General Meeting*, pages 1–8. IEEE, 2011.

[38] Jennifer DeCesaro, Kevin Porter, and Michael Milligan. Wind energy and power system operations: A review of wind integration studies to date. *The Electricity Journal*, 22(10):34–43, 2009.

[39] Juan Rivier Abbad. Electricity market participation of wind farms: the success story of the spanish pragmatism. *Energy policy*, 38(7):3174–3179, 2010.

[40] GM Joselin Herbert, Selvaraj Iniyan, E Sreevalsan, and S Rajapandian. A review of wind energy technologies. *Renewable and sustainable energy Reviews*, 11(6): 1117–1145, 2007.

[41] Frede Blaabjerg and Ke Ma. Wind energy systems. *Proceedings of the IEEE*, 105 (11):2116–2131, 2017.

[42] Jens Fortmann. *Modeling of wind turbines with doubly fed generator system.* Springer, 2014.

[43] Bin Wu, Yongqiang Lang, Navid Zargari, and Samir Kouro. *Power conversion and control of wind energy systems.* John Wiley & Sons, 2011.

[44] Mohit Singh and Surya Santoso. *Dynamic models for wind turbines and wind power plants.* National Renewable Energy Laboratory, 2011.

[45] Ming Cheng and Ying Zhu. The state of the art of wind energy conversion systems and technologies: A review. *Energy Conversion and Management*, 88:332–347, 2014.

[46] Henk Polinder, Jan Abraham Ferreira, Bogi Bech Jensen, Asger B Abrahamsen, Kais Atallah, and Richard A McMahon. Trends in wind turbine generator systems. *IEEE Journal of Emerging and Selected Topics in Power Electronics*, 1(3):174–185, 2013.

[47] Gonzalo Abad, Jesus Lopez, Miguel Rodriguez, Luis Marroyo, and Grzegorz Iwanski. *Doubly fed induction machine: modeling and control for wind energy generation*, volume 85. John Wiley & Sons, 2011.

[48] John Fletcher and Jin Yang. *Introduction to the doubly-fed induction generator for wind power applications.* INTECH Open Access Publisher, 2010.

[49] Anca D Hansen and Gabriele Michalke. Fault ride-through capability of dfig wind turbines. *Renewable energy*, 32(9):1594–1610, 2007.

[50] Dawei Xiang, Li Ran, Peter J Tavner, and Shunchang Yang. Control of a doubly fed induction generator in a wind turbine during grid fault ride-through. *IEEE Transactions on Energy Conversion*, 21(3):652–662, 2006.

[51] Lasantha Gunaruwan Meegahapola, Tim Littler, and Damian Flynn. Decoupled-dfig fault ride-through strategy for enhanced stability performance during grid faults. *IEEE Transactions on Sustainable Energy*, 1(3):152–162, 2010.

[52] Cristina Vázquez Hernández, Thomas Telsnig, and Anahí Villalba Pradas. Jrc wind energy status report 2016 edition. *Market, Technology and Regulatory Aspects of Wind Energy*, 2017.

[53] Australian Energy Market Operator (AEMO). Wind Turbine Plant Capabilities Report . Technical report, 2013. [Online]. Available: https://www.aemo.com.au/-/media/Files/PDF/Wind_Turbine_Plant_Capabilities_Report.pdf/.

[54] Nicholas W Miller, William W Price, and Juan J Sanchez-Gasca. Dynamic modeling of GE 1.5 and 3.6 wind turbine-generators.

[55] SM Muyeen, Md Hasan Ali, R Takahashi, T Murata, J Tamura, Y Tomaki, A Sakahara, and E Sasano. Comparative study on transient stability analysis of wind turbine generator system using different drive train models. *IET Renewable Power Generation*, 1(2):131–141, 2007.

[56] Janaka B Ekanayake, Lee Holdsworth, XueGuang Wu, and Nicholas Jenkins. Dynamic modeling of doubly fed induction generator wind turbines. *IEEE Transactions on Power systems*, 18(2):803–809, 2003.

[57] Wei Qiao. Dynamic modeling and control of doubly fed induction generators driven by wind turbines. In *Power Systems Conference and Exposition, 2009. PSCE'09. IEEE/PES*, pages 1–8. IEEE, 2009.

[58] JG Slootweg, Henk Polinder, and WL Kling. Dynamic modelling of a wind turbine with doubly fed induction generator. In *Power Engineering Society Summer Meeting, 2001*, volume 1, pages 644–649. IEEE, 2001.

[59] Kara Clark, Nicholas W Miller, and Juan J Sanchez-Gasca. Modeling of ge wind turbine-generators for grid studies. *GE energy*, 4:0885–8950, 2010.

[60] Yazhou Lei, Alan Mullane, Gordon Lightbody, and Robert Yacamini. Modeling of the wind turbine with a doubly fed induction generator for grid integration studies. *IEEE transactions on energy conversion*, 21(1):257–264, 2006.

[61] Jamal A Baroudi, Venkata Dinavahi, and Andrew M Knight. A review of power converter topologies for wind generators. *Renewable Energy*, 32(14):2369–2385, 2007.

[62] Markus A Poller. Doubly-fed induction machine models for stability assessment of wind farms. In *Power Tech Conference Proceedings, 2003 IEEE Bologna*, volume 3, pages 6–pp. IEEE, 2003.

[63] JB Ekanayake, L Holdsworth, and N Jenkins. Comparison of 5th order and 3rd order machine models for doubly fed induction generator (dfig) wind turbines. *Electric Power Systems Research*, 67(3):207–215, 2003.

[64] Mustafa Kayikçi and JV Milanovic. Assessing transient response of dfig-based wind plants—the influence of model simplifications and parameters. *IEEE Transactions on power systems*, 23(2):545–554, 2008.

[65] Poul Sørensen, Anca D Hansen, Torsten Lund, and Henrik Bindner. Reduced models of doubly fed induction generator system for wind turbine simulations. *Wind Energy*, 9(4):299–311, 2006.

[66] Jianxiao Zou, Chao Peng, Yan Yan, Hong Zheng, and Yan Li. A survey of dynamic equivalent modeling for wind farm. *Renewable and sustainable energy reviews*, 40: 956–963, 2014.

[67] Vladislav Akhmatov and Hans Knudsen. An aggregate model of a grid-connected, large-scale, offshore wind farm for power stability investigations importance of windmill mechanical system. *International Journal of Electrical Power & Energy Systems*, 24(9):709–717, 2002.

[68] JG Slootweg and WL Kling. Aggregated modelling of wind parks in power system dynamics simulations. In *Power Tech Conference Proceedings, 2003 IEEE Bologna*, volume 3, pages 6–pp. IEEE, 2003.

[69] Muhammad Ali, Irinel-Sorin Ilie, Jovica V Milanovic, and Gianfranco Chicco. Wind farm model aggregation using probabilistic clustering. *IEEE Transactions on Power Systems*, 28(1):309–316, 2013.

[70] Luis M Fernández, Francisco Jurado, and José Ramón Saenz. Aggregated dynamic model for wind farms with doubly fed induction generator wind turbines. *Renewable energy*, 33(1):129–140, 2008.

[71] LM Fernandez, CA Garcia, JR Saenz, and F Jurado. Equivalent models of wind farms by using aggregated wind turbines and equivalent winds. *Energy conversion and management*, 50(3):691–704, 2009.

[72] MA Chowdhury, WX Shen, N Hosseinzadeh, and HR Pota. A novel aggregated DFIG wind farm model using mechanical torque compensating factor. *Energy conversion and management*, 67:265–274, 2013.

[73] Muhammad Ali, JV Milanovic, Irinel-Sorin Ilie, and Gianfranco Chicco. Comparison of wind farm aggregate models for transient stability studies. In *Proc. 17th Power System Computation Conf.(PSCC)*, 2011.

[74] Miguel Garcia-Gracia, M Paz Comech, Jesus Sallan, and Andrés Llombart. Modelling wind farms for grid disturbance studies. *Renewable energy*, 33(9):2109–2121, 2008.

[75] Wei Qiao, Ronald G Harley, and Ganesh K Venayagamoorthy. Dynamic modeling of wind farms with fixed-speed wind turbine generators. In *Power Engineering Society General Meeting, 2007. IEEE*, pages 1–8. IEEE, 2007.

[76] Sung-ho Hur. Modelling and control of a wind turbine and farm. *Energy*, 156: 360–370, 2018.

[77] M Dicorato, G Forte, and M Trovato. Wind farm stability analysis in the presence of variable-speed generators. *Energy*, 39(1):40–47, 2012.

[78] Markus Pöller and Sebastian Achilles. Aggregated wind park models for analyzing power system dynamics. In *4th International Workshop on Large-Scale Integration of Wind Power and Transmission Networks for Offshore Wind Farms, Billund, Denmark*, 2003.

[79] Marcelo A Elizondo, Shuai Lu, Ning Zhou, and Nader Samaan. Model reduction, validation, and calibration of wind power plants for dynamic studies. In *2011 IEEE Power and Energy Society General Meeting*, pages 1–8. IEEE, 2011.

[80] Mohammed A Badr, Ahmed M Atallah, and Mona A Bayoumi. Comparison between aggregation techniques for pmsg wind farm. *Energy Procedia*, 74:1162–1173, 2015.

[81] Yu Ni, Chongtao Li, Zhengchun Du, and Gang Zhang. Model order reduction based dynamic equivalence of a wind farm. *International Journal of Electrical Power & Energy Systems*, 83:96–103, 2016.

[82] Carlos Andrés García, Luis M Fernández, and Francisco Jurado. Evaluating reduced models of aggregated different doubly fed induction generator wind turbines for transient stabilities studies. *Wind Energy*, 18(1):133–152, 2015.

[83] MJ Mercado-Vargas, D Gomez-Lorente, O Rabaza, and E Alameda-Hernandez. Aggregated models of permanent magnet synchronous generators wind farms. *Renewable Energy*, 83:1287–1298, 2015.

[84] Toshiya Nanahara, Masahiro Asari, Takamitsu Sato, Koji Yamaguchi, Masaaki Shibata, and Tsutomu Maejima. Smoothing effects of distributed wind turbines. part 1. coherence and smoothing effects at a wind farm. *Wind Energy*, 7(2):61–74, 2004.

[85] Toshiya Nanahara, Masahiro Asari, Tsutomu Maejima, Takamitsu Sato, Koji Yamaguchi, and Masaaki Shibata. Smoothing effects of distributed wind turbines. part 2. coherence among power output of distant wind turbines. *Wind Energy: An International Journal for Progress and Applications in Wind Power Conversion Technology*, 7(2):75–85, 2004.

[86] Poul Sørensen, Nicolaos Antonio Cutululis, Antonio Vigueras-Rodríguez, Henrik Madsen, Pierre Pinson, Leo E Jensen, Jesper Hjerrild, and Martin Donovan. Modelling of power fluctuations from large offshore wind farms. *Wind Energy*, 11(1): 29–43, 2008.

[87] Poul Sørensen, Anca D Hansen, and Pedro André Carvalho Rosas. Wind models for simulation of power fluctuations from wind farms. *Journal of wind engineering and industrial aerodynamics*, 90(12-15):1381–1402, 2002.

[88] Luciano De Tommasi, Madeleine Gibescu, and Arno J Brand. A dynamic wind farm aggregate model for the simulation of power fluctuations due to wind turbulence. *Journal of Computational Science*, 1(2):75–81, 2010.

[89] Antonio Vigueras-Rodríguez, P Sørensen, A Viedma, MH Donovan, and E Gómez Lázaro. Spectral coherence model for power fluctuations in a wind farm. *Journal of Wind Engineering and Industrial Aerodynamics*, 102:14–21, 2012.

[90] Jay Apt. The spectrum of power from wind turbines. *Journal of Power Sources*, 169(2):369–374, 2007.

[91] Jon Olauson and Mikael Bergkvist. Correlation between wind power generation in the European countries. *Energy*, 114:663–670, 2016.

[92] Nathaniel S Pearre and Lukas G Swan. Spatial and geographic heterogeneity of wind turbine farms for temporally decoupled power output. *Energy*, 145:417–429, 2018.

[93] Lluís Trilla, Oriol Gomis-Bellmunt, Adrià Junyent-Ferre, Montserrat Mata, J Sanchez Navarro, and Antoni Sudria-Andreu. Modeling and validation of DFIG 3MW wind turbine using field test data of balanced and unbalanced voltage sags. *IEEE Trans. Sustain. Energy*, 2(4):509–519, 2011.

[94] Abram Perdana, Sanna Uski-Joutsenvuo, Ola Carlson, and Bettina Lemström. Comparison of an aggregated model of a wind farm consisting of fixed-speed wind turbines with field measurement. *Wind Energy*, 11(1):13–27, 2008.

[95] Asma Aziz, Aman Than Oo, and Alex Stojcevski. Frequency regulation capabilities in wind power plant. *Sustainable Energy Technologies and Assessments*, 26: 47–76, 2018.

[96] Mohammad Dreidy, H Mokhlis, and Saad Mekhilef. Inertia response and frequency control techniques for renewable energy sources: A review. *Renewable and Sustainable Energy Reviews*, 69:144–155, 2017.

[97] Miller, Nicholas and Lew, Debra and Piwko, Richard . Technology Capabilities for Fast Frequency Response. Technical report, GE Energy Consulting, 2017. [Online]. Available: https://www.aemo.com.au/-/media/Files/Electricity/NEM/Security_and_Reliability/Reports/2017/2017-03-10-GE-FFR-Advisory-Report-Final---2017-3-9.pdf.

[98] Panayiotis Moutis, Stavros A Papathanassiou, and Nikos D Hatziargyriou. Improved load-frequency control contribution of variable speed variable pitch wind generators. *Renewable Energy*, 48:514–523, 2012.

[99] Xue Yingcheng and Tai Nengling. Review of contribution to frequency control through variable speed wind turbine. *Renewable energy*, 36(6):1671–1677, 2011.

[100] Rogério G De Almeida and JA Peças Lopes. Participation of doubly fed induction wind generators in system frequency regulation. *IEEE transactions on power systems*, 22(3):944–950, 2007.

[101] HT Ma and BH Chowdhury. Working towards frequency regulation with wind plants: combined control approaches. *IET Renewable Power Generation*, 4(4): 308–316, 2010.

[102] Australian Energy Market Operator (AEMO). Fast frequency response in the NEM. Technical report, 2017. [Online]. Available: https://www.aemo.com.au/-/media/Files/Electricity/NEM/Security_and_Reliability/Reports/2017/FFR-Working-Paper---Final.pdf.

[103] Nicholas W Miller, Kara Clark, and Miaolei Shao. Impact of frequency responsive wind plant controls on grid performance. In *9th International Workshop on Large-Scale Integration of Wind Power into Power Systems*, 2010.

[104] Francisco Díaz-González, Melanie Hau, Andreas Sumper, and Oriol Gomis-Bellmunt. Participation of wind power plants in system frequency control: Review of grid code requirements and control methods. *Renewable and Sustainable Energy Reviews*, 34:551–564, 2014.

[105] Sudipta Ghosh, Sukumar Kamalasadan, Nilanjan Senroy, and Johan Enslin. Doubly fed induction generator (dfig)-based wind farm control framework for primary frequency and inertial response application. *IEEE Transactions on Power Systems*, 31(3):1861–1871, 2015.

[106] NW Miller, Kara Clark, and Miaolei Shao. Frequency responsive wind plant controls: Impacts on grid performance. In *2011 IEEE Power and Energy Society General Meeting*, pages 1–8. IEEE, 2011.

[107] Zhao-Sui Zhang, Yuan-Zhang Sun, and Lin Cheng. Potential of trading wind power as regulation services in the california short-term electricity market. *Energy policy*, 59:885–897, 2013.

[108] Jiaqi Liang, Santiago Grijalva, and Ronald G Harley. Increased wind revenue and system security by trading wind power in energy and regulation reserve markets. *IEEE Transactions on Sustainable Energy*, 2(3):340–347, 2011.

[109] Elena Saiz-Marin, Javier García-González, Julian Barquin, and Enrique Lobato. Economic assessment of the participation of wind generation in the secondary regulation market. *IEEE Transactions on Power systems*, 27(2):866–874, 2012.

[110] Tiago Soares, Pierre Pinson, Tue V Jensen, and Hugo Morais. Optimal offering strategies for wind power in energy and primary reserve markets. *IEEE Transactions on Sustainable Energy*, 7(3):1036–1045, 2016.

[111] Le-Ren Chang-Chien, Chih-Min Hung, and Yao-Ching Yin. Dynamic reserve allocation for system contingency by dfig wind farms. *IEEE Transactions on Power Systems*, 23(2):729–736, 2008.

[112] Anca D Hansen, Poul Sørensen, Florin Iov, and Frede Blaabjerg. Centralised power control of wind farm with doubly fed induction generators. *Renewable energy*, 31 (7):935–951, 2006.

[113] Sara Siniscalchi-Minna, Fernando D Bianchi, Mikel De-Prada-Gil, and Carlos Ocampo-Martinez. A wind farm control strategy for power reserve maximization. *Renewable energy*, 131:37–44, 2019.

[114] TMI Mahlia, TJ Saktisahdan, A Jannifar, MH Hasan, and HSC Matseelar. A review of available methods and development on energy storage; technology update. *Renewable and Sustainable Energy Reviews*, 33:532–545, 2014.

[115] SBC Energy Institute. Electicity storage. [Online]. Available: https://www.cpuc.ca.gov/WorkArea., 2013. [Accessed: 2019-09-10].

[116] Anya Castillo and Dennice F Gayme. Grid-scale energy storage applications in renewable energy integration: A survey. *Energy Conversion and Management*, 87: 885–894, 2014.

[117] Behnam Zakeri and Sanna Syri. Electrical energy storage systems: A comparative life cycle cost analysis. *Renewable and sustainable energy reviews*, 42:569–596, 2015.

[118] Haisheng Chen, Thang Ngoc Cong, Wei Yang, Chunqing Tan, Yongliang Li, and Yulong Ding. Progress in electrical energy storage system: A critical review. *Progress in Natural Science*, 19(3):291–312, 2009.

[119] Marc Beaudin, Hamidreza Zareipour, Anthony Schellenberglabe, and William Rosehart. Energy storage for mitigating the variability of renewable electricity sources: An updated review. *Energy for Sustainable Development*, 14(4):302–314, 2010.

[120] Richard Baxter. *Energy storage: a nontechnical guide*. PennWell Books, 2006.

[121] Francisco Díaz-González, Andreas Sumper, Oriol Gomis-Bellmunt, and Roberto Villafáfila-Robles. A review of energy storage technologies for wind power applications. *Renewable and Sustainable Energy Reviews*, 16(4):2154–2171, 2012.

[122] Abbas A Akhil, Georgianne Huff, Aileen B Currier, Benjamin C Kaun, Dan M Rastler, Stella Bingqing Chen, Andrew L Cotter, Dale T Bradshaw, and William D Gauntlett. Doe/epri electricity storage handbook in collaboration with nreca. *Sandia national laboratories*, 2015.

[123] Lukas Geissbühler, Viola Becattini, Giw Zanganeh, Simone Zavattoni, Maurizio Barbato, Andreas Haselbacher, and Aldo Steinfeld. Pilot-scale demonstration of advanced adiabatic compressed air energy storage, part 1: Plant description and tests with sensible thermal-energy storage. *Journal of Energy Storage*, 17:129–139, 2018.

[124] Frank S Barnes and Jonah G Levine. *Large energy storage systems handbook*. CRC press, 2011.

[125] Haoran Zhao, Qiuwei Wu, Shuju Hu, Honghua Xu, and Claus Nygaard Rasmussen. Review of energy storage system for wind power integration support. *Applied Energy*, 137:545–553, 2015.

[126] Xing Luo, Jihong Wang, Mark Dooner, and Jonathan Clarke. Overview of current development in electrical energy storage technologies and the application potential in power system operation. *Applied Energy*, 137:511–536, 2015.

[127] KC Divya and Jacob Østergaard. Battery energy storage technology for power systems—an overview. *Electric Power Systems Research*, 79(4):511–520, 2009.

[128] Lazard. Levelized cost of storage analysis - version 3.0. Technical report, 2017.

[129] Ioannis Hadjipaschalis, Andreas Poullikkas, and Venizelos Efthimiou. Overview of current and future energy storage technologies for electric power applications. *Renewable and sustainable energy reviews*, 13(6):1513–1522, 2009.

[130] David Linden and Thomas B Reddy. Handbook of batteries. 3rd, 2002.

[131] Mathew Aneke and Meihong Wang. Energy storage technologies and real life applications–a state of the art review. *Applied Energy*, 179:350–377, 2016.

[132] AB Gallo, JR Simões-Moreira, HKM Costa, MM Santos, and E Moutinho dos Santos. Energy storage in the energy transition context: A technology review. *Renewable and Sustainable Energy Reviews*, 65:800–822, 2016.

[133] Ling Ai Wong, Vigna K Ramachandaramurthy, Phil Taylor, JB Ekanayake, Sara L Walker, and Sanjeevikumar Padmanaban. Review on the optimal placement, sizing and control of an energy storage system in the distribution network. *Journal of Energy Storage*, 21:489–504, 2019.

[134] Tarik Kousksou, Pascal Bruel, Abdelmajid Jamil, T El Rhafiki, and Youssef Zeraouli. Energy storage: Applications and challenges. *Solar Energy Materials and Solar Cells*, 120:59–80, 2014.

[135] Claire Curry. Lithium-ion battery costs and market. *Bloomberg New Energy Finance*, 5, 2017.

[136] Sergio Vazquez, Srdjan M Lukic, Eduardo Galvan, Leopoldo G Franquelo, and Juan M Carrasco. Energy storage systems for transport and grid applications. *IEEE Transactions on Industrial Electronics*, 57(12):3881–3895, 2010.

[137] Zhi Zhou, Todd Levin, and Guenter Conzelmann. Survey of us ancillary services markets. Technical report, Argonne National Lab.(ANL), Argonne, IL (United States), 2016.

[138] Yuqing Yang, Stephen Bremner, Chris Menictas, and Merlinde Kay. Battery energy storage system size determination in renewable energy systems: A review. *Renewable and Sustainable Energy Reviews*, 91:109–125, 2018.

[139] Yi Luo, Lin Shi, and Guangyu Tu. Optimal sizing and control strategy of isolated grid with wind power and energy storage system. *Energy Conversion and Management*, 80:407–415, 2014.

[140] Paul D Brown, JA Peças Lopes, and Manuel A Matos. Optimization of pumped storage capacity in an isolated power system with large renewable penetration. *IEEE Transactions on Power systems*, 23(2):523–531, 2008.

[141] Ted KA Brekken, Alex Yokochi, Annette Von Jouanne, Zuan Z Yen, Hannes Max Hapke, and Douglas A Halamay. Optimal energy storage sizing and control for wind power applications. *IEEE Transactions on Sustainable Energy*, 2(1):69–77, 2010.

[142] Fengji Luo, Ke Meng, Zhao Yang Dong, Yu Zheng, Yingying Chen, and Kit Po Wong. Coordinated operational planning for wind farm with battery energy storage system. *IEEE Transactions on Sustainable Energy*, 6(1):253–262, 2015.

[143] Abdulaziz Alanazi and Amin Khodaei. Optimal battery energy storage sizing for reducing wind generation curtailment. In *2017 IEEE Power & Energy Society General Meeting*, pages 1–5. IEEE, 2017.

[144] Yasser Moustafa Atwa and EF El-Saadany. Optimal allocation of ess in distribution systems with a high penetration of wind energy. *IEEE Transactions on Power Systems*, 25(4):1815–1822, 2010.

[145] Sonja Wogrin and Dennice F Gayme. Optimizing storage siting, sizing, and technology portfolios in transmission-constrained networks. *IEEE Transactions on Power Systems*, 30(6):3304–3313, 2014.

[146] Wei Li and Géza Joós. Comparison of energy storage system technologies and configurations in a wind farm. In *2007 IEEE Power Electronics Specialists Conference*, pages 1280–1285. IEEE, 2007.

[147] M Khalid and AV Savkin. Minimization and control of battery energy storage for wind power smoothing: Aggregated, distributed and semi-distributed storage. *Renewable Energy*, 64:105–112, 2014.

[148] Kyle Bradbury, Lincoln Pratson, and Dalia Patiño-Echeverri. Economic viability of energy storage systems based on price arbitrage potential in real-time US electricity markets. *Applied Energy*, 114:512–519, 2014.

[149] Ted KA Brekken, Alex Yokochi, Annette Von Jouanne, Zuan Z Yen, Hannes Max Hapke, and Douglas A Halamay. Optimal energy storage sizing and control for wind power applications. *IEEE Transactions on Sustainable Energy*, 2(1):69–77, 2011.

[150] Chad Abbey and Géza Joós. A stochastic optimization approach to rating of energy storage systems in wind-diesel isolated grids. *IEEE Transactions on Power Systems*, 24(1):418–426, 2009.

[151] Dylan McConnell, Tim Forcey, and Mike Sandiford. Estimating the value of electricity storage in an energy-only wholesale market. *Applied Energy*, 159:422–432, 2015.

[152] Ramteen Sioshansi, Paul Denholm, Thomas Jenkin, and Jurgen Weiss. Estimating the value of electricity storage in pjm: Arbitrage and some welfare effects. *Energy economics*, 31(2):269–277, 2009.

[153] Simon Gill, GW Ault, and Ivana Kockar. The optimal operation of energy storage in a wind power curtailment scheme. In *2012 IEEE Power and Energy Society General Meeting*, pages 1–8. IEEE, 2012.

[154] Edgardo D Castronuovo and Joao A Pecas Lopes. Optimal operation and hydro storage sizing of a wind–hydro power plant. *International Journal of Electrical Power & Energy Systems*, 26(10):771–778, 2004.

[155] Mir-Akbar Hessami and David R Bowly. Economic feasibility and optimisation of an energy storage system for portland wind farm (victoria, australia). *Applied Energy*, 88(8):2755–2763, 2011.

[156] Hossein Akhavan-Hejazi and Hamed Mohsenian-Rad. Optimal operation of independent storage systems in energy and reserve markets with high wind penetration. *IEEE Transactions on Smart Grid*, 5(2):1088–1097, 2013.

[157] Trishna Das, Venkat Krishnan, and James D McCalley. Assessing the benefits and economics of bulk energy storage technologies in the power grid. *Applied Energy*, 139:104–118, 2015.

[158] Asmae Berrada and Khalid Loudiyi. Operation, sizing, and economic evaluation of storage for solar and wind power plants. *Renewable and sustainable energy Reviews*, 59:1117–1129, 2016.

[159] Rahul Walawalkar, Jay Apt, and Rick Mancini. Economics of electric energy storage for energy arbitrage and regulation in new york. *Energy Policy*, 35(4): 2558–2568, 2007.

[160] Asmae Berrada, Khalid Loudiyi, and Izeddine Zorkani. Valuation of energy storage in energy and regulation markets. *Energy*, 115:1109–1118, 2016.

[161] Magnus Korpaas, Arne T Holen, and Ragne Hildrum. Operation and sizing of energy storage for wind power plants in a market system. *International Journal of Electrical Power & Energy Systems*, 25(8):599–606, 2003.

[162] Javier Garcia-Gonzalez, RocÍo Moraga Ruiz de la Muela, Luz Matres Santos, and Alicia Mateo Gonzalez. Stochastic joint optimization of wind generation and pumped-storage units in an electricity market. *IEEE Transactions on Power Systems*, 23(2):460–468, 2008.

[163] Huajie Ding, Zechun Hu, and Yonghua Song. Stochastic optimization of the daily operation of wind farm and pumped-hydro-storage plant. *Renewable Energy*, 48: 571–578, 2012.

[164] Peng Zou, Qixin Chen, Qing Xia, Guannan He, and Chongqing Kang. Evaluating the contribution of energy storages to support large-scale renewable generation in joint energy and ancillary service markets. *IEEE Transactions on Sustainable Energy*, 7(2):808–818, 2015.

[165] Guannan He, Qixin Chen, Chongqing Kang, Qing Xia, and Kameshwar Poolla. Cooperation of wind power and battery storage to provide frequency regulation in power markets. *IEEE Transactions on Power Systems*, 32(5):3559–3568, 2016.

[166] T Rodrigues, PJ Ramírez, and G Strbac. The value of storage for a wind farm offering energy and spinning reserve. 2016.

[167] Junli Wu, Buhan Zhang, Hang Li, Zhongcheng Li, Yi Chen, and Xiaogang Miao. Statistical distribution for wind power forecast error and its application to determine optimal size of energy storage system. *International Journal of Electrical Power & Energy Systems*, 55:100–107, 2014.

[168] Hans Bludszuweit, José Antonio Domínguez-Navarro, and Andrés Llombart. Statistical analysis of wind power forecast error. *IEEE Transactions on Power Systems*, 23(3):983–991, 2008.

[169] Morteza Zare Oskouei and Ahmad Sadeghi Yazdankhah. Scenario-based stochastic optimal operation of wind, photovoltaic, pump-storage hybrid system in frequency-based pricing. *Energy Conversion and Management*, 105:1105–1114, 2015.

[170] Saurabh Tewari, Charles J Geyer, and Ned Mohan. A statistical model for wind power forecast error and its application to the estimation of penalties in liberalized markets. *IEEE Transactions on Power Systems*, 26(4):2031–2039, 2011.

[171] Y Yuan, Q Li, and W Wang. Optimal operation strategy of energy storage unit in wind power integration based on stochastic programming. *IET renewable power generation*, 5(2):194–201, 2011.

[172] Technical specifications of Senvion MM92 wind turbine 2.05 MW. https://www.senvion.com/global/en/products-services/wind-turbines/mm/mm92/. (accessed: 2019-05-26).

[173] Julius S Bendat and Allan G Piersol. *Random data: analysis and measurement procedures*, volume 729. John Wiley & Sons, 2011.

[174] GAMS - cutting edge modeling. [Online]. Available: https://www.gams.com/. [Aaccessed: 2019-05-26].

[175] Andrei Nikolaevich Kolmogorov. The local structure of turbulence in incompressible viscous fluid for very large reynolds numbers. *Proceedings of the Royal Society of London. Series A: Mathematical and Physical Sciences*, 434(1890):9–13, 1991.

[176] Warren Katzenstein, Emily Fertig, and Jay Apt. The variability of interconnected wind plants. *Energy policy*, 38(8):4400–4410, 2010.

[177] Masahiro Asari, Toshiya Nanahara, Tsutomu Maejima, Koji Yamaguchi, and Takamitsu Sato. A study on smoothing effect on output fluctuation of distributed wind power generation. In *Transmission and Distribution Conference and Exhibition 2002: Asia Pacific. IEEE/PES*, volume 2, pages 938–943. IEEE, 2002.

[178] IBM ILOG CPLEX Optimization. [Online]. Available: https://www.ibm.com/analytics/cplex-optimizer. [Accessed: 2019-05-26].

[179] Australian Energy Market Operator (AEMO). Australian Wind Energy Forecasting System (AWEFS). Technical report, 2016. [Online]. Available: https://www.aemo.com.au/-/media/Files/PDF/Australian-Wind-Energy-Forecasting-System-AWEFS.pdf.

[180] NRECA, CoBank, and NRTC. Battery energy storage overview. 2017.

[181] Todd Aquino, Mathew Roling, Chris Baker, and Lucas Rowland. Battery energy storage technology assessment. Platte River Power Authority, 2017-11-29.

[182] Susan M Schoenung and William V Hassenzahl. Long-vs. short-term energy storage technologies analysis: a life-cycle cost study: a study for the DOE energy storage systems program. Technical report, Sandia National Laboratories, 2003.

[183] Ran Fu, Timothy W Remo, and Robert M Margolis. 2018 US utility-scale photovoltaics-plus-energy storage system costs benchmark. Technical report, National Renewable Energy Lab.(NREL), Golden, CO (United States), 2018.

[184] Torben Knudsen, Thomas Bak, and Mikael Svenstrup. Survey of wind farm control—power and fatigue optimization. *Wind Energy*, 18(8):1333–1351, 2015.

[185] Causer Pays 4-second data. [Online]. Available: http://www.nemweb.com.au/Reports/Current/Causer_Pays/. [Accessed: 2019-07-10].

[186] Australian Energy Market Commission (AEMC). National electricity rules version 123. Technical report, 2019. [Online]. Available: https://www.aemc.gov.au/sites/default/files/2019-07/National%20Electricity%20Rules%20Version%20123%20excluding%20Chapter%204A_0.pdf.

[187] Sarah Probert, Akeelesh Kusrutsing, Matthew Jeppesen, David Rundell, and Mostafa Naemi. Alcoa FCAS Provision. Private Communication, 2018.

[188] Ma Lei, Luan Shiyan, Jiang Chuanwen, Liu Hongling, and Zhang Yan. A review on the forecasting of wind speed and generated power. *Renewable and Sustainable Energy Reviews*, 13(4):915–920, 2009.

[189] Saurabh S Soman, Hamidreza Zareipour, Om Malik, and Paras Mandal. A review of wind power and wind speed forecasting methods with different time horizons. In *North American Power Symposium 2010*, pages 1–8. IEEE, 2010.

[190] T.S. Brinsmead, P. Graham, J. Hayward, E.L. Ratnam, and L. Reedman. Future energy storage trends: An assessment of the economic viability, potential uptake and impacts of electrical energy storage on the nem 2015–2035. Technical report, CSIRO, 2015.

[191] Jane S Peters and Jun Suzuki. Baseline market evaluation metrics for energy storage. Technical report, Research Into Action, Inc, 2017.

[192] Electricity storage and renewables: Costs and markets to 2030. Technical report, Interational Renewable Energy Agency (IRENA), 2017.

[193] U.S. battery storage market trends. Technical report, Energy Information Administration (EIA), 2018.

[194] Final energy storage potential evaluation. Technical report, PacifiCorp, 2018.